2018

THE BIOPHYSICAL AND BIOCHEMICAL IMPACTS OF FOREST DISTURBANCES ACROSS ECOSYSTEMS

Leila Ann Cooper

THE BIOPHYSICAL AND BIOCHEMICAL IMPACTS OF FOREST DISTURBANCES ACROSS ECOSYSTEMS

By

LEILA ANN COOPER

Bachelor of Arts, Whitman College, Walla Walla, WA, 2012

Dissertation

presented in partial fulfillment of the requirements
for the degree of

Doctor of Philosophy
in Systems Ecology

The University of Montana
Missoula, MT

May 2018

Approved by:

Scott Whittenburg, Dean of The Graduate School
Graduate School

Ashley P. Ballantyne, Chair
Department of Ecosystem and Conservation Sciences

Solomon Z. Dobrowski
Department of Forest Management

Zachary A. Holden
United States Forest Service

Erin L. Landguth
Division of Biological Sciences

Andrew J. Larson
Department of Forest Management

Cooper, Leila, Ph.D., Spring 2018 Systems Ecology

The Biophysical and Biochemical Impacts of Forest Disturbances Across Ecosystems

Chairperson: Ashley Ballantyne

Forest disturbances result in numerous impacts on ecosystem services. In the western United States, disturbances such as wildfires and bark beetle outbreaks have resulted in millions of hectares of dead trees. Despite the potential for these events to have significant climatic impacts, it remains a challenge both to effectively locate and characterize disturbance events across landscapes, and to identify the disturbance biophysical and biochemical impacts. The objective of my dissertation research was to improve the ways in which we locate and classify forest disturbances over large areas, as well as to increase our understanding of disturbance biophysical and biochemical impacts and how those impacts vary according to ecosystem properties.

In chapter 1, I researched how a severe mountain pine beetle outbreak in western Montana influenced the future characteristics of lodgepole pine forests through the use of dendrochronological and climate station data. I investigated whether the outbreak had differentially impacted differing growth phenotypes, resulting in changes in forest productivity, and how growth phenotype related to patterns of growth-climate sensitivity. In chapter 2, I moved up in scale to investigate the biophysical and biochemical impacts of multiple forest disturbance classes, as well as how impacts of forest disturbances differed across varying ecoregions around the western United States. For chapter 3, I sought to improve our ability to understand the climatic impacts of forest disturbances by developing a logical framework to more accurately and efficiently detect and attribute forest disturbances using satellite imagery.

The results of my work demonstrate the potential for large-scale impacts of forest disturbances on climate, and also suggest that current disturbances may alter the future forest-climate interactions. Additionally, the results from chapters 1 and 2 suggest that there is significant variability in the impacts of forest disturbances on climate, both within and among ecoregions and among disturbance types. This variability is mostly ignored in large-scale simulations of disturbance, despite its potential to significantly alter model and simulation results. The framework developed for my 3rd chapter will enable a better understanding of the variability of forest disturbances and allow for better prediction of their impacts on climate and other ecosystem properties.

ACKNOWLEDGEMENTS

This work has come together with the help of numerous people, to whom I am extremely thankful. First, I would like to thank my advisor, Ash Ballantyne, without whom I would not have been able to complete this research. I am very grateful to him for funding me for my initial first couple of years, for his effort in parsing my many drafted funding requests and papers, and for his humor and tireless career advice. Second, I would like to thank Zack Holden for his help with several components of this research, including providing computational resources and help getting my 2nd chapter ready for publication. I would like to thank my remaining committee members – Erin Landguth, Solomon Dobrowski, and Andrew Larson, for their continuous support throughout my Ph.D. process and for their help with various aspects of projects, from providing occasional funding and computational resources, to answering questions on statistics and disturbance ecology. Finally, I would like to thank the members of the Global Climate and Ecology Lab – Charlotte Reed, Zhihua Liu, Tams Fletcher, and Andrew Hursh, for their formal and informal input on my research and for always being willing to get tea and chat about life and science.

I also am indebted to my family, who have provided support throughout the ups and downs of my graduate career. Lastly, I could not have completed my dissertation without my fiancée, Seth, there to support me and provide feedback. I cannot express how thankful I am for his unwavering support over the past five years.

TABLE OF CONTENTS

LIST OF FIGURES

LIST OF TABLES

DISSERTATION OVERVIEW

My dissertation is organized into three chapters, covering the biochemical and biophysical impacts of disturbances across ecosystems and climatic gradients, as well as new methods with which to detect and attribute forest disturbances using satellite data. Combined, these chapters improve our understanding of how disturbance impacts vary according to local or regional environmental characteristics, and also improve on our ability to study these disturbance impacts in more detail in future research. A brief summary of each chapter follows.

Chapter 1: Mountain pine beetle attack faster growing lodgepole pine at low elevations in western Montana, USA

Global change has impacted forests through altered disturbance regimes. In the western US, climate change has resulted in extensive and severe mountain pine beetle outbreaks. These outbreaks have the potential to impact forest function through the selection of certain phenotypes. We investigated the potential for bark beetle-induced selection by way of measuring growth and climate response in mountain pine beetle-killed and surviving lodgepole pine in the Northern Rockies. We had three objectives: (1) investigate differences in growth between beetle-killed and surviving lodgepole pine prior to a recent outbreak, (2) compare the climate-growth relationships for beetle-killed and surviving lodgepole pine and how those relationships explain observed growth differences and predict mortality risk, and (3) investigate growth differences and growth-climate relationships across north- and south-facing aspects and over an elevation range representing local climate gradients. Significant differences in growth rate were observed at low-elevation sites, with beetles killing large, faster-growing, trees. While aspect influenced overall growth, it did not have a significant influence on the difference in

growth between beetle-killed and surviving trees. Growth showed significant relationships with several climate variables (i.e., previous-year August temperatures, October temperatures, annual precipitation, and summertime climatic water deficit), with slight differences in those relationships between beetle-killed and surviving trees. Mixed effects models demonstrated that higher growth rates and age increased the probability of mortality during the outbreak at all elevations, and also that climatic water deficit and previous-year August maximum temperatures were related to the magnitude of growth differences between beetle-killed and surviving trees. Overall, mountain pine beetles tended to attack large, fast-growing, lodgepole trees, especially at lower elevations where trees may be more susceptible to seasonal water stress.

Chapter 2: Disturbance impacts on land surface temperature and gross primary productivity in the western United States

Forest disturbances influence forest structure, composition, and function, and may impact climate through changes in net radiation or through shifts in carbon exchange. Climate impacts vary depending on environmental variables and disturbance characteristics, yet few studies have investigated disturbance impacts over large, environmentally heterogeneous, regions. We used satellite data to objectively determine the impacts of fire, bark beetles, defoliators, and 'unidentified disturbances' (UD) on land surface temperature (LST) and gross primary productivity (GPP) across the western United States (US). We investigated immediate disturbance impacts, the drivers of those impacts, and long-term post-disturbance LST and GPP recovery patterns. All disturbance types caused LST increases (ºC; Fire: 3.45±3.02, Bark Beetles: 0.76±3.04, Defoliators: 0.49±3.12, UD: 0.76±3.03). Fire and insects resulted in GPP declines (%; Fire: -25.05±21.67, Bark Beetles: -2.84±21.06, Defoliators: -0.23±15.40), while UDs resulted

in slightly enhanced GPP (1.89±24.20 %). Disturbance responses also varied between ecoregions. Severity and interannual changes in air temperature were the primary drivers of short-term disturbance responses, and severity also had a strong impact on long-term recovery patterns. These results suggest a potential climate feedback due to disturbance-induced biophysical changes that may strengthen as disturbance regimes shift due to climate change.

Chapter 3: Application of Random Forest for the detection and attribution of forest disturbance

Accurate assessments of current and future disturbance characteristics and trends are essential for understanding the ecological processes and interactions within and among landscapes. Current methods for disturbance detection rely primarily on temporal change detection. These approaches areas are fairly accurate in regions where they have been tuned but are less accurate when applied to regions where they have not been tuned. Here, we introduce a new approach for both disturbance detection and attribution that exploits both temporal and spatial variability. Our objectives with this new approach were to determine the usefulness of both temporal and spatial information for disturbance detection and attribution, and to determine whether a machine learning (i.e., Random Forest) approach utilizing both types of information would improve the accuracy of detection across multiple regions. The results of our analysis are also useful for providing information on how disturbances differ across forest types, and how those differences might complicate conventional temporal approaches to disturbance detection. Specifically, with this approach, we were able to ask, how do variables important for disturbance detection and attribution vary among regions? We found that while accuracy varied across regions and among disturbance types, the false positive (3-23%) and

negative (3-40%) rates using these new methods were similar to those from strictly temporal approaches. In addition, we found that the variables important for disturbance detection and attribution varied considerably across regions, with at least one spatial and one temporal variable included in each model. This suggests that both disturbance characteristics and the environment in which they occur vary considerably by forest type and location. This difference among predictor variables may explain why previous detection algorithms are accurate in one region, but are less accurate when applied to other regions. The detection methods developed for this study may be useful for detecting and attributing disturbance at the landscape scale, and have the potential to be scaled up from regional to global scales in the future.

CHAPTER 1

Mountain pine beetle attack faster growing lodgepole pine at low elevations in western Montana, USA

Corresponding publication:

Cooper, L.A., Reed, C.C. & Ballantyne, A.P. (*In press*) Mountain pine beetle attack faster growing lodgepole pine at low elevations in western Montana, USA, *Forest Ecology and Management*.

INTRODUCTION

Forests are globally important due to the ecosystem services they provide [Trumbore et al., 2015]. Recently, widespread mountain pine beetle (*Dendroctonus ponderosae* Hopkins) outbreaks have occurred in the western United States and Canada, resulting in mass mortality across large areas of forest [Meddens et al., 2012]. These outbreaks are driven in part by changes in regional climate, where temperatures have increased and precipitation patterns have shifted [IPCC, 2014]. Warmer and drier conditions stress host trees and provide a longer period of temperatures suitable to beetles [Dale et al., 2001; Raffa et al., 2008; Bentz et al., 2010]. Thus, beetles are both more capable of reproducing rapidly and can more easily overwhelm tree defenses [Mitton and Ferrenberg, 2012]. As water stress is predicted to increase in many ecosystems in the western US [Seager et al., 2007; IPCC, 2014], the need to more fully understand the relationship between host trees, bark beetles, and climate is significant. Specifically, it is important to understand how host trees interact with climate and to determine the impact of those interactions on host tree susceptibility to beetle attack.

Mountain pine beetles are a native, ‘irruptive,’ insect in western North America. Beetles attack trees by burrowing through the tree’s bark and into the phloem. Successful attacks occur when sufficient numbers of beetles are recruited to attack the tree via the release of pheromones by the initial attackers [Raffa, 1988]. These mass attacks succeed by overwhelming tree defenses, and result in mortality of the host tree. Beetles also

introduce blue-stain fungus to trees during attacks, which helps to kill trees by blocking the xylem with fungal spores. Tree defenses include producing resins to physically expel beetles and producing defensive compounds, processes that require a substantial investment of resources [Raffa and Berryman, 1983]. Trees become more susceptible to successful attack when climate conditions are stressful because their resources are already limited [Waring and Pitman, 1983]. Additionally, climate conditions that are stressful to host trees are typically beneficial to the beetles, with warmer temperatures allowing some species to grow and mature faster [Bentz et al., 2010]. While mountain pine beetles attack several species, their most common host is lodgepole pine (*Pinus contorta* Douglas ex Loudon) [Raffa, 1988].

Numerous climatological variables have been linked to bark beetle outbreaks, including vapor pressure deficit (VPD) [Littell et al., 2010; Hart et al., 2014], climatic water deficit (CWD) [Millar et al., 2012], high previous-year summer and fall temperatures [Berg et al., 2006; Chapman et al., 2012], and multi-decadal oscillations such as the Atlantic Decadal Oscillation [Hart et al., 2014]. Similar climate variables have been found to limit the growth of lodgepole pine [Chhin et al., 2008; Lo et al., 2010], reinforcing the link between climate and host tree resource limitation. All of these climate conditions decrease the availability of water to the host tree, inhibiting both its ability to grow and its ability to produce resin with which to pitch out attacking beetles [Kane and Kolb, 2010].

Mountain pine beetle outbreaks have the potential to influence the characteristics of host stands through beetle preference for certain host tree characteristics, as well as through differential success of beetle attacks based on tree traits. Resistance to mountain

pine beetles may vary among stands and individuals due to environmental or genetic variation [Raffa and Barryman, 1983; Alberto et al., 2013], such that in the right outbreak conditions, trees with lower resistance may be killed more readily than trees with naturally higher resistance [Ferrenberg et al., 2014]. During severe outbreaks, it is therefore possible that the phenotypic traits of host stands may shift due to extensive mortality within one resistance group [de la Mata et al., 2017].

The results of previous studies on selection for certain phenotypes, both in lodgepole pine and other pine species, are highly variable. High levels of mortality in ponderosa pine were found to primarily affect slower-growing individuals, leading towards selection for faster-growing trees [Knapp et al., 2013]. Similarly, Millar et al. [2012] found evidence for selection towards faster-growing whitebark pine in the eastern Sierra Nevada, CA due to higher mortality among slower-growing individuals from mountain pine beetle. However, a separate study on ponderosa pine found that a greater number of individuals from fast-growing families were killed during an intense bark beetle outbreak, resulting in selection towards slower growth in the population [de la Mata et al., 2017]. Results from a study in British Columbia, Canada on lodgepole pine also found that faster-growing families within populations were more susceptible to mountain pine beetle attack [Yanchuk et al., 2008]. In an Aleppo pine (*Pinus halepensis* Mill.) plantation in Spain, high bark beetle mortality was observed in both fast- and slow-growing individuals. However, individuals that were more responsive to annual climate variations were less likely to have been killed [Sanguesa-Barreda et al., 2015]. The ages of the stands in these studies differed substantially, with the Knapp et al. [2013] and Millar et al. [2012] studies focusing on relatively old (>150 years) stands, and the de la

Mata et al. [2017], Yanchuk et al. [2008], and Sanguesa-Barreda et al. [2015] studies focusing on a younger (<50 years) stands. These studies suggest high variability in the impacts of bark beetles on pine stands, potentially due to variations in local climate, host species, stand age, and topographic variables. Studies have consistently found that water deficit plays a role in regulating annual tree growth and pine susceptibility to attack, and that climate-related growth differences may exist between trees that succumbed to pine beetles and trees that survived outbreaks. Further research is therefore necessary to illuminate the relationship between climate (e.g., water deficit) impacts on growth and how that relationship translates into mountain pine beetle susceptibility.

Differences in growth between beetle-killed and surviving trees may suggest a difference in the allocation of resources [Ruel and Whitham, 2002; Bigler and Veblen, 2009]. Trees may differ in the amount of carbon allocated towards growth versus defensive compounds [Herms and Mattson, 1992], or carbon compounds used for growth and maintenance when drought limits photosynthetic activity. Trees that are affected more by drought may also have a higher chance of successful beetle attack [Hanks et al., 1999]. If an outbreak occurs with sufficient severity, this could push the local host tree population towards having lower growth, but higher defenses. However, this has not been demonstrated consistently [Lahr and Krokene, 2013; Hood and Sala, 2015], suggesting that differences in growth may instead be explained by environmental context. Trees growing in more or less favorable environments may naturally react differently to climate stress, resulting in differential mortality during bark beetle outbreaks. While the trees may appear phenotypically different when examining growth and growth-climate responses, they may not have any natural differences in allocation strategies. In this

scenario, trees with higher growth might also have greater natural resistance to pine beetles [Mitchell et al., 1983] due to greater access to resources [Christiansen et al., 1987].

For this study, we had three objectives: (1) investigate differences in growth between beetle-killed and surviving lodgepole pine prior to a recent outbreak, (2) determine and compare the climate-growth relationships for beetle-killed and surviving lodgepole pine and how those relationships explain observed growth differences and predict mortality risk, and (3) investigate growth differences and growth-climate relationships across north- and south-facing aspects and over an elevation range representing a local gradient in climate stress.

METHODS

Study area

Our study sites occur within the Boulder Mountains of the Beaverhead-Deerlodge National Forest (Fig. 1.1), where elevation ranges from ~1400 m to ~3100 m. The area experienced a severe mountain pine beetle outbreak in the mid-2000s. Primary tree species in the area are lodgepole pine, Douglas-fir (*Pseudotsuga menziesii* (Mirb.) Franco), subalpine fir (*Abies lasiocarpa* (Hook.) Nutt), and whitebark pine (*Pinus albicaulis* Engelm.). Douglas-fir and lodgepole pine are dominant species at low to mid elevations, and whitebark pine, subalpine fir, and lodgepole pine are dominant species at higher elevations. According to the nearest climate station, located ~34 km away in Boulder, MT, January was the coldest month between 1949 and 2015, with an average temperature of -12.4 ºC. July was the warmest month with an average temperature of 28.2 ºC [http://www.wrcc.dri.edu/cgi-bin/cliMAIN.pl?mt1008]. Within this period,

annual precipitation averaged 279 mm, with most precipitation falling in June. The actual study site temperature and precipitation are likely slightly colder and wetter, as Boulder, MT is located just outside the forested area at a lower elevation (1521 m).

Plot selection and design

Twelve plots were selected for the study from the Thunderbolt Creek and Boulder River drainages. The plots span both north and south aspects, and three elevational bands across a 600 m gradient. Potential plot locations were selected based on apparent lodgepole pine dominance, significant mortality due to mountain pine beetle, and stand access [Montana Natural Heritage Program, 2017; USDA Forest Service, 2000-2014]. Actual plots were selected upon visiting the sites, with selection determined by (1) dominance of lodgepole pine in the canopy, (2) substantial mountain pine beetle-caused mortality in the stand (>40%), and (3) survival of at least 10 trees in the plot and immediate vicinity. In order to capture more of the variability in stand dynamics, two plots were chosen within each aspect-elevation combination (e.g., south – low #1 = SL1, south – mid #2 = SM2, etc.). Plots were required to be a minimum of 100 m from one another so as to limit spatial autocorrelation.

Ten beetle-killed trees were selected within a 10 m radius circular plot, and two increment cores were taken at 1.37 m height on opposite sides of the tree, perpendicular to the slope. Beetle-killed trees were randomly selected across the plot to obtain an even distribution of samples. Ten surviving trees of similar diameter to the beetle-killed trees were selected and cored within the plot. If ten surviving trees were not found within the plot, additional surviving trees close to the boundary of the plot (i.e., within 1 m) were used. Non-random sampling of surviving trees was used in order to minimize the

difference in ages between surviving and beetle-killed trees. Six of the plots did not have sufficient surviving trees within the plot radius, necessitating that trees outside the plot be sampled (Table 1.1). No plots required more than 40% of surviving trees to be sampled outside the plot radius. A total of 482 tree cores were collected for the study. Of the 482 tree cores collected, 444 were included in the analysis. Thirty-eight cores were discarded from the analysis due to poor correlations with the master chronologies. Additionally, age, DBH, and the coefficient of variation for annual growth within trees were assessed in order to provide context for other results.

Climate data

Climate data were obtained from the Boulder, MT climate station [http://www.wrcc.dri.edu/cgi-bin/cliMAIN.pl?mt1008]. Monthly maximum temperature, minimum temperature, and precipitation were prepared for the analysis. Vapor pressure deficit (VPD) was calculated from climate station data [Buck et al., 1981], using the equations

$$e_s = 0.6108e^{\frac{17.27T}{237.3+T}}$$

$$VPD = \frac{100 - RH}{100} e_s$$

where e_s is saturated vapor pressure, T is temperature in degrees Celsius, and RH is relative humidity as measured at the climate station. Hydrologic year (annual) precipitation was calculated from the monthly data, and previous-year values of all variables were determined. RH data came from the Helena, MT climate station [https://wrcc.dri.edu/cgi-bin/cliMAIN.pl?mthele] because the Boulder station did not record the variable. Monthly climatic water deficit (CWD) [Dobrowski et al., 2013] was also included in the analysis as a variable representative of drought, and because it has

been demonstrated to have significant relationships with growth in other study locations [Millar et al., 2012]. All data preparation was completed in R [R Core Team, 2013].

Tree core preparation

Increment cores were prepared according to standard dendrochronological techniques [Stokes and Smiley, 1968]. Master chronologies for each aspect-elevation combination were created using approximately ten cores from surviving trees at each location. Cores were cross-dated, then scanned at 2400 dpi. Annual ring widths were measured using CooRecorder 7.8 [Cybis Elektronik, 2014], and final chronologies quantitatively validated in COFECHA [Holmes, 1983].

Basal area increment (BAI), a measure of growth, was calculated using ring widths and estimated distance to pith with the *dplR* package [Bunn et al., 2015] in R. Distance to pith was estimated based on growth and curvature of the earliest observed rings if the pith was not present in the core [Larsson et al., 2014]. Converting annual ring widths to BAI overcomes the decrease in ring width that occurs as a function of increasing tree size [Biondi and Qeadan, 2008].

Statistical analyses

Climate correlations

In order to determine which climate variables to include in models of mortality risk and growth differences, correlations between BAI and climate variables were tested using Pearson correlations. Correlations were considered significant if p-values were ≤ 0.05. Climate variables were tested for correlations with zero (current-year) and one year (previous-year) lag times.

Mortality models

A binomial mixed effects model was used to model mortality risk as a function of elevation, aspect, tree age, mean 1950 – 2005 BAI, and growth resistance to extreme values of correlated climate variables. Stress resistance was calculated for each tree as the BAI during stressful years relative to the BAI during 'normal' years. Stressful years were determined as years in which the value of the variable exceeded the 75th percentile of its distribution over the 1950 – 2005 period. All years in which the variable did not exceed the 75th percentile were designated as 'normal.' None of the variables included in the binomial mortality model showed signs of collinearity. Models were fit according to protocols in Zuur et al. [2009]. Both plot and tree were considered as random effects in the model.

BAI-climate models

General linear mixed effects models (GLMMs) were used to model BAI as a function of climate variables, mortality, and tree age [Fernández-de-Uña et al., 2016]. Climate variables shown to be significant in the BAI-climate correlation analysis were considered for the models. Potential climate variables were checked for collinearity and the variable deemed most ecologically important was chosen if two variables were collinear. Variables were considered sufficiently independent with variance inflation factors less than 10.

One model was created for each aspect-elevation combination in order to determine the growth controls at each site, and whether pre-outbreak growth differed significantly between mortality categories. Both plot and tree were considered as random effects in each model, and autocorrelation was modeled between years. Residual heterogeneity was allowed to vary by plot for the mid- and high-elevation models.

Residual heterogeneity did not vary significantly between plots at low elevations and was not included in those models.

Growth difference models

Plot-level differences in BAI between beetle-killed and surviving trees were also modeled using GLMMs. These models predicted BAI differences as a function of aspect, elevation, and climate variables. Plot was considered as a random effect. Residual heterogeneity was allowed to vary by plot and autocorrelation was again modeled between years.

RESULTS

Site characteristics

All plots showed high levels of mortality ranging from 49 – 86% (Table 1.1), with most mortality occurring between 2006 and 2008. Stands were similar in density, with no discernable pattern across elevations and aspects, although the diameter and age of trees did increase with elevation (Table 1.1; Figs. S1.2 & S1.5). While it was possible to locate stands spaced evenly along the elevation gradient, the exact aspect of stands varied slightly from north-south alignment.

Climate correlations

Correlations between BAI and maximum temperature, minimum temperature, precipitation, and VPD were significant ($p \leq 0.05$) for several months, with similar correlation patterns between aspects (Table S1.1). Beetle-killed trees generally showed slightly stronger correlations with climate variables, and while the coefficient of variation for BAI was slightly lower over the study period in beetle-killed trees relative to surviving trees, this was not related to climate variation (Fig S1.3) nor significant across

plots. In general, late-summer maximum temperatures and VPD of the previous growing season were negatively related to growth across elevations and aspects, with only a few exceptions. Additionally, current-year October temperatures and VPD were generally positively related to growth across high-, and sometimes mid-elevation sites. Annual precipitation was positively correlated with BAI at both aspects of low elevations for both beetle-killed and surviving trees. Summertime CWD was correlated with BAI at low-elevation sites across both aspects for both beetle-killed and surviving trees.

Mortality model

Mortality risk was explained by both mean 1950 – 2005 BAI and tree age (Table 1.2). Growth rate was the most significant predictor of mortality ($p < 0.001$) followed by age. Resistance to instances of high previous-year August temperatures and high CWD were both tested as potential variables due to their high and consistent correlations with BAI, but neither were found to be significant predictors in the model. The differences in growth rate (Fig. S1.8) found in the model were also clearly seen when comparing overall BAI time series for each elevation-aspect combination (Fig. 1.2), especially at low-elevation sites. The final model did not include either elevation or aspect as being important for overall mortality risk.

BAI-climate models

The fixed effects components of the GLMMs demonstrated that climate influences on growth at each site differed across elevations, and also differed slightly by aspect (Table 1.3, Fig. S1.6). Notably, mortality was only a factor in determining growth at low elevations and tree age was not important in any of the models. Low-elevation models showed significantly higher pre-outbreak growth rates in beetle-killed trees than

surviving trees. All elevations and aspects showed previous-year August maximum temperatures to be important for growth. October maximum temperatures negatively impacted growth for low-elevation sites and south-facing sites across elevations. Annual precipitation positively influenced growth at low elevations and the north-facing mid-elevation sites. CWD had a negative impact on growth at high-elevation sites and at south-facing mid-elevation sites.

Growth difference model

Differences between beetle-killed and surviving tree BAI were explained by CWD, previous-year August maximum temperature, and elevation (Table 1.3, Fig. S1.7). The model results found that beetle-killed trees were typically faster growing than surviving trees, with elevation strongly determining the value of that difference. Low-elevation sites had significantly larger growth differences than mid and high sites, whereas the mid and high site growth difference results were indistinguishable from one another and were not significantly different from 0. The overall difference between beetle-killed and surviving tree BAI decreased with increasing CWD as well as with increasing previous-year August maximum temperature. However, the sites with the largest growth differences also coincided with the highest CWD and August temperature values [Reed et al., 2018].

DISCUSSION

Growth differences across elevations and aspects

We found that beetle-killed trees grew consistently faster than surviving trees in the half century prior to a severe mountain pine beetle outbreak at low-elevation sites, while there were no significant differences in growth rate at the mid- and high-elevation

sites. This finding is consistent with results from some studies on lodgepole, ponderosa, and limber pine from similar locales [Yanchuk et al., 2008; de la Mata et al., 2017], but contrasts with others [Millar et al., 2012; Knapp et al., 2013; Ferrenberg et al., 2014]. Our results provide further evidence that observed differences in growth between beetle-killed and surviving trees vary substantially across host species and climate regions, as well as with stand age and along gradients of bark beetle population densities. Additionally, we found evidence that growth differences vary by elevation, which may explain some of the variation seen in results from previous studies.

There are a number of possibilities as to why we observed faster growth in beetle killed trees. Beetle outbreak pressure may have a strong influence on host selection, with particularly large epidemics having the ability to override the defenses of host trees, regardless of their relative resistance to attack [Boone et al., 2011]. As beetle populations increase in density, host trees that are naturally more resistant (i.e., larger or faster growing) [Christensen et al., 1987] to beetle invasion may become more susceptible than less resistant trees because they provide more resources to beetles [Boone et al., 2011], Similarly, trees with thicker phloem also tend to have higher growth rates [Shrimpton and Thomson, 1985]. As trees with thicker phloem can support more beetles [Amman, 1972; Safranyik and Carroll, 2006], it follows that the faster-growing trees are more likely to be attacked during a severe outbreak. The high stand mortality rates seen in this study ($\tilde{x}$ = 70%) may therefore explain the observed patterns of growth differences [Boone et al., 2011].

Growth differences between surviving and beetle-killed trees appear to diminish with increasing elevation, with significant differences only observed at low-elevation,

more water-limited sites. Growth at low elevations was indeed positively correlated with precipitation (Table 1.3; Table S1.1), demonstrating some control of moisture on growth. This implies that there may be some difference in resource allocation strategy between mortality groups, which is shown best when trees are under high water stress and competing for very limited resources. Specifically, trees that are fast-growing might allocate fewer carbon resources to defenses and therefore suffer more in water-limited conditions, resulting in higher susceptibility to beetle-related mortality. However, stress due to water limitation does not prove that there were differences in allocation strategy between mortality groups. At dry, low-elevation sites, the larger, faster-growing, trees may have simply been more water-stressed than the smaller trees within the plot due to higher water requirements, resulting in their defenses being more easily overcome by the beetles than equivalent trees at higher elevations. Additionally, while climate was related to the magnitude of growth differences at low-elevation sites, resistance to high CWD and late summer temperatures was not a significant predictor of mortality risk in our models as would be expected if trees occupied sites with substantially different microclimates.

While growth differences between mortality categories changed along an elevational gradient, there were no significant differences between aspects. We had expected that the growth differences would be smaller on less water-limited, north-facing aspects, and the lack of significant differences suggests that the changes in climate along an elevational transect are greater than those across aspects. Alternatively, the similarity in results among aspects may be due to the larger range of size classes on north-facing

slopes (Fig. S1.5), with beetles being able to choose larger, faster-growing, trees on north-facing slopes.

Variation in mortality across elevations

Beetle pressure, as measured by stand level mortality, may vary across elevations and can influence growth differences between beetle-killed and surviving trees. Simard et al. [2012] found that beetle-related lodgepole pine mortality increased with elevation in the Greater Yellowstone ecosystem, although this may have been due to increased basal area in stands at higher elevations [Klutsch et al., 2009; Simard et al., 2012]. Conversely, mortality decreased with elevation in a meta-analysis including plots across the mountain pine beetle native range [Björklund and Lindgren, 2009]. This elevational pattern could be explained by a negative correlation between beetle survival and cold winter temperatures [Logan and Powell, 2001; Carroll et al., 2003; Hicke et al., 2006; Björklund and Lindgren, 2009]. We did not find any significant differences in beetle-induced mortality with elevation in our study (Table 1.1), despite decreasing differences in BAI between mortality categories over the elevation range.

One possible explanation for this phenomenon is that the higher elevation trees were older than those at low elevations (Table 1.1; Fig. S1.2). Competition may have been lower in older stands, resulting in decreased competition for resources and more similarity in stress levels among trees within a stand. Additionally, growth at higher elevations was more correlated with late summer temperatures than precipitation (Table S1.1), so high CWD and late summer temperatures may have impacted trees less at higher elevations. Physiological responses to stress may also vary with age [Knapp and

Soulé, 2011], so the older median age of the higher elevation sites may further explain the different climatic responses at those sites relative to low-elevation sites.

Growth-climate relationships and comparisons between mortality categories

Growth of both beetle-killed and surviving trees was influenced by the same climate variables and showed mostly similar correlation strengths. Consistent with results from lodgepole pine in interior British Columbia, low-elevation tree growth was correlated with precipitation, while mid- and high-elevation growth was most strongly correlated with late summer temperatures [Lo et al., 2010]. While beetle-killed trees did have somewhat stronger correlations with climate, the pattern was not consistent. Interactions between mortality and climate variables were insignificant in all growth models, and mortality category only had a significant impact on growth at low elevations. This suggests that both surviving and beetle-killed trees generally respond similarly, but may differ when conditions are stressful to growth as is the case at lower, more water-limited, sites. The model of growth difference magnitude (Table 1.3) supports this theory, as both late summer temperatures and CWD were significant in influencing the low-elevation BAI differences. However, overall, our correlation and model results do not provide substantial evidence that beetle-killed trees are more sensitive to stressful climatic conditions and thus more vulnerable to beetle outbreaks.

Increased allocation towards defenses over growth theoretically should result in increased resistance to stressful climate conditions due to enhanced stored carbon resources. As such, we expected to find interactions between mortality categories and climate variables in the mortality risk and BAI-climate models. Our results were contrary to this expectation, with both beetle-killed and surviving trees showing similar responses

to stressful climate events, according to the models. While unexpected, these results may be in line with Bentz et al., [2015], in which no significant differences in phloem chemistry were found between attacked and non-attacked lodgepole pine in the Greater Yellowstone Ecosystem. In this case, beetles had no apparent selective preference for trees that were less chemically resistant to mountain pine beetles, but rather focused on the larger trees in the study stands [Bentz et al., 2015]. In short, while trade-offs between growth and defense may exist, they may not significantly influence mortality risk during severe pine beetle outbreaks.

Caveats

Trees have varying growth patterns depending on their age [Shrimpton and Thomson, 1985], thus it is possible that tree age may have had some influence on our results. However, no strong patterns emerged for differences in age and age-growth relationships between mortality categories (Table 1.1; Fig. S1.2). While beetle-killed trees were older, the trees had no identifiable trend in growth over the study period and were mature, with a median age of $\tilde{x} = 124$ ($\tilde{x}_{BK} = 125$; $\tilde{x}_{S} = 122$). In short, age may have resulted in a greater size of those trees which died, but those trees also had higher growth rates. Further research controlling for age would be useful in disentangling the two variables. Interestingly, there was no substantial relationship between age and growth rate for this study, and our BAI model results suggest that age did not have a strong influence on growth rate.

Additionally, while faster-growing trees may have greater constitutive defenses [Hood and Sala, 2015; Pinnell, 2016], slower-growing trees may have greater induced defenses [de la Mata et al., 2017]. The trade-off between constitutive and induced

defenses [Moreira et al., 2014] is such that the allocation of resources towards defenses may have differed between mortality categories in a way that we did not measure in this study. This phenomenon could explain why we found growth differences, despite few clear differences in host tree climate-growth relationships, as those conditions would not activate induced defenses.

Management implications

Our results indicate that severe mountain pine beetle outbreaks in lodgepole pine forests may lead to a dominance of slower-growing individuals by way of higher mortality rates among faster-growing individuals. Further work should be done to determine the heritability of growth rate, and whether or not slower growth rate is in fact being selected for during these outbreaks. It should also be noted that the preference of beetles for fast-growing trees, either due to increased size or reduced defenses, runs counter to the aim of many breeding programs which seek high growth. A more moderated program in which increased growth diversity is sought would be beneficial for the resilience of forests to future outbreaks.

CONCLUSIONS

In conclusion, we found differences in growth between beetle-killed and surviving trees, with significant differences seen at low elevations. Models demonstrated that higher growth rates and age increased the probability of mortality during the outbreak, and also that CWD and previous-year August maximum temperatures were related to the magnitude of growth differences between mortality categories. Overall, while there was limited evidence that beetle-killed trees were more susceptible to successful bark beetle attack due to increased climatic stress, the impact was potentially diminished by

differences in growth environment between the trees. It is likely that many of the beetle-killed trees grew more quickly simply due to earlier recruitment, better slope position, or lower resource competition. The extreme pressure of the outbreak may also have partially masked or reversed any natural differences in mountain pine beetle resistance within stands, particularly at more water-limited low elevations where the largest growth differences were observed. Our results do not rule out that some individuals are more or less susceptible to bark beetle attack, but they do not provide strong evidence in that direction. Further work should compare responses to past beetle outbreaks, investigate growth differences following a lower severity beetle outbreak, and investigate genetic differences between beetle-killed and surviving trees.

FIGURES AND TABLES

Figure Legends

Figure 1.1. Study location in Montana, USA. Low elevation plots (-L) are in yellow, mid elevation plots (-M) are in green, and high elevation plots (-H) are in blue. South (S-) and North (N-) aspects are designated by the direction of the arrow symbol.

Figure 1.2. Basal area increment (i.e., BAI) over time on (a) south-facing, and (b) north-facing slopes. Open symbols represent mean annual BAI values of surviving trees and filled symbols represent mean annual BAI values of beetle-killed trees.

Figure 1.1.

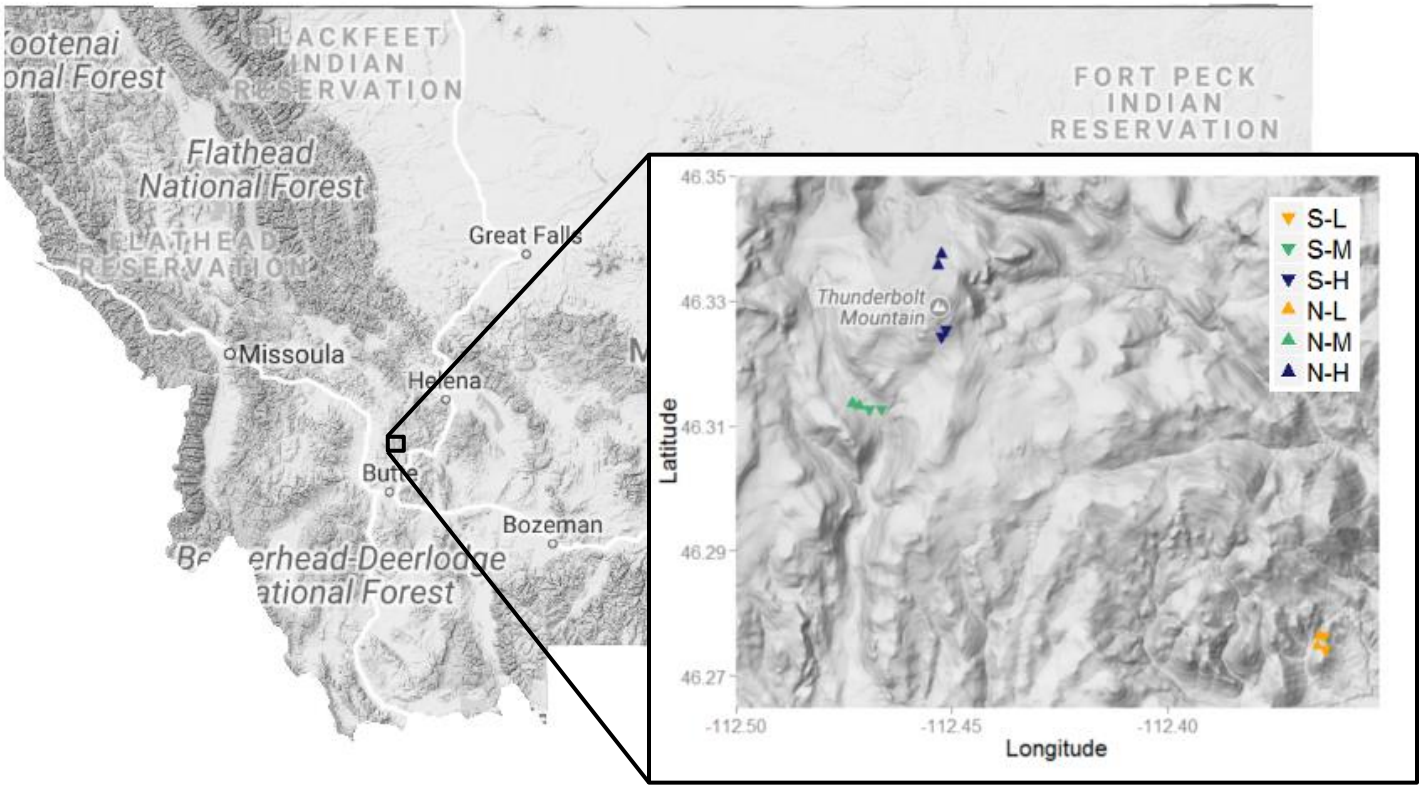
ootenai
onal Forest
BLACKFEET
INDIAN
RESERVATION
FORT PECK
INDIAN
RESERVATION
Flathead
National Forest
FLATHEAD
RESERVATION
Great Falls
Missoula
Helena
Butte
Bozeman
Beaverhead-Deerlodge
National Forest
Thunderbolt
Mountain
S-L
S-M
S-H
N-L
N-M
N-H
46.35
46.33
46.31
46.29
46.27
Latitude
-112.50
-112.45
-112.40
Longitude

Figure 1.2.

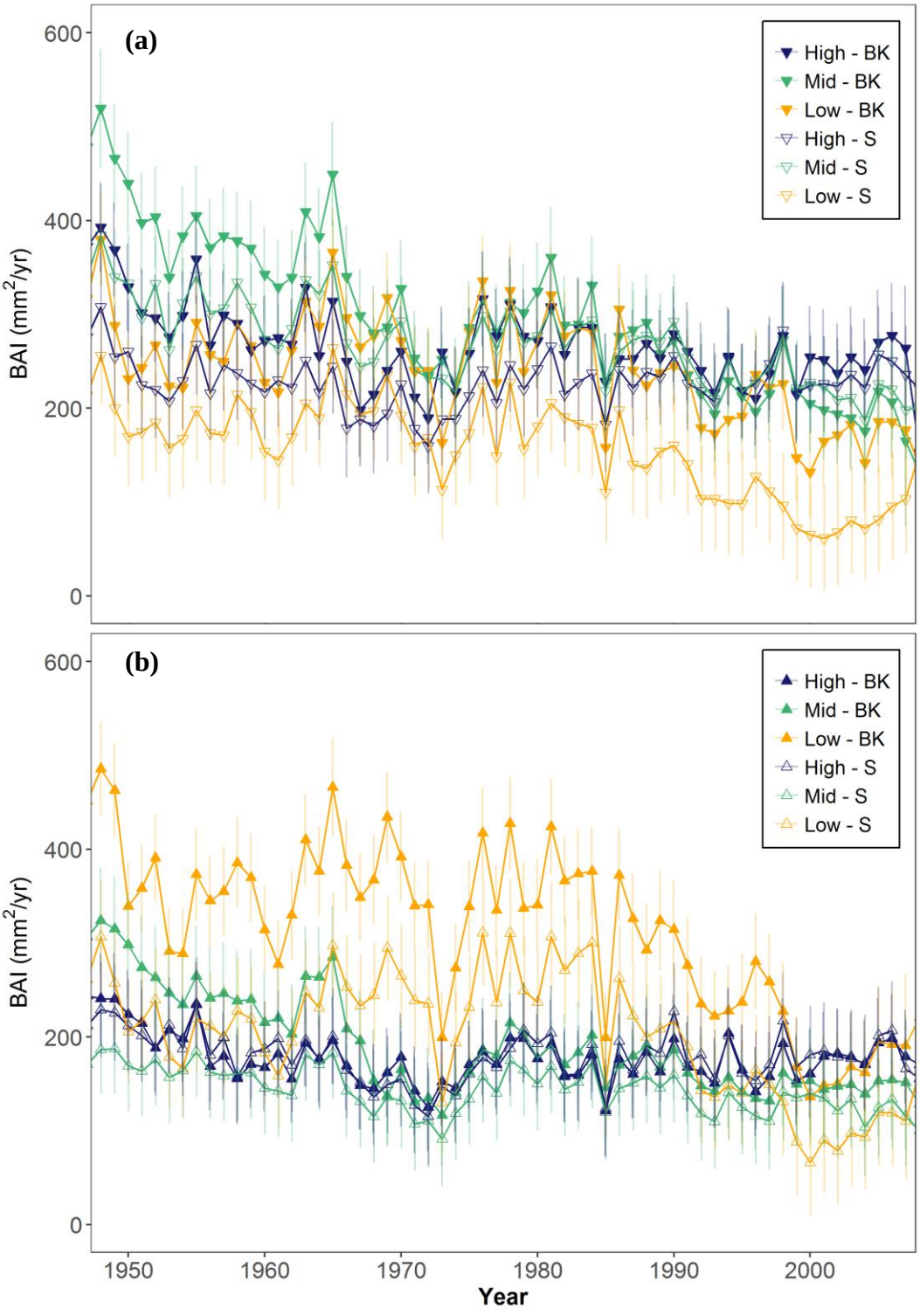
(a)
(b)
High - BK
Mid - BK
Low - BK
High - S
Mid - S
Low - S
BAI (mm²/yr)
0
200
400
600
1950
1960
1970
1980
1990
2000
Year

Tables

Table 1.1. Characteristics of chosen study sites. Plot names are determined by aspect (North/South), elevation (Low/Mid/High), and plot number within the aspect-elevation combination. *n* indicates number of trees sampled. If surviving *n* is higher than the surviving trees within the plot, additional surviving trees were sampled within 1m of the plot boundary. The surviving trees within plot column indicates the total number of surviving trees > 5in DBH in the plot, not just those sampled. Median age represents the age of the trees in 2005, when the outbreak began. The median BAI values were calculated for 1950-2005 with units of mm^2/year. Plot density and percent mortality at each plot were measured in September 2017. All other plot variables were measured in July 2016. Median mortality year was rounded to the nearest year. PICO indicates measurements of lodgepole pine (*Pinus contorta)*.

Plot	Surviving *n*	Beetle-kill *n*	Surviving median age	Beetle-kill median age	Median BAI (S)	Median BAI (BK)	Elevation (m)	Aspect (º)	Slope (º)	PICO Plot Density (trees/m^2)	Total Plot Density (trees/m^2)	% PICO Mortality	Median Mortality Year	Surviving Trees within Plot
SL1	9	10	108	107	145.3	235.4	1873	160	20	0.11	0.12	62	2008	13
SL2	11	13	100	101	136.0	198.0	1859	116	18	0.11	0.13	73	2007	9
NL1	11	12	94	96	214.7	336.4	1861	270	18	0.10	0.11	74	2007	8
NL2	9	9	120	110	137.7	246.6	1854	302	14	0.10	0.13	69	2006	10
SM1	10	10	115	140	226.7	186.2	2132	184	15	0.11	0.12	49	2007	18
SM2	10	10	114	120	285.6	379.1	2152	184	20	0.06	0.06	63	2006	7
NM1	10	8	124	163	139.0	169.4	2152	58	20	0.13	0.14	71	2007	12
NM2	10	11	124	124	129.6	151.0	2173	38	12	0.14	0.15	74	2008	11
SH1	10	10	100	126	205.4	283.5	2505	138	14	0.12	0.13	82	2007	7
SH2	10	10	131	138	189.1	209.8	2481	182	24	0.08	0.09	68	2007	8
NH1	10	11	212	225	154.9	168.3	2504	328	12	0.12	0.12	56	2008	17
NH2	10	10	208	215	160.3	171.8	2482	328	6	0.13	0.15	86	2008	6

Table 1.2. Results of the binomial mixed effects model predicting mortality risk. Coefficient β is the coefficient of the predictor variable, SE(β) is the standard error of that coefficient, *z* is the z-score of the coefficient, and *p* is the p-value of the coefficient. The χ^2 metrics show the significance of each predictor variable by way of comparing the model with and without the variable. Measures of model fit are reported for scaled values of the predictor variables in order to provide more context for their relative influence on mortality risk.

Predictor	*Coef. β*	*SE(β)*	*z*	*p*		χ^2	*df*	p_{χ^2}
Intercept	-0.04	0.14	-0.25	0.8				
Growth Rate (1950-2005)	-0.54	0.15	-3.48	<0.001		13.4	1	<0.001
Age in 2005	-0.29	0.14	-2.03	0.04		4.2	1	0.04

Table 1.3. Model results for BAI-climate relationships and BAI difference-climate relationships. Coefficient β is the coefficient of the predictor variable, SE(β) is the standard error of that coefficient, *z* is the z-score of the coefficient, and *p* is the p-value of the coefficient. The AIC metrics show the AIC of the final model (AIC_{final}) relative to that of a model without a variable (AIC_{drop}). p_L is the p-value for the likelihood that the models are different from one another.

Model	Predictor	Coef. β	SE(β)	t	p	AIC_{final}	df_{final}	AIC_{drop}	df_{drop}	p_L
South Low BAI	*Intercept*	14.74	0.63	23.51	<0.001					
	Mortality (S)	-3.02	0.92	-3.26	0.003	8168.9	9	8176.2	8	0.002
	Previous-year August Tmax	-0.14	0.01	-9.62	<0.001			8257	8	<0.001
	October Tmax	-0.05	0.01	-3.58	<0.001			8179.6	8	<0.001
	Annual Prcp	0.007	0	14.3	<0.001			8361.1	8	<0.001
North Low BAI	*Intercept*	16.76	1.19	14.11	<0.001					
	Mortality (S)	-3.23	1.05	-3.08	0.004	8943.3	9	8949.7	8	0.004
	Previous-year August Tmax	-0.14	0.02	-7.97	<0.001			9003.7	8	<0.001
	October Tmax	-0.05	0.02	-3.22	0.001			8951.7	8	0.001
	Annual Prcp	0.007	0	12.1	<0.001			9082.7	8	<0.001
South Mid BAI	*Intercept*	16.44	1.52	10.82	<0.001					
	Previous-year August Tmax	-0.18	0.01	-14.14	<0.001	7879.2	8	8066.5	7	<0.001
	CWD	-0.002	0	-5.41	<0.001			7906.2	7	<0.001
	October Tmax	-0.07	0.01	-5.74	<0.001			7909.9	7	<0.001
North Mid BAI	*Intercept*	12.3	0.45	27.34	<0.001					
	Previous-year August Tmax	-0.14	0.01	-12.54	<0.001	7066.9	7	7215.3	6	<0.001
	Annual prcp	0.001	0	2.96	0.003			7073.6	6	0.003
South High BAI	*Intercept*	15.42	0.51	30.5	<0.001					
	Previous-year August Tmax	-0.24	0.01	-18.6	<0.001	7671.7	8	7985.5	7	<0.001
	CWD	-0.002	0	-5.54	<0.001			7700.2	7	<0.001
	October Tmax	-0.07	0.01	-6.18	<0.001			7707.5	7	<0.001
North High BAI	*Intercept*	13.35	0.32	41.39	<0.001					
	Previous-year August Tmax	-0.25	0.01	-21.49	<0.001	7327.3	7	7732.8	6	<0.001
	CWD	-0.002	0	-3.84	<0.001			7340	6	<0.001
Growth Difference	*Intercept*	17.57	13.29	1.32	0.19					
	CWD	-0.03	0.01	-4.29	<0.001	5954.28	19	5969.29	18	<0.001
	Previous-year Aug. Tmax	-0.78	0.28	-2.81	0.005			5959.68	18	0.007
	Elevation (Low)	80.91	19.18	4.22	0.002			5961.38	17	0.004
	Elevation (High)	24.27	18.78	1.29	0.23					

SUPPLEMENTARY INFORMATION

Supplemental Figure Legends

Figure S1.1. BAI for entire time series on (a) south-facing, and (b) north-facing slopes.

Figure S1.2. Average age (in 2005) of cored trees. Age was cut off at 2005 because most mortality occurred after 2006. * marks significant differences between mortality categories ($p \leq 0.05$). BK stands for beetle-killed, and S stands for surviving.

Figure S1.3. Average CV of cored trees. * marks significant differences between mortality categories ($p \leq 0.05$). BK stands for beetle-killed, and S stands for surviving.

Figure S1.4. Average year of recruitment of cored trees. * marks significant differences between mortality categories ($p \leq 0.05$). BK stands for beetle-killed, and S stands for surviving.

Figure S1.5. Average DBH of cored trees. * marks significant differences between mortality categories ($p \leq 0.05$). BK stands for beetle-killed, and S stands for surviving.

Figure S1.6. Model fits for all BAI models. (a) South-Low, (b) North-Low, (c) South-Mid, (d) North-Mid, (e) South-High, (f) North-High. The black line in each plot is the model fit, and the red line is the 1-1 line. R^2 and RMSE values are for the fit of the line between predicted and actual values. See table 1.3 in the main text for measures of model fit.

Figure S1.7. Model fit for the BAI difference model. The black line shows the relationship between predicted and actual BAI differences, and the red line is the 1-1 line. R^2 and RMSE values are for the fit of the line between predicted and actual values. See table 1.3 in the main text for measures of model fit.

Figure S1.8. Differences between beetle-killed and surviving tree BAI across aspects and elevations.

Figure S1.1.

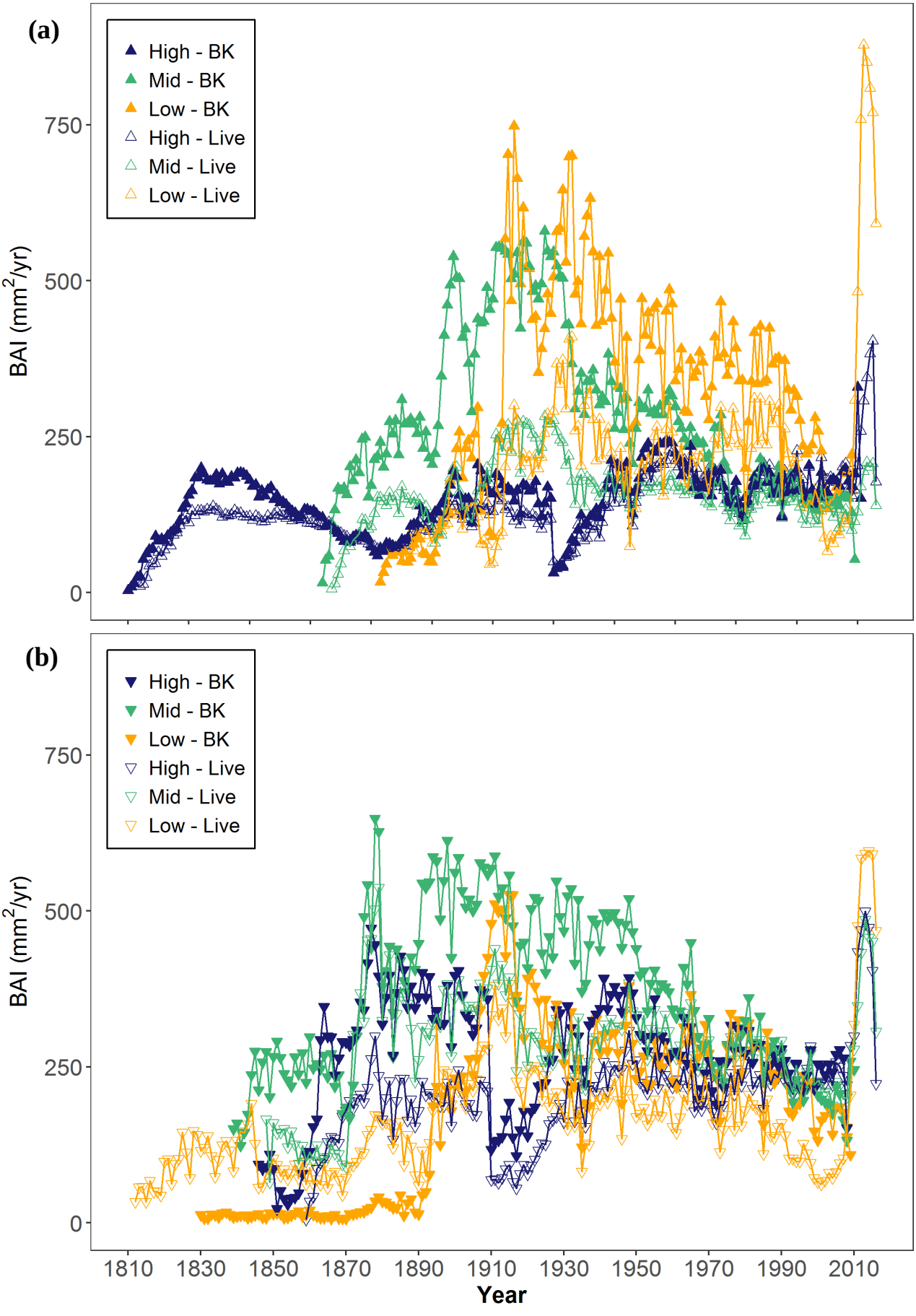
(a)
High - BK
Mid - BK
Low - BK
High - Live
Mid - Live
Low - Live
BAI (mm²/yr)
0
250
500
750
(b)
High - BK
Mid - BK
Low - BK
High - Live
Mid - Live
Low - Live
BAI (mm²/yr)
0
250
500
750
1810
1830
1850
1870
1890
1910
1930
1950
1970
1990
2010
Year

Figure S1.2.

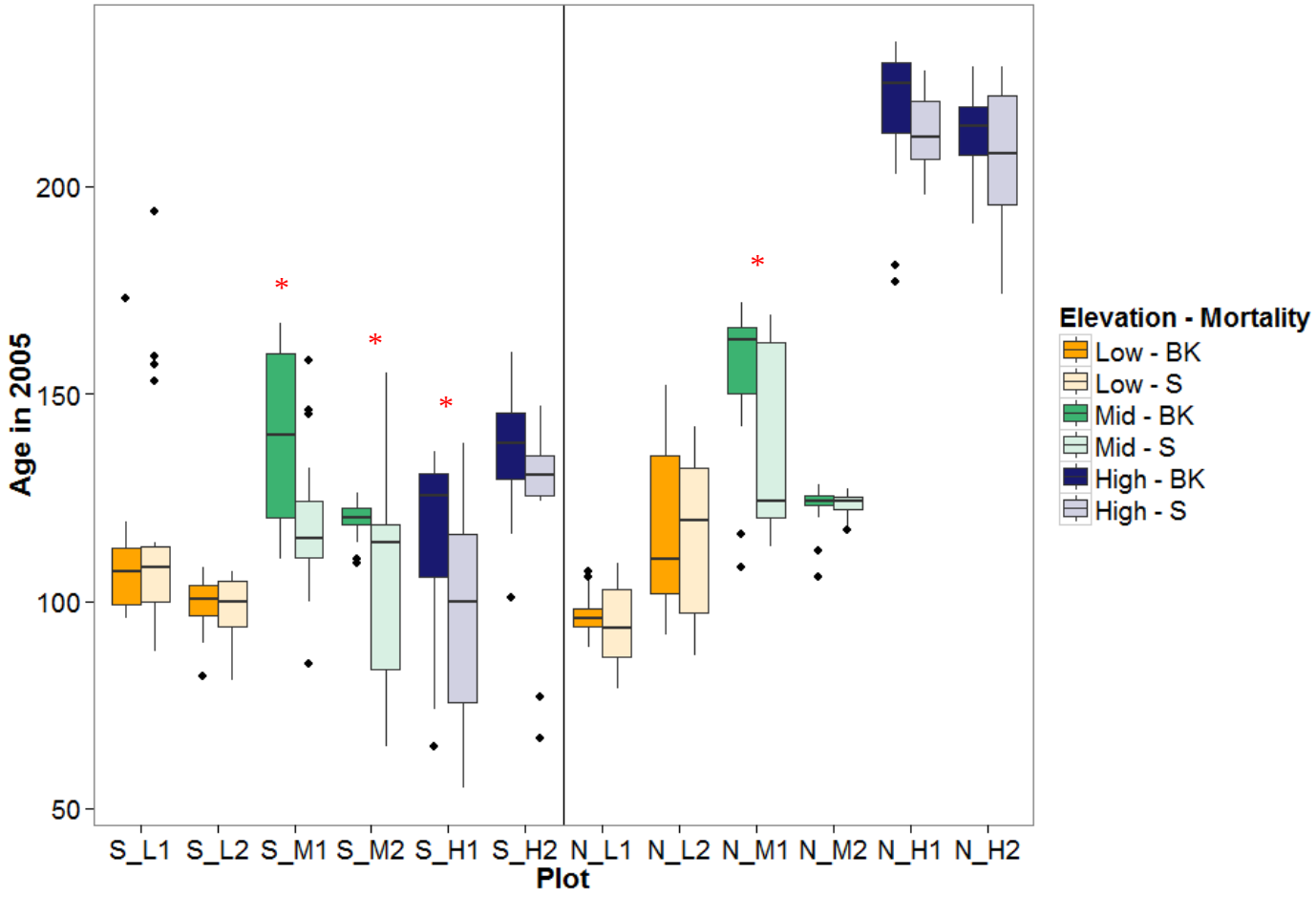
Age in 2005
200
150
100
50
S_L1
S_L2
S_M1
S_M2
S_H1
S_H2
N_L1
N_L2
N_M1
N_M2
N_H1
N_H2
Plot
Elevation - Mortality
Low - BK
Low - S
Mid - BK
Mid - S
High - BK
High - S

Figure S1.3.

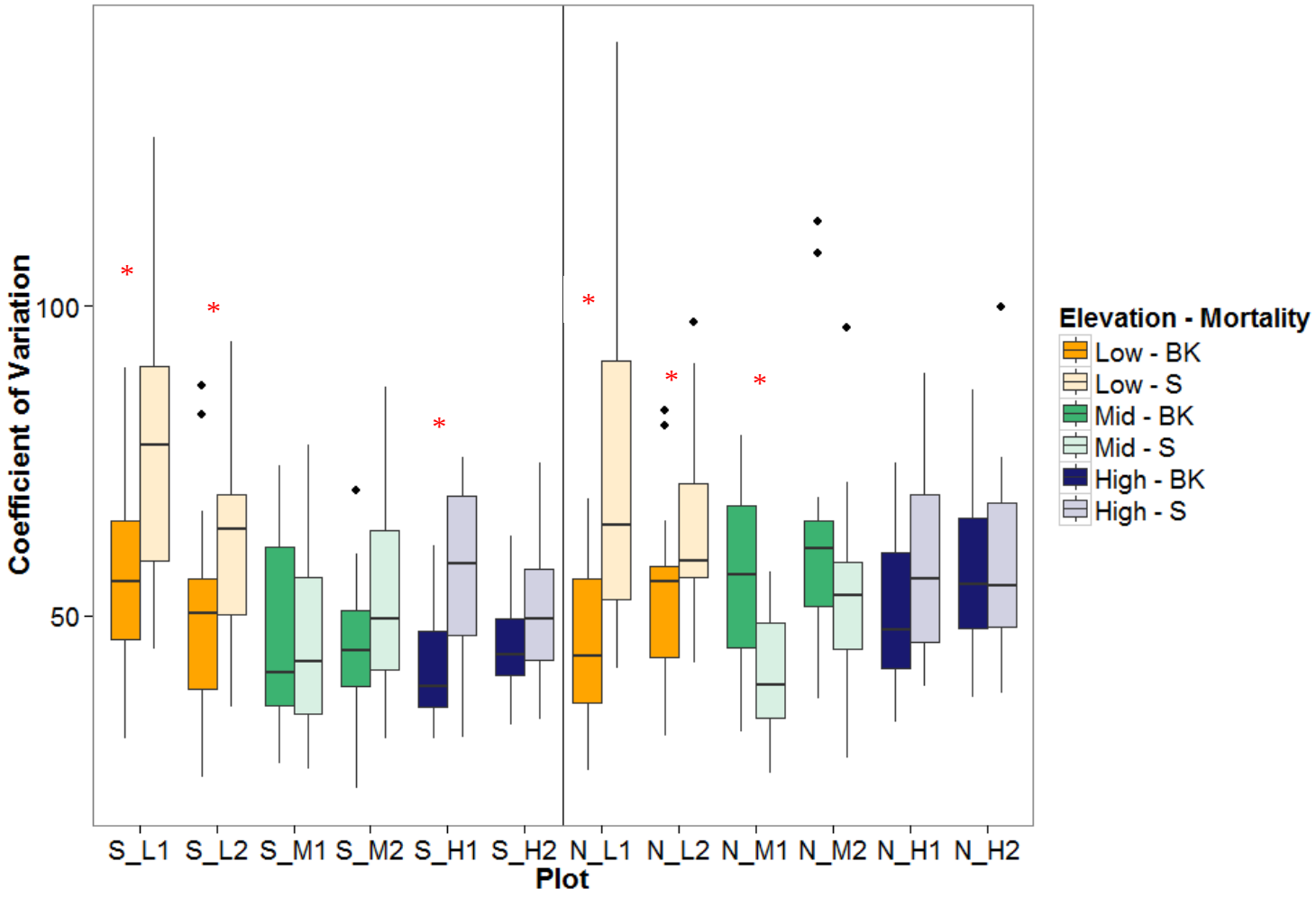
Coefficient of Variation
100
50
S_L1
S_L2
S_M1
S_M2
S_H1
S_H2
N_L1
N_L2
N_M1
N_M2
N_H1
N_H2
Plot
Elevation - Mortality
Low - BK
Low - S
Mid - BK
Mid - S
High - BK
High - S

Figure S1.4.

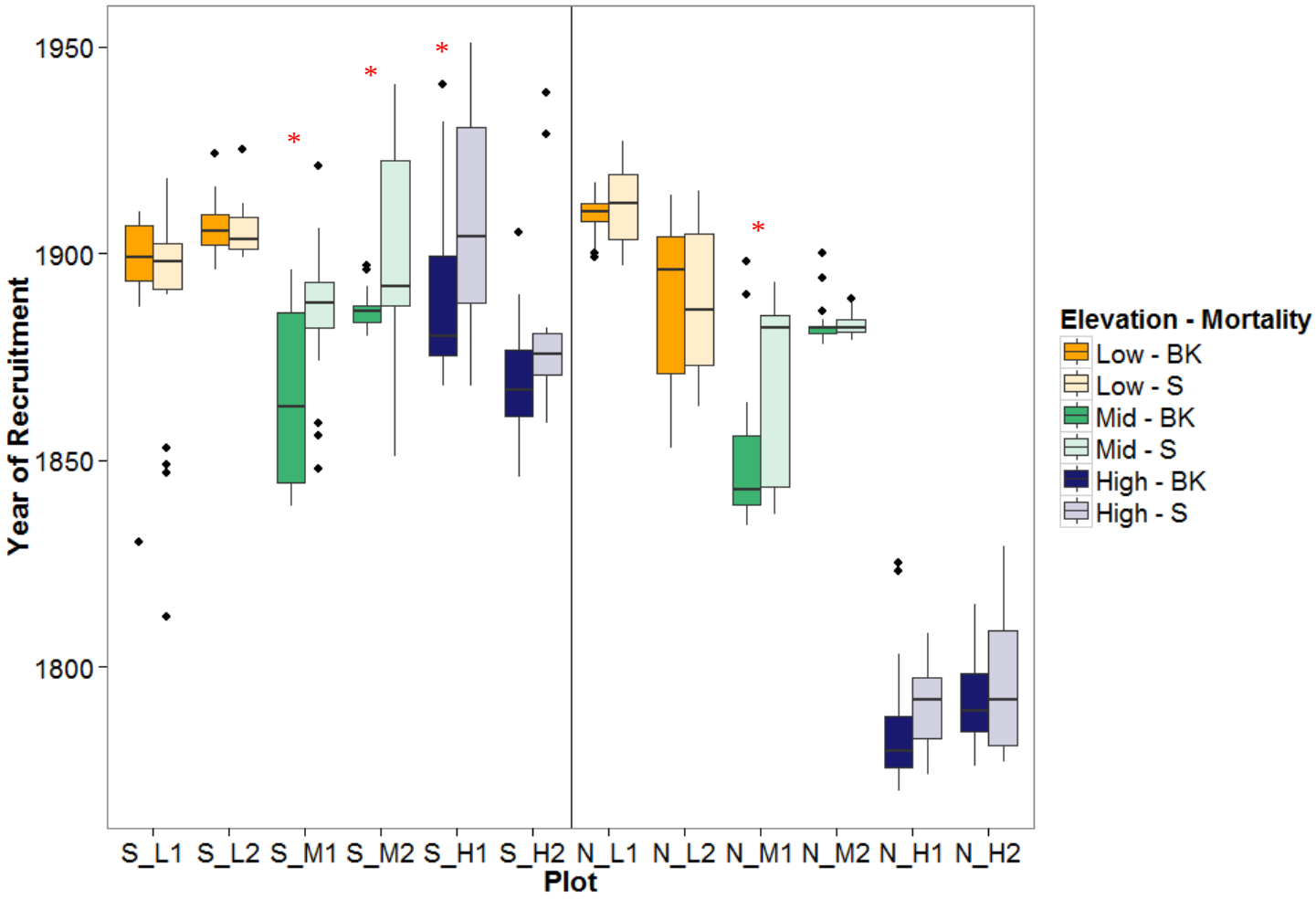
1950
1900
1850
1800
Year of Recruitment
S_L1
S_L2
S_M1
S_M2
S_H1
S_H2
N_L1
N_L2
N_M1
N_M2
N_H1
N_H2
Plot
Elevation - Mortality
Low - BK
Low - S
Mid - BK
Mid - S
High - BK
High - S

Figure S1.5.

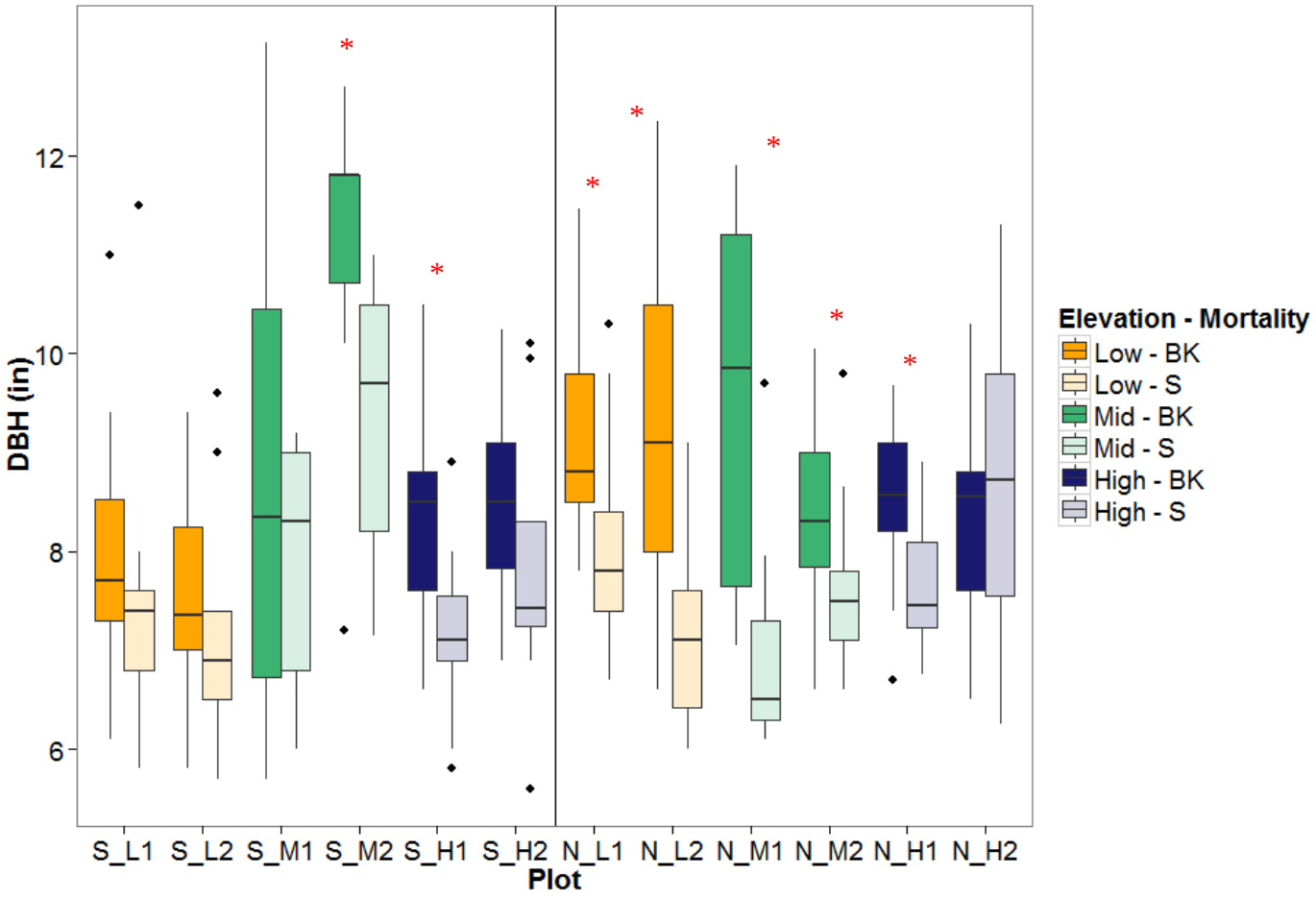
DBH (in)
12
10
8
6
S_L1
S_L2
S_M1
S_M2
S_H1
S_H2
N_L1
N_L2
N_M1
N_M2
N_H1
N_H2
Plot
Elevation - Mortality
Low - BK
Low - S
Mid - BK
Mid - S
High - BK
High - S

Figure S1.6.

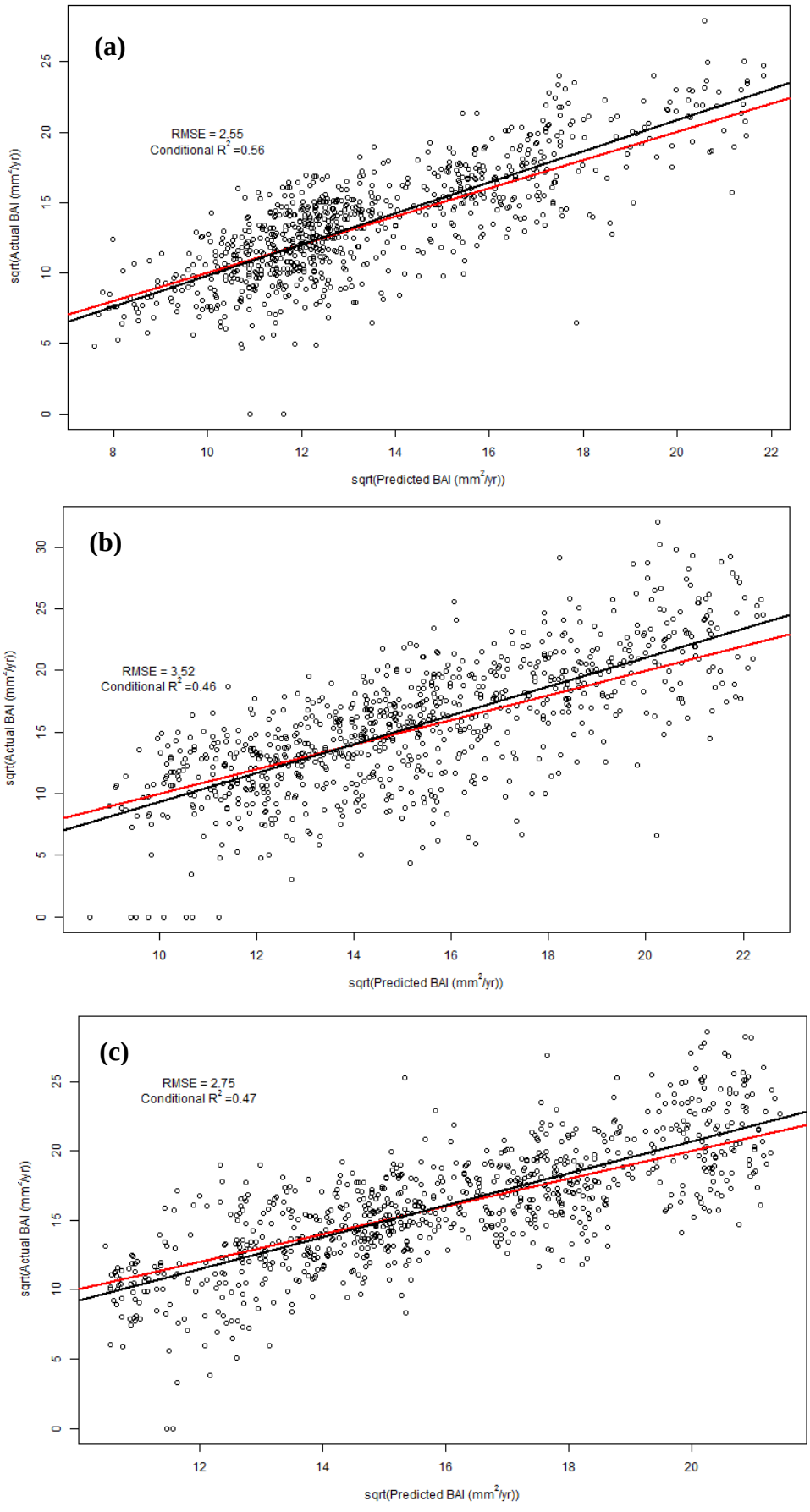
(a)
RMSE = 2.55
Conditional R^2 =0.56
sqrt(Actual BAI (mm^2/yr))
sqrt(Predicted BAI (mm^2/yr))
(b)
RMSE = 3.52
Conditional R^2 =0.46
sqrt(Actual BAI (mm^2/yr))
sqrt(Predicted BAI (mm^2/yr))
(c)
RMSE = 2.75
Conditional R^2 =0.47
sqrt(Actual BAI (mm^2/yr))
sqrt(Predicted BAI (mm^2/yr))

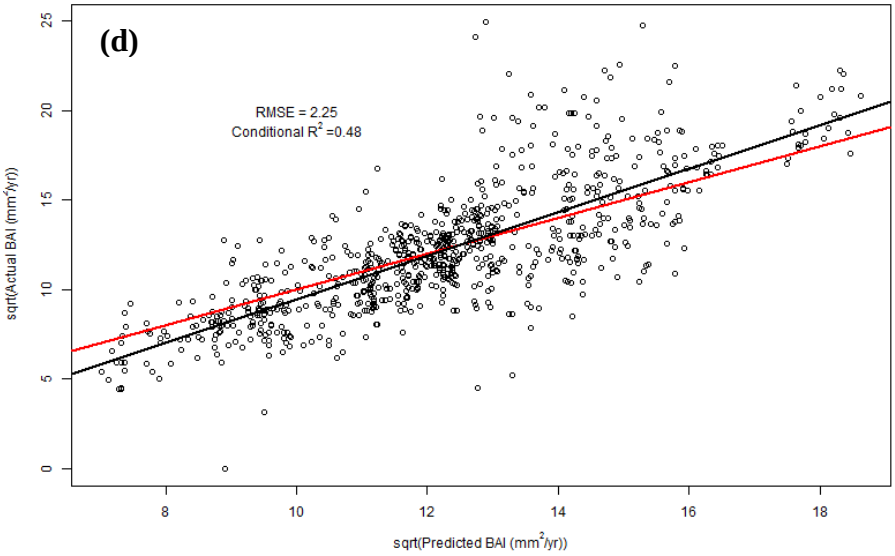
(d)
RMSE = 2.25
Conditional R2 =0.48
sqrt(Actual BAI (mm2/yr))
sqrt(Predicted BAI (mm2/yr))
0
5
10
15
20
25
8
10
12
14
16
18

Figure S1.7.

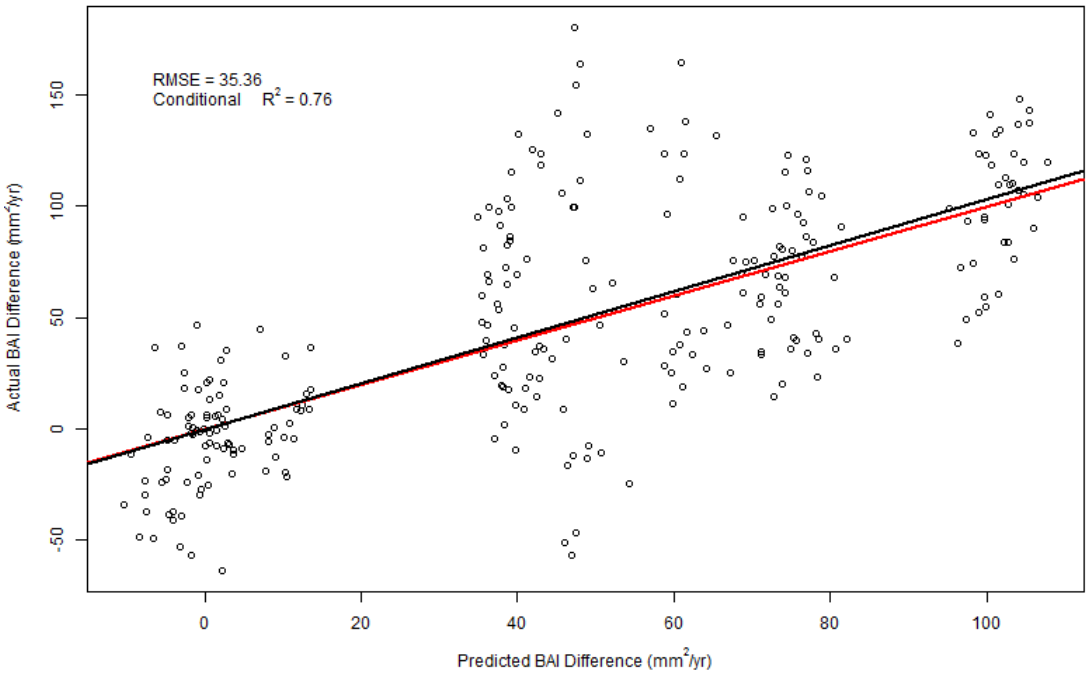
RMSE = 35.36
Conditional R^2 = 0.76
Actual BAI Difference (mm^2/yr)
Predicted BAI Difference (mm^2/yr)
-50
0
50
100
150
0
20
40
60
80
100

Figure S1.8.

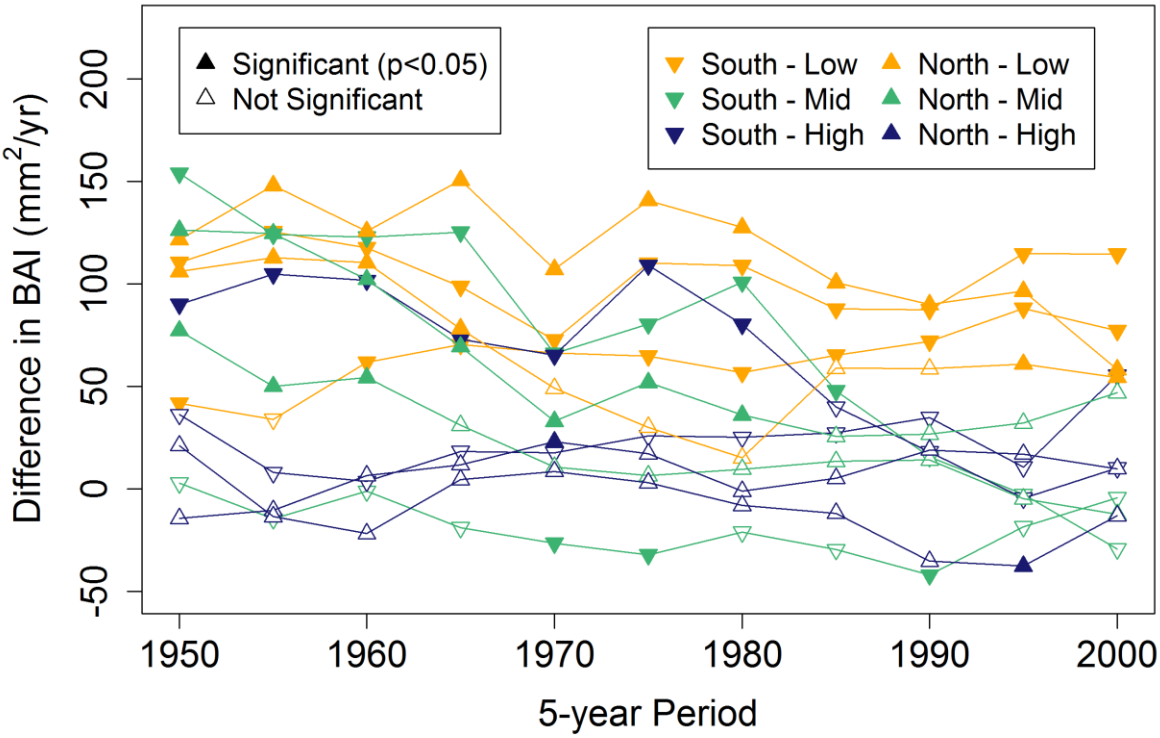
Significant (p<0.05)
Not Significant
South - Low
South - Mid
South - High
North - Low
North - Mid
North - High
Difference in BAI (mm²/yr)
-50
0
50
100
150
200
1950
1960
1970
1980
1990
2000
5-year Period

Supplementary Tables

Table S1.1. Correlations between BAI and climate variables for (a) beetle-killed and (b) surviving trees. Only months with significant results are shown here. Yellow highlighting indicates positively correlated significant variables, and blue highlighting indicates negatively correlated significant variables. Asterisks denote significance level (*: $p \leq 0.05$; **: $p \leq 0.01$).

(a)

Aspect	Climate Variable	Elevation	Previous-Year						Climate-Year				
			Jan	Jun	Jul	Aug	Oct	Dec	Apr	Jun	Jul	Aug	Annual
South	Tmax	Low	-0.03	-0.03	0.06	-0.16	0.18	0.12	0.03	-0.08	-0.06	0.03	
		Mid	-0.15	-0.03	-0.08	**-0.29***	**0.27***	0.15	0.08	-0.09	-0.05	0.03	
		High	**-0.37****	0.03	-0.11	**-0.46****	**0.27***	0.16	-0.05	-0.16	-0.07	0.07	
	Tmin	Low	-0.1	0.01	0.09	-0.2	0.2	0.05	0.08	-0.1	-0.04	0.01	
		Mid	-0.2	0.03	-0.02	-0.18	**0.31***	0.11	0.13	-0.09	-0.01	0.04	
		High	**-0.41****	0.07	0.02	-0.26	0.22	0.14	0.13	-0.1	0	0.06	
	Prcp	Low	0.15	0.06	0.06	-0.1	0.04	-0.06	0.08	0.18	0.11	-0.07	**0.31***
		Mid	0.18	0.11	0.2	0.02	0.02	-0.04	0.11	0.24	0.11	-0.1	0.2
		High	0.2	-0.01	0.25	0.1	-0.11	-0.08	**0.28***	0.23	0.18	-0.07	0.25
	VPD	Low	0.05	-0.03	0.09	-0.06	0.15	0.15	0.02	-0.12	-0.08	0.1	
		Mid	-0.02	-0.08	-0.09	-0.18	0.23	0.2	0.01	-0.1	-0.09	0.15	
		High	**-0.29***	-0.03	-0.13	**-0.37****	**0.35****	0.24	-0.15	-0.18	-0.22	0.13	
	CWD	Low			**-0.14****						**-0.16****		
		Mid			-0.03						-0.01		
		High			**-0.06***						0		
North	Tmax	Low	-0.04	-0.05	-0.01	-0.14	0.1	0.17	0.05	-0.07	-0.07	0.09	
		Mid	-0.06	-0.09	-0.09	**-0.41****	**0.32***	0.18	0.09	-0.05	0.06	0.02	
		High	-0.2	0.04	-0.07	**-0.54****	**0.31***	0.09	-0.02	-0.03	0.07	0.04	
	Tmin	Low	-0.1	-0.01	0.07	-0.18	0.2	0.12	0.07	-0.08	-0.07	0.05	
		Mid	-0.1	-0.04	-0.05	-0.24	**0.39****	0.15	0.16	-0.12	0.04	0.03	
		High	-0.25	0	0.02	-0.25	**0.27***	0.05	0.12	-0.07	0.05	-0.02	
	Prcp	Low	0.19	0.06	0.16	-0.09	0.06	-0.06	0.08	0.18	0.11	-0.08	**0.29***
		Mid	0.03	0.09	0.25	0.05	0.01	-0.05	0.18	0.17	0.07	-0.09	0.18
		High	0.06	-0.05	0.22	0.16	-0.14	0.13	0.24	0.11	0.06	-0.04	0.12
	VPD	Low	0.03	-0.07	0.01	-0.06	0.1	0.18	0.04	-0.12	-0.1	0.13	
		Mid	0.06	-0.08	-0.11	**-0.26***	0.19	**0.28***	0.05	-0.02	0.03	0.2	
		High	-0.19	0.03	-0.09	**-0.38****	**0.31***	0.14	-0.09	0.01	-0.02	0.16	
	CWD	Low			**-0.19****						**-0.21****		
		Mid			-0.01						0.01		
		High			0.03						0.03		

(b)

Aspect	Climate Variable	Elevation	Previous-Year					Current-Year					
			Jan	Jun	Jul	Aug	Oct	Feb	Apr	Jun	Jul	Aug	Annual
South	Tmax	Low	-0.09	-0.01	0.02	-0.26	0.2	-0.03	-0.01	-0.16	-0.1	0.06	
		Mid	-0.08	-0.01	-0.06	-0.23	0.2	0.07	0.05	-0.05	0	-0.01	
		High	-0.15	0.02	-0.08	**-0.48****	**0.29***	0.1	0.07	-0.08	0.01	0.02	
	Tmin	Low	-0.17	0.03	0.12	-0.26	0.24	-0.02	0.05	-0.13	-0.06	0.03	
		Mid	-0.13	0.01	-0.02	-0.16	0.24	0.05	0.09	-0.05	0.01	-0.05	
		High	-0.19	0.01	0.03	-0.22	0.23	0.05	0.19	-0.08	0.09	0.06	
	Prcp	Low	0.17	0.03	0.16	-0.08	0.03	**0.30***	0.11	**0.27***	0.18	-0.1	**0.40****
		Mid	0.09	0.1	0.15	-0.02	0	0.11	0.11	0.17	0.06	-0.12	0.18
		High	0.19	0	0.22	0.19	-0.08	0.02	0.17	0.15	0.14	-0.06	0.17
	VPD	Low	-0.03	-0.04	0.02	-0.16	0.22	-0.05	-0.04	-0.22	-0.19	0.11	
		Mid	0.02	-0.01	-0.02	-0.1	0.15	0.04	0.03	-0.03	0.01	0.1	
		High	-0.02	0.01	-0.06	**-0.35****	**0.34***	0.12	0.05	0	-0.03	0.18	
	CWD	Low			**-0.18****						**-0.22****		
		Mid			-0.05						-0.01		
		High			-0.03						-0.01		
North	Tmax	Low	-0.06	-0.01	0	-0.16	0.13	-0.03	0.07	-0.07	-0.11	0.07	
		Mid	-0.05	-0.02	-0.07	**-0.28***	0.18	0.07	0.04	-0.01	0	-0.08	
		High	-0.2	-0.02	-0.15	**-0.53****	**0.27***	0.09	-0.06	-0.09	0.06	0.07	
	Tmin	Low	-0.14	0.02	0.06	-0.22	0.2	-0.03	0.08	-0.05	-0.1	0.02	
		Mid	-0.08	0	-0.04	-0.17	0.22	0.05	0.09	-0.03	0.01	-0.05	
		High	**-0.27***	-0.03	-0.01	**-0.28***	0.22	0.06	0.05	-0.14	0.08	-0.01	
	Prcp	Low	0.17	0.07	0.14	-0.11	0.08	**0.27***	0.07	0.2	0.13	-0.11	**0.32***
		Mid	0	0.11	0.17	0.03	-0.01	0.1	0.12	0.13	0.08	-0.05	0.18
		High	0.17	0.01	**0.27***	0.17	-0.07	-0.01	**0.28***	0.14	0.11	-0.07	0.18
	VPD	Low	-0.01	-0.06	0.01	-0.06	0.14	-0.05	0.04	-0.13	-0.14	0.11	
		Mid	0.04	0.02	-0.01	-0.1	0.12	0.11	0.05	0.03	0.04	0.07	
		High	-0.15	-0.01	-0.12	**-0.37****	**0.27***	0.14	-0.12	-0.04	-0.06	0.18	
	CWD	Low			**-0.16****						**-0.15****		
		Mid			**-0.08***						0.01		
		High			-0.02						0.04		

CHAPTER 2

Disturbance impacts on land surface temperature and gross primary productivity in the western United States

Corresponding publication:

Cooper, L.A., Ballantyne, A.P., Holden, Z.A. & Landguth, E.L. (2017) Mountain pine beetle attack faster growing lodgepole pine in western Montana, USA, *Journal of Geophysical Research – Biogeosciences 122* (4), 930-946. https://doi.org/10.1002/2016JG003622.

INTRODUCTION

Forests cover roughly 30% of Earth's land surface and provide vital ecosystem services, such as water quality, wildlife habitat, and timber production, as well as climate services [Bonan, 2008]. The ability of forests to continue providing these ecosystem services depends on forest characteristics, such as stand structure, composition, and functional processes. The primary drivers of forest characteristics are state factors including climate, soils, and topography. However, secondary drivers, such as disturbance (e.g., wildfire, insect attack, or windthrow), are often more important than state factors in determining ecosystem services at the regional scale [Law et al., 2003; Pregitzer and Euskirchen, 2004; Bond-Lamberty et al., 2007], influencing stand composition and stand age, as well as C fluxes, nutrient cycling, and energy dynamics. As such, disturbance is an integral process in all forest ecosystems and altered disturbance regimes have the potential to impact forest health globally.

Although disturbance agents such as insect outbreaks and stand-replacing wildfires play a major role in shaping forest ecosystems, global change may be altering disturbance regimes in the United States (US) and elsewhere. Disturbance events affect large swathes of forest in North America every year, with wildfires affecting approximately 760,000 ha/yr [Littell et al., 2009] and insect-induced mortality affecting approximately 100,000 to 1,000,000 ha/yr [Hicke et al., 2012; Meddens et al., 2012]. While disturbance regimes vary in frequency and severity, more severe disturbance

events, such as stand-replacing wildfires and severe bark beetle outbreaks, may be increasing in frequency as global temperatures rise [Watson et al., 1998; Adams et al., 2009; Bentz et al., 2010; Westerling et al., 2011; Hicke et al., 2012; Millar and Stephenson, 2015]. The extent and magnitude to which disturbance has altered certain ecosystem services, including climate regulation, is often regionally specific [Randerson et al., 2006].

Disturbance events vary widely in severity and extent and their ecological impacts are mediated by climate, topography, and pre-disturbance vegetation characteristics [Holden et al., 2009; Dillon et al., 2011]. These impacts can include everything from decreases in stand-level productivity [Hanson and Weltzin, 2000; Kurz et al., 2008] to changes in the radiative budget of the surface [Randerson et al., 2006; Maness et al., 2013]. Many studies have focused on the impacts of disturbance on successional patterns, forest structure, and composition [e.g., Sousa, 1984; Johnson et al., 1998]; however, disturbance effects on local and regional climate are less studied. Therefore, understanding how disturbances of varying severity and frequency impact climate is critical for predicting forest resilience and the recovery of vital ecosystem services.

Disturbance can influence climate in several ways, including altering the radiative budget of forests or by affecting the uptake and release of C by forests. Kurz et al. [2008] estimated that large forested regions of British Columbia (BC), Canada switched from a C sink to a C source following a large and severe mountain pine beetle (MPB) outbreak. The conversion in net C flux was expected to occur over several decades, suggesting that severe biotic disturbances have gradual, but long-term, impacts. These modeled results were supported by an observed 15-20% decline in satellite-derived GPP immediately

post-outbreak [Coops and Wulder, 2010]. Although increased albedo following beetle outbreaks in both BC and the western US results in a decline in absorbed radiation [O'Halloran et al., 2012; Maness et al., 2013; Vanderhoof et al., 2013], a decrease in summertime evapotranspiration (ET) results in an increase in the sensible to latent heat ratio (i.e., Bowen ratio). These effects combined to ultimately result in a ~1 °C increase in surface temperature following the BC outbreak [Maness et al., 2013].

Despite the relatively consistent findings regarding post-MPB outbreak C fluxes, these studies focused on an area with a very large and severe insect outbreak; results may differ when outbreaks occur on smaller scales or under different environmental conditions. For example, the effects of less severe disturbance and mortality events, such as smaller-scale insect outbreaks and drought, are more ambiguous than the results from the MPB outbreak in BC. Hanson and Weltzin [2000] determined that the likely effects of drought are reductions in net primary production and stand water use, both phenomena resulting in positive radiative forcing (i.e., an atmospheric warming effect). However, changes in albedo or heterotrophic respiration were not included in the analysis, making it difficult to assess the net radiative forcing resulting from smaller and less severe disturbances such as drought. Thus, the exact climate effects of these disturbances are unclear and likely depend on the extent and severity of the event as well as the environmental characteristics of the forest ecosystem (e.g., vegetation type).

Wildfire also appears to have a large effect on the net radiative forcing of ecosystems [Randerson et al., 2006], although the effect is not well understood across different forest ecosystems. Fires in boreal Alaska were found to have differing impacts on climate depending on the time since disturbance [Randerson et al., 2006]. Initially,

observations showed that fires resulted in positive radiative forcing due to large C emissions and the deposition of black C on ice and snow, decreasing the albedo of the surface and increasing absorbed radiation. However, according to model simulations, after several decades, boreal forest fires resulted in a net negative radiative forcing due to increases in surface albedo as a result of decreased canopy cover, ultimately leading to a potential cooling of the land surface. This is one of the few studies to develop a physical framework to evaluate the net radiative impacts of the effects of forest disturbance, but it only addressed a relatively small forested site and a single fire event.

Another study [O'Halloran et al., 2012] addressed the radiative impacts of fire, bark beetle attack, and hurricanes due to changes in albedo and the net ecosystem carbon balance over several locations across North America. The authors found results similar to those of Randerson et al. [2006] for boreal wildfire, with an initial warming effect, followed several decades later by a slight cooling effect. However, they found that bark beetle attack increased wintertime albedo, resulting in negative radiative forcing. This complicates the longer-term results of Kurz et al. [2008], which suggest positive radiative forcing from bark beetle attack over many decades. These results demonstrate differences in climate impacts among disturbances and disturbance locations and highlight the need for systematic analyses across larger areas.

Several other studies have addressed the potential for disturbances to impact climate in temperate regions through both biogeochemical [Hanson and Weltzin, 2000; Kurz et al., 2008; Hicke et al., 2012; Seidl et al., 2014] and biogeophysical [Vanderhoof et al., 2013; Maness et al., 2013] effects, with results indicating that temperate disturbances may generally result in a long-term net positive radiative forcing, although

the forcing depends on disturbance location, timing, type, and severity. The continued complexity of disturbance-related climate forcing in forest ecosystems indicates that an analysis evaluating the patterns of effects of multiple disturbance types on local to regional climate across multiple ecosystems is a novel contribution to the field. There is a general consensus that forests will become more vulnerable to disturbance as a result of increasing water and heat stress [Allen et al., 2010; Heyder et al., 2011; Anderegg et al., 2013], but in order to better manage for forest resilience to climate change it is also necessary to understand the effects of forest disturbances on local- to regional-scale climate.

The aim of this study is to determine the impact of fires, bark beetles, defoliators, and 'unidentified disturbances' (UD) on land surface temperature (LST) and gross primary productivity (GPP) in the western US from 2002 – 2012. Specifically, our analysis seeks to answer the following research questions: (1) How do LST and GPP change immediately following disturbance in forests of the western US?, (2) How do these short-term effects differ among ecoregions and disturbance types?, (3) How important are severity, extent, and interannual air temperature change to the short-term disturbance response of LST and GPP?, and (4) How do LST and GPP change over twelve years following disturbance? This study adds to the literature through an analysis of disturbance effects across ecoregions and four disturbance categories. It covers a large geographical region and provides a summary of the relative importance of disturbances of varying types and locations on local- to regional-scale climate.

METHODS

Study area

We assessed the impacts of disturbance over the western US (Fig. 2.1a), a region encompassing substantial topographic and climatic variation. Mean annual temperatures range from -3 ºC in the intermountain West to 24 ºC in the Southwest [PRISM Climate Group, 2011] and mean annual precipitation ranges from 5925 mm in the Pacific Northwest to 62 mm in the desert Southwest [PRISM Climate Group, 2011].

A range of disturbances are known to impact western forests, including prescribed and wildland fires, insects and pathogens, windthrow, and timber harvest. Substantial efforts to map wildfires and insect-induced mortality have resulted in spatially explicit annual maps of these disturbance types. We therefore focus primarily on these disturbance types, and classify all other forms of disturbance as UD. Furthermore, as our disturbance detection approach was limited to detecting only disturbances affecting moderately large areas of the landscape, insect species included in the insect damage categories were limited to species of aggressive bark beetles and defoliators [see Hicke et al., 2012; USDA Forest Service, 2000-2014]. Bark beetle species included mountain pine beetle (*Dendroctonus ponderosae*), western pine beetle (*Dendroctonus brevicomis*), and species of ips (*Ips sp.*). Defoliators included western spruce budworm (*Choristoneura occidentalis*), western blackheaded budworm (*Acleris gloverana*), western hemlock looper (*Lambdina fiscellaris spp. lugubrosa*), pine needlesheath miner (*Zelleria haimbachi*), sawflies (Suborder *Symphyta*), tent caterpillars (*Malacosoma sp.*), and douglas-fir tussock moth (*Orygia pseudostugata*).

Disturbance detection and grouping by disturbance and ecoregion

Disturbances were mapped using a combination of satellite imagery and aerial data sources, including Moderate Resolution Imaging Spectroradiometer (MODIS)

Enhanced Vegetation Index (EVI) time series imagery [http://lpdaac.usgs.gov], Monitoring Trends in Burn Severity (MTBS) data [Eidenshink et al., 2007], and Aerial Detection Survey (ADS) maps [USDA Forest Service, 2000-2014]. EVI time series data for 2000-2014 were accessed between July and September 2014. These data are available at 250 m resolution and are collected via the Terra satellite every 16 days. EVI was used rather than the Normalized Difference Vegetation Index (NDVI) because it is less susceptible to saturation in dense canopies [Liu and Huete, 1995]. The index is calculated as:

$$EVI = G \times \frac{(\rho_{nir} - \rho_{red})}{(L + \rho_{nir} + C_1\rho_{red} + C_2\rho_{blue})} \quad (1)$$

where G is the gain factor, ρ_{nir} and ρ_{red} are atmospherically corrected surface reflectances, L is the canopy background adjustment term, and C_1 and C_2 are coefficients for the aerosol resistance term [Huete et al., 2002]. While the blue band used for correcting residual atmospheric effects ($C_2\rho_{blue}$) is only available at 500 m rather than 250 m, this should have negligible impacts on results [lpdaac.usgs.gov].

Raw EVI images were pre-processed for quality assurance, and pixels determined to be either cloudy or unreliable due to satellite measurement abnormalities were removed. Images were further processed to remove non-forested pixels according to a 20% forest mask created from the 250 m resolution MODIS Vegetation Continuous Fields product [DiMiceli et al., 2011; Townshend et al., 2011]. Forested images were then mosaicked to cover the western US and run through a pre-processing algorithm to remove outliers and replace missing values by interpolation, using the 'interpts' function in the 'wq' package [Jassby and Cloern, 2015] in R [R Core Team, 2013], resulting in spatially and temporally continuous time series of EVI values. Outliers were determined

as values lying outside of 150% of the first or third quartiles of the EVI value distribution. Because the time series were evaluated for change at the pixel level, we were further able to selectively remove pixels where: (a) more than one quarter of the total measurement days were missing, or (b) more than 20 consecutive measurement days were missing.

We then used the Breaks for Additive Season and Trend (BFAST) change-detection algorithm [Verbesselt et al., 2010a, 2010b] to determine areas of likely disturbance between 2002 and 2012 at the pixel level (i.e., 250 m). The BFAST algorithm decomposes time series into seasonal, trend, and noise components, and then compares slopes of trend segments iteratively to find breakpoints [Verbesselt et al., 2010a, 2010b]. We used the BFAST algorithm with a harmonic seasonal component and a single allowable breakpoint. With a single breakpoint, only one year per pixel could show disturbance, resulting in the pixel disturbance being the largest break in the time series (if breaks were detected) and thus the most severe disturbance in that pixel. BFAST could not detect disturbance 2000-2001 and 2013-2014 due to lead-in requirements within the algorithm. Pixels with significant detected decreases in the EVI time series were labeled with the year of change and compiled into annual raster files.

In an effort to improve the detection of disturbed pixels in cloud- and snow-contaminated areas, we augmented the BFAST results with data on forest loss from Hansen et al. [2013]. The Hansen data were originally computed annually at 30 m resolution using Landsat imagery, thus increasing the likelihood of catching a cloud-free segment of the landscape. For this analysis, these 30 m data were aggregated to 240 m resolution to approximate the resolution of the MODIS data. The coarser resolution forest

loss files were then placed onto a grid equivalent in resolution and extent to the BFAST results grid, with Hansen raster values added to the nearest BFAST-equivalent grid pixels. Once equivalent grids were achieved, the Hansen and BFAST detection rasters were mosaicked to a final disturbance raster, with disturbances marked if they were shown on either of the two detection rasters (Fig. 2.1b). Data from Hansen et al. [2013] were prepared and downloaded from Google Earth Engine [see Hansen et al., 2013] in August 2015. Raster files were mosaicked in ArcGIS [ESRI, 2010].

The combined disturbance data were split into four distinct disturbance type categories - (1) fire, (2) bark beetles, (3) defoliators, and (4) UD. Fire disturbance pixels were identified as pixels where the combined disturbance data for a given year overlapped MTBS fire polygons for that same year. Insect disturbance pixels, including bark beetles and defoliators, were determined as pixels where the combined disturbance data for a given year overlapped the ADS polygons labeled as bark beetle or defoliator mortality for any year between 2002 and 2012. Insect damage may only reach an EVI-detectable severity after several years, although the outbreak may be detected in the ADS maps at the very start of the outbreak. Alternatively, ADS data may mark the disturbance after it is detected by satellite methods. Thus, it was assumed that if the pixel was within the bounds of the ADS polygon, it was most likely an insect damage pixel. This assumption was not made for fires because all damage occurs within a single year, allowing for much more accurate identification and timing. Where fire and insect damage polygons overlapped, the pixel was labeled ‘fire’ if the detection year matched the year of the fire, and labeled ‘bark beetle’ or ‘defoliator’ if the detection year did not match the

year of the fire. The UD category was applied to all other pixels that did not fall under the previous categories.

MTBS and ADS presence or absence values were extracted at disturbance detection points in ArcGIS [ESRI, 2010] in order to indicate the mode of disturbance for that pixel. ADS polygons were limited to those containing damage attributed to the bark beetle and defoliator species listed in section 2.1. We chose not to use a cut-off for trees killed per acre within ADS polygons, as mortality area is patchy within the affected area polygons, making polygon-level trees killed per acre unrepresentative of all pixels within each polygon.

Lastly, results were evaluated by ecoregions as defined by the Environmental Protection Agency's Level II ecological region product [Omernik, 1987; Omernik and Griffith, 2014]. Data were grouped into ecoregions according strictly to the level II regions at first, and then regions with fewer than fifty detected disturbance pixels were combined with the ecoregion nearest to them in both location and vegetation type (Fig. 2.1a).

Detection results were evaluated for accuracy using two methods, (1) evaluation relative to ADS [USDA Forest Service, 2000-2014] and MTBS polygons [Eidenshink et al., 2007], and (2) comparison with 2002-2010 detection results from the well-validated Vegetation Change Tracker (VCT) project [Huang et al., 2010; Zhao et al., 2015]. The first method indicated mixed results for the number of ADS and MTBS polygons that were detected by the combined BFAST and Hansen dataset (Table S2.3). For example, ADS bark beetle polygons were often undetected, but most MTBS polygons were detected. Those polygons that were not detected by the dataset tended to be smaller and

had lower recorded severity (Table S2.3). The second validation method demonstrated similar overlap between VCT detected pixels and ADS and MTBS polygons as method 1, suggesting general agreement between VCT and the dataset used here in detecting disturbance (Table S2.3). Additionally, an examination of the distances between BFAST/Hansen points and VCT points indicated similarities in areas of detection (Fig. S2.9, Table S2.4). The detection areas that did not match were primarily in UD areas.

Response and predictor variable preparation

Mean summertime (June-July-August; JJA) Landsat-based 30 m LST data were prepared in Google Earth Engine in August 2015 using methods described in Weng et al. [2004] and Sobrino et al. [2004]. In short, this method for estimating LST uses an estimated land surface emissivity based on NDVI [Sobrino et al., 2004] as input into the equation

$$LST = \frac{T_B}{1+\left(\lambda \times \frac{T_B}{\rho}\right)} \ln \varepsilon \quad (2)$$

where T_B is the effective at-satellite temperature (K), λ is the wavelength of emitted radiance (μm), ε is NDVI-based emissivity, and $\rho = h \times {}^{c}/_{\sigma}$, with h equal to Planck's constant (J·s), c equal to the speed of light ($m \cdot s^{-1}$), and σ equal to the Boltzmann constant ($J \cdot K^{-1}$) [Weng et al., 2004]. The resulting product was aggregated to 240 m to better match the detection data. Landsat data are available from the U.S. Geological Survey.

Changes in GPP were estimated using the 1 km, 8-day, MOD17A2 GPP product. Data were downloaded via the Land Processes Distributed Active Archive Center (LP DAAC) in September 2015 and pixels flagged as low quality were removed.

Factors (i.e., predictor variables) potentially influencing the disturbance response variables included disturbance severity (*S*), extent (*E*), and local interannual change in air

temperature (T_{air}). *S* was determined as the per-pixel change in pre- to post-disturbance EVI (see Eq. (5) and (6)). The *E* of fire disturbance events was labeled as the total acres burned, retrieved from the MTBS fire polygon data. Each fire pixel was labeled with the total area of the fire. The *E* of bark beetle, defoliator, and UD events was estimated as the size of the area covered by adjoining pixels detected in the same year. The calculation of area for insect and UD disturbances was done in ArcGIS [ESRI, 2010]. We chose to label each pixel with the area of the total disturbance (encompassing several pixels), because we were interested in how disturbance in surrounding pixels influences the effects within single pixels. For example, a large fire may cause a larger increase in LST in some pixels because surrounding pixels no longer have surviving vegetation, and thus higher ET, to mitigate that pixel's rising LST.

PRISM monthly 800 m temperature data [PRISM Climate Group, 2011] averaged for JJA were used to represent local air temperatures, for use in determining how the disturbance response results were influenced by non-disturbance-related differences in temperature. T_{air} was calculated as the pre- to post-disturbance change in the variable (see Eq. (5) and (6)). Data were downloaded from the PRISM website in October 2015.
It should be noted that the aim of this analysis was not to identify the drivers of fires, bark beetle outbreaks, or defoliator attacks, but rather to identify what disturbance or environmental factors have the strongest influences on the responses of LST and GPP following disturbance. Many other studies have identified the drivers of disturbance [e.g., Raffa et al., 2008; Dillon et al., 2011; Westerling et al., 2011].

Analysis of disturbance-related changes in LST and GPP

The LST difference and GPP percent change following the disturbance were calculated at the pixel level. Only changes in the JJA values of the variable were analyzed for this study. Values for each variable before (V_{pre}) and after (V_{post}) the detected disturbance were calculated as follows:

$$V_{pre} = \frac{(V_{t-1}+V_{t-2})}{2} \quad (3)$$

$$V_{post} = \frac{(V_t+V_{t+1})}{2} \quad (4)$$

where V_t is the variable at t years before or after the detected disturbance. We then calculated the absolute (ΔV) and percent change ($\%\,\Delta V$) in each variable as:

$$\Delta V = V_{post} - V_{pre} \quad (5)$$

$$\%\Delta V = \left(\frac{V_{post} - V_{pre}}{V_{pre}}\right) \times 100 \quad (6)$$

All calculations were completed in R [*R Core Team*, 2013].

Statistical analysis

After response variables were extracted at each detected disturbance point, differences in disturbance effects between ecoregions and disturbance types were examined. The significance of the differences between both ecoregions and disturbance types were determined using multivariate analysis of variance (MANOVA) tests. If significant differences in disturbance response variables (LST, GPP) were found, discriminant function analysis was conducted to determine the ability of the response variables to predict the type of disturbance that caused the response and the ecoregion in which the disturbance occurred. MANOVA tests were conducted in R [R Core Team, 2013]. Discriminant function analysis was also done in R using the 'lda' function in the 'MASS' package [Venables and Ripley, 2002].

To analyze the influence of the potential drivers of disturbance impacts, regression trees were created using the 'randomForest' function within the 'randomForest' package [Liaw and Wiener, 2002] in R. One model was created for each response variable (i.e., LST, GPP), resulting in two total models. The importance *S*, *E*, and T_{air} to the response variables was identified by mean squared error (MSE) importance values from the random forest models. Ecoregion and disturbance type were also included in the models as potential driving factors (Table 2.1).

To determine how the disturbance responses of LST and GPP change through time, data were collected for all years following disturbance events through 2014. Pre- to post-disturbance changes in LST and GPP were used to identify the patterns in recovery following disturbances segregated by four severity classes (0-20%, 21-40%, 41-60%, and > 60%), with percent decline in EVI used as a proxy for severity (Fig. S2.10). Recovery data were prepared with the same methods used to calculate initial disturbance response (Eq. (5) and Eq. (6)), with V_{post} representing only one year rather than the average of two years. Line graphs of recovery were analyzed by time to stabilization and compared by disturbance type, ecoregion, and severity category. The time period of the analysis (2002-2012) was insufficient to see full recovery following disturbance. However, "stabilization," or leveling in the response variables following the disturbance, may result due to other factors, including regrowth of non-canopy vegetation. This stabilization, if seen, indicated some degree of recovery and is used here as an indication of future trends in recovery.

RESULTS

Changes in LST and GPP in response to disturbance

Fire

We observed a significant increase in LST and a decline in GPP following fire events (Fig. 2.2; Table S2.2). The mean LST increase (°C) was 3.45 ± 3.02 (μ ± σ) over all regions (Fig. 2.2a), although there was considerable interregional variation (Fig. 2.3). Cold Deserts experienced the largest increases in LST (4.57 ± 3.45) while the Marine West Coast Forests experienced the smallest increases (1.10 ± 1.98). Fires also resulted in significant declines in GPP (Fig. 2.2b). Across all regions, the mean GPP percent change was -25.05 ± 21.67. The fire effect on GPP varied significantly by ecoregion (Fig. 2.3). The largest declines in GPP were seen in the Warm Deserts (-41.49 ± 23.81) and the smallest declines were observed in Marine West Coast Forests (-4.72 ± 11.38).

Bark Beetles

Following bark beetle outbreaks, LST generally increased, and response of GPP was variable across ecoregions (Fig. 2.2; Table S2.2). All but two regions, the Sierra Madre and Temperate/West Central Semi-Arid Prairies, showed increases in LST following bark beetle outbreaks (Fig. 2.2a). The mean impact of bark beetles on LST (°C) was 0.76 ± 3.04. The largest increase in LST was seen in the Western Cordillera (0.92 ± 3.00) and the smallest increase was seen in Warm Deserts (0.01 ± 0.87). Bark beetle disturbance occurring in Sierra Madre and Temperate/West Central Semi-Arid Prairies resulted in slight decreases in LST (-0.05 ± 3.13; -0.18 ± 2.89). The mean impact of bark beetle outbreaks was a percent change in GPP of -2.84 ± 21.06, although seven of the nine ecoregions showed a slight increase in GPP (Fig. 2.3). The greatest increase in GPP occurred in Warm Deserts (29.86 ± 37.09), although there were also increases in the Cold Deserts, Sierra Madre, Upper Gila Mountains, Marine West Coast Forests, and all Semi-

Arid Prairies. GPP decreased post-disturbance in Mediterranean California and the Western Cordillera (-1.02 ± 17.01; -4.43 ± 13.80).

Defoliators

Overall, LST increased slightly and GPP decreased slightly following defoliator attacks (Fig. 2.2, Table S2.2). The average LST effect over all regions was 0.49 ± 3.12 °C, with four ecoregions showing increases in LST and two ecoregions showing decreases. An additional three ecoregions had no data. The largest increases in LST following defoliator attack occurred in Cold Deserts (2.68 ± 3.00). The Sierra Madre and Upper Gila Mountain ecoregions showed decreases in LST (-0.56 ± 2.12; -0.48 ± 2.94). The overall defoliator effect on GPP (%) was very small (-0.23 ± 15.40), with substantial variation between ecoregions. The Upper Gila Mountain ecoregion showed large increases in GPP following defoliator attacks (9.68 ± 27.91), while Mediterranean CA showed moderate GPP declines (-4.51 ± 10.97).

Unidentified Disturbance

In general, LST and GPP increased following UDs (Fig. 2.2; Table S2.2). The mean LST effect (0.76 ± 3.03 °C) and regional variability were very similar to the patterns following insect outbreaks (Fig. 2.2). The ecoregion with the largest increase in LST was the Marine West Coast Forest ecoregion (1.48 ± 3.24). LST decreased in the South Central Semi-Arid Prairies following UDs (-0.15 ± 2.97). GPP generally increased following UDs, with variation in response between ecoregions (Fig. 2.3). The mean percent change in GPP was 1.89 ± 24.20. The largest increases in GPP occurred in four regions: Warm Deserts (9.13 ± 42.16), Sierra Madre (11.48 ± 68.57), Upper Gila

Mountains (8.03 ± 36.55), and South Central Semi-Arid Prairies (9.26 ± 34.99). The Western Cordillera showed a slight decrease in GPP (-0.35 ± 20.28).

Differences in disturbance response between disturbance types and ecoregions

MANOVA tests indicated that there were highly significant differences in LST and GPP responses due to disturbance type ($F(6,4883470) = 59{,}477$, $p < 0.01$), ecoregion ($F(16, 4883470) = 4735$, $p < 0.01$), and the interactive effect of disturbance type and ecoregion ($F(42, 4883470) = 516$, $p < 0.01$). In order to ensure that the large sample size was not confounding the significance of the results, MANOVA tests were also conducted on 2000 samples of 1000 detected disturbance points, and the statistics of each of those 2000 samples averaged to determine the significance of lower sample size on the factor differences. Disturbance ($F(6,1960) = 25.98$, $p < 0.01$) and ecoregion ($F(16,1960) = 3.47$, $p < 0.01$) remained significant, despite the lower sample size. The interactive effect between disturbance type and ecoregion became insignificant ($F(17,1960) = 1.66$, $p = 0.20$).

Discriminate function analysis was used to determine whether the responses of LST and GPP were sufficiently different to classify detected pixels into disturbance types and ecoregions. A linear model using the response variables (LST, GPP) as predictor variables predicted disturbance type with 83.98% accuracy. The response variables resulted in lower accuracy when predicting ecoregion (49.76% accuracy). However, when the data were subset by disturbance type, linear models predicted ecoregion with higher accuracy for bark beetle attack (72.92%) and defoliator damage (92.95% accuracy) than for fire (57.25% accuracy) and UDs (46.36% accuracy).

Importance of severity, extent, and local interannual change in air temperature for LST and GPP responses

The random forest models used to determine the importance of *S*, *E*, and T_{air} to the post-disturbance response in LST and GPP were cross-validated using a 60% testing subset of the data. R^2 values of the relationship between predicted and actual data were 0.39 for LST and 0.45 for GPP (Table 2.2).

Across both response variable models, both *S* and T_{air} were the most important continuous variables in determining disturbance impacts according to MSE importance (Table 2.2). Both models also underscored the importance of disturbance type and ecoregion on LST and GPP. *E* had relatively low importance in the random forest models. The models had somewhat low predictive power, likely because all potential predictor variables were not included in the model. While the residual sum of squares (RSS) importance values were not used to determine variable importance, they corroborate the results using MSE importance (Table 2.2).

Long-term patterns and trends in disturbance response

Fire

LST and GPP showed a short time to stabilization across all ecoregions following fire. In general, LST rose quickly in the first year post-disturbance, and then followed a slight decline over the next 1-4 years (Fig. 2.4; Fig. S2.1), although LST remained elevated from pre-disturbance LST and even rose gradually over the remainder of the years following the decline. This pattern was consistent across ecoregions, with slight variations in the timing of the decline and in the level to which LST declined post-disturbance. As predicted, the severity (% decline in EVI) of the disturbance had a strong influence on the LST increase post-disturbance. Surprisingly, severity did not have an effect on the duration of the post-disturbance difference in LST. Ecosystem LST values

appeared to decline just as quickly following high severity fires as lower severity fires, although they retained higher LST than lower severity fires. GPP decreased over the first 1-2 years following fire and then increased back to a stable level over the following 2-12 years (Fig. 2.5; Fig. S2.5), although GPP remained lower than pre-disturbance levels for higher severity fires. Most regions showed a similar pattern, with varying degrees of differences between the severity categories. The highest severity fires (> 60% decline in EVI) showed the largest declines in GPP. However, these fires did not show significantly different stabilization times than fires in other severity categories.

Bark Beetles

Generally, LST increased gradually in the 1-2 years following bark beetle disturbance, and then stabilized at higher temperatures for the remainder of the post-disturbance years, with some recovery to slightly lower temperatures (Fig. 2.4; Fig. S2.2). This pattern was fairly consistent across ecoregions and severity levels, despite many of the ecoregions not having any bark beetle detections. In general, GPP declined in the year of the disturbance event, and then recovered gradually over the next 3-12 years (Fig. 2.5; Fig. S2.6). Higher severity attacks resulted in the sharpest declines and longest recovery times of GPP. Several regions did not show significant impacts of bark beetle disturbance on GPP.

Defoliators

The regions with data available for defoliator attacks showed an increase in LST in the 1-2 years after an attack (Fig. 2.4; Fig. S2.3), with higher severity disturbances resulting in a larger increase in temperature. LST never fully recovered to pre-disturbance levels and actually increased over the period of observation, although the rate of increase

slowed over time. In several regions and with lower severity disturbances, LST increased but did not decline over the period of available data. GPP declined in the year of disturbance in the Western Cordillera and Upper Gila Mountains ecoregions (Fig. 2.5; Fig. S2.7) and increased slightly in the Cold Desert and West/Central Semi-Arid Prairie ecoregions. GPP increased back to pre-disturbance levels over the remainder of the available time period in the two ecoregions that showed initial declines. In the ecoregions that showed GPP increases, GPP levels fluctuated around pre-disturbance levels.

Unidentified Disturbances

For the first 1-3 years following UDs, LST increased from pre-disturbance levels (Fig. 2.4; Fig. S2.4). LST showed slight indications of recovery (i.e., decreasing LST) in the 1-5 years following maximum LST increases, but tended to stabilize at higher temperatures. Following UDs, GPP declined for 1-2 years (Fig. 2.5; Fig. S2.8) and then gradually increased for 1-9 years until stabilizing. In the Marine West Coast Forests it took a much longer period of time for the very high severity disturbances to recover compared to the other three disturbance categories.

Relationships between recovery and initial impacts

Recovery patterns following bark beetle, defoliator, and fire effects (Fig. 2.4, Fig. 2.5) are of similar magnitude and sign, seeming to contradict the results from the previous section regarding immediate post-disturbance changes in LST and GPP (Fig. 2.3). This is due to the separation of severity in the recovery figures. The severity categories do not contain equal numbers of pixels, and thus if the average is taken, bark beetle and defoliator LST and GPP responses are smaller than those following fire simply due to the inclusion of more low-severity disturbances. Additionally, as many of the

pixels lie within the Western Cordillera ecoregion, the results of that ecoregion dominate the recovery results.

DISCUSSION

Mechanisms behind LST and GPP responses to disturbance

Our results indicate that LST increases and GPP decreases following forest disturbances in the western US, although these responses vary by ecoregion. These responses to tree mortality are expected, as mortality results in a loss of canopy photosynthesis, and thus GPP. Previous research [e.g., Bright et al., 2013; Maness et al., 2013] has indicated that ET declines coincident with photosynthesis following disturbance. Decreases in ET result in shifts in the exchange of heat from latent to sensible heat, resulting in increased LST. Decreased albedo following fires also enhances absorption of radiation at the surface, further increasing LST. There are mixed results regarding the importance of albedo for impacting LST and radiative forcing following insect outbreaks or drought, with some results indicating little importance [Bright et al., 2013], and some indicating higher importance [O'Halloran et al., 2012]. Disturbance-related albedo changes may be more or less important to LST and radiative forcing at varying times of the year, with more importance in the winter due to snowpack effects (i.e., more exposed snow due to a loss of canopy cover) [Randerson et al., 2006; O'Halloran et al., 2012], and less importance in summer. Decreased surface shading by the canopy due to needle loss and/or snagfall and subsequent changes in soil moisture may also impact post-disturbance LST.

Despite showing a broad scale reduction in GPP, some ecoregions showed an increase in GPP. This may occur through several mechanisms: (1) false classification of a

pixel as disturbance due to natural fluctuations in the EVI signal, (2) pre-disturbance limitation of GPP by climate conditions, (3) release of the remaining vegetation from resource (light, nutrient, and/or water) limitation or, (4) an increase in the length of the growing season. The first and second mechanisms are the most probable in the case of UDs where detections may reflect random or phenological fluctuations in canopy greenness or temporary climate-induced declines in photosynthesis (e.g., due to drought). Natural fluctuations in the EVI signal may have been labeled as disturbance in some instances, resulting in false positives. Removal of climate limitations post-detection would allow 'disturbance' pixels to increase in GPP, also resulting in false positives because no actual mortality occurred. The third mechanism is that partial canopy mortality, as may occur in insect outbreaks, may release any remaining vegetation from resource limitation, enhancing the productivity of the remaining vegetation enough to compensate for the partial or complete loss of the canopy, increasing GPP. Several studies [Veblen et al., 1991; Brown et al., 2012; Reed et al., 2014; Pec et al., 2015] have cited this mechanism to explain potential increases in productivity following insect disturbance. While the relatively low resolution of MODIS GPP is unlikely to detect small changes in GPP due to this mechanism, if the affected area is large enough, it may be sufficient. Finally, sites with increased GPP typically also had increased LST. As minimum temperature is a variable in the current GPP algorithm, slight increases in LST could extend the growing season and thus increase GPP.

Causes and implications of differences in response among disturbance types and ecoregions

There were differences in LST and GPP responses to disturbance both between disturbance categories and ecoregions, although the general response patterns matched

those from previous studies [e.g., Coops and Wulder, 2010; Bright et al., 2013; Maness et al., 2013; Moore et al., 2013]. We hypothesize that insect disturbances and UDs resulted in less severe responses than fires due to both the detection method used and the nature of the disturbances. Our disturbance detection algorithm may have recorded some pixels as disturbed that were experiencing decreased greenness that did not cause significant mortality, diminishing the category's overall disturbance response results. Additionally, bark beetle outbreaks, defoliator attacks, and UDs tend to be somewhat species specific and may occur over several years [Raffa et al., 2008; Bentz et al., 2010]. Thus, small patches within larger pixels might be at differing successional stages at the time of observation [e.g., Penn et al., 2016]. These disturbance characteristics could decrease the disturbance LST and GPP response because few trees may be affected in a given area annually. This also could result in the inclusion of some mortality in our pre-disturbance LST and GPP response estimates. However, our recovery figures (Fig. 2.4, Fig. 2.5) indicate that the largest changes in magnitude of the variables occurred in the year of the detection. This suggests that most of the mortality or decrease in productivity occurred in the year of detection and not in previous years. Thus, we believe that the muting effect of gradual disturbances is very slight.

The variation in disturbance response among ecoregions is likely a result of regional variation in climate, forest composition and structure, soils, and hydrology, as well as disturbance regime. For example, post-fire increases in LST were much lower in ecoregions with high precipitation and moderate temperatures (e.g., Marine West Coast Forests) than in ecoregions with low precipitation and higher temperatures (e.g., Upper Gila Mountains), likely due to greater water availability for latent heat exchange and

lower atmospheric demand. Differences between ecoregions in terms of cloudiness may also account for some of the differences in disturbance responses. However, all response variables were pre-processed to minimize cloud cover and were JJA averages, when clouds are the least prevalent. The exact influence of environmental variables other than air temperature was not investigated in this study and merits further research.

The observed differences in disturbance response between ecoregions reinforce the importance of management strategies that are dependent on the disturbance locale. Current and predicted future climate [PRISM Climate Group, 2011; Dobrowski et al., 2013] and disturbance regimes [Fulé et al., 1997; Franklin et al., 2002] differ substantially between ecoregions. We show that response regimes (i.e., response magnitude, direction, and duration) also differ significantly. Variation in management strategies among ecoregions and other management divisions will have increasing importance as these components (i.e., climate, disturbance regime, and response regime) of climate-disturbance feedbacks interact. This is especially true in areas where high-severity disturbance events may be increasing in frequency, as recovery to pre-disturbance biophysical characteristics may not occur, indicating longer-term shifts in ecosystem type or function. Managers should be wary of applying strategies aimed at mitigating disturbance-climate feedbacks from one region to another without validation.

Potential disturbance feedbacks to local and regional climate

Disturbance severity (*S)* is critical to LST and GPP responses, as has been noted in many previous studies [Randerson et al., 2006; Bond-Lamberty et al., 2007; Kurz et al., 2008; Maness et al., 2013]. Disturbances are projected to increase in severity due to climate change [Adams et al., 2009; Littell et al., 2009; Bentz et al., 2010; Westerling et

al., 2011; Seidl et al., 2014], indicating the presence of a positive feedback loop whereby changes in climate may result in more frequent and more severe disturbances, which then may result in greater LST and GPP feedbacks to climate. As severity was also linked to differences in post-disturbance recovery, longer feedbacks from disturbance to local climates may result as severity increases due to climate change. Longer disturbance impacts may lead to shifts in ecosystem type, as prolonged changes in the energy budgets of the area prevent the vegetation from fully recovering [e.g., Breshears et al., 2009; Allen et al., 2010]. However, the impacts of changes in disturbance regime on recovery patterns may be mitigated somewhat by a CO_2 fertilization effect, which potentially allows vegetation to grow more quickly due to enhanced photosynthetic efficiency [Foster et al., 2010; McMahon et al., 2010; Williams et al., 2012].

Years with warmer air temperatures also resulted in larger LST and GPP responses. As such, disturbance impacts are likely to be enhanced in areas where climate change will result in warmer conditions. Forest function may change more in response to future disturbances than it did in response to historic disturbances with the same severity and extent.

Scale and its role in disturbance-induced climate forcing

The variation in disturbance responses between disturbance types highlights the importance of scale in disturbance studies. Previous studies [e.g., Kurz et al., 2008; Hicke et al., 2013] found that insect outbreaks can result in potential impacts at least as large as fire. We did not see this in our results. However, non-fire disturbances are typically more spatially and temporally patchy than fires. Less continuous spatial patterns mean that, when aggregated across large pixels (e.g., 250 m), the disturbances appear to have a

smaller effect. The use of 1 km GPP data may have exaggerated this effect. Penn et al. [2016] found that despite large impacts on ET observed at the hillslope scale following a bark beetle outbreak, only small effects were seen at the watershed scale due to the mediating contribution of nearby healthy vegetation.

Disturbance detection

The detection of low-severity disturbances and in particular insect-induced damage and mortality remains a challenge for remote sensing, particularly in cloud dominated and mountainous regions. Evaluation efforts are further hampered by the limited availability of broad-scale repeated ground survey data. The BFAST/Hansen and VCT remotely-sensed datasets we evaluated agreed well with each other and with MTBS polygons (Table S2.3). However, both datasets showed poor agreement with ADS maps (Table S2.3). This is not surprising, as ADS maps, while very useful at coarse resolutions for research or for forest planning purposes, have only low to moderate accuracy when compared to field plots [Johnson and Ross, 2008]. While ADS are increasingly used in research studies on the extent and impacts of insect disturbance, these data have their own issues. For example, different observers conduct the surveys each year, and the methods used vary from region to region. More specifically, one observer might draw a small polygon around only a few trees, while another might draw a very large polygon around the same small area. ADS maps are subjective and represent general areas of disturbance, not precise disturbance locations [Hall et al., 2006; Johnson and Ross, 2008; Johnson and Wittwer, 2008]. Despite low agreement between our detection product and ADS, we believe that our combined approach, whereby we limit our ecosystem response results to areas where ADS also detected insect damage, is justified and preferable to

using ADS alone to represent non-fire disturbances. The approach uses remotely detected data as a complement to ADS and MTBS data to more finely resolve the temporal and spatial variation in disturbance locations. Several studies have used this combined approach [Hall et al., 2006; Assal et al., 2014], in which aerial surveys bound an area, but remote sensing algorithms are used to discover the exact locations and timing of disturbances within those bounds. It is highly unlikely that detected disturbances within an aerial polygon represent a disturbance other than that marked by the survey. Although our disturbance detection is not perfectly accurate, it is statistically comparable to the results from the similar VCT remote sensing approach (Table S2.3; Table S2.4; Fig. S2.9). By limiting our data extent to areas of known disturbance, we can be confident that the detected points are indeed disturbance.

Assumptions and errors

Several assumptions may have contributed to increased uncertainty in the results. While the BFAST method has proven effective at detecting disturbances such as fires, floods, and deforestation [Verbesselt et al., 2010a; Watts et al., 2014; DeVries et al., 2015], the method's success may vary depending on local vegetation and disturbance type [Watts et al., 2014]. We demonstrated that BFAST and Hansen data combined are able to detect the majority of large, moderate to severe, disturbances (Fig. S2.9, Fig. S2.10, Table S2.3; Table S2.4). However, small or patchy disturbances may be missed at this resolution (250 m), leading to conservative results that are likely to be underestimates rather than overestimates of the total impacts of disturbance on forest ecosystems.

We may have also introduced some error by using all MTBS and ADS polygons, regardless of the severity reported in those polygons. However, our detection methods

were designed to represent more spatially and temporally explicit disturbance locations and tended to pick up higher severity disturbances than would have been found in a random subset of the disturbance polygons (Table S2.3). It is therefore unlikely that we include many non-disturbance pixels in low-severity polygons.

We also assume that the detected decline in EVI represents mortality, not simply a decline in canopy 'greenness' related to temporary stressors such as high vapor pressure deficit. It is likely that these false positives are few [Watts et al., 2014; Dutrieux et al., 2015] and occur primarily in the UD category. The use of fire, bark beetle, and defoliator polygons decreased the likelihood of false positives in those categories. Detected declines in EVI that did not represent mortality should result in a decrease in the magnitude of the response results, as non-mortality detections will decrease the average change observed. Additionally, we demonstrate the validity of EVI-based severity in Fig. S2.10.

Issues of scale, especially pertaining to our use of 1 km GPP, may have also resulted in increased uncertainty. However, several other studies have investigated the effects of MPB on GPP and found reductions in GPP that overlap the 10-90% quantiles of our results (-27-21%). Results in the upper and lower quantiles of our data are not considered due to outliers. Bright et al. [2013], Coops and Wulder [2010], and Moore et al. [2013] found GPP declines of 5-26%, 15-20%, and 13-30%, respectively. Coops and Wulder [2010] studied MPB disturbance in British Columbia, and Bright et al. [2013] and Moore et al. [2013] studied MPB disturbance in Colorado. Both regions have experienced severe MPB damage. While our results overlapped zero and used the same MODIS GPP product to estimate changes in the variable, we also used coarser resolution

data to locate areas of likely disturbance (i.e., 240 m vs. 30 m or field data) and included less severely disturbed areas in addition to severely disturbed areas.

Finally, the calculation of extent (*E*) may have contributed towards its insignificant relationship with disturbance responses. *E* was determined as the area of adjoining pixels that were affected by the same disturbance type. This method is slightly problematic as it assumes that bark beetle and defoliator disturbances in the same area represent the same outbreak. However, it is logical that *E* is less important than severity and interannual changes in air temperature for determining disturbance effects on LST and GPP.

CONCLUSIONS

We used satellite data to objectively determine the effects of four categories of disturbance on LST and GPP across nine ecoregions in the western US. We found that all disturbance types resulted in overall increased LST in the 2 years following disturbance, and all disturbance types but UD resulted in decreased GPP, although the exact magnitude and direction of these changes varied significantly both among disturbance types and ecoregions. Fires showed the largest and clearest impacts in all response variables, whereas bark beetle, defoliator, and UD responses were much less pronounced. Severity and interannual changes in air temperature were the primary drivers of the magnitude of disturbance response regardless of the type or location, and disturbances of higher severity resulted in longer recovery times. The results of this study suggest a strong potential climate feedback due to biophysical changes in forests following disturbance events that may strengthen as disturbances grow in frequency and severity in the coming decades. Despite several assumptions made in the study, to our knowledge

this analysis remains the first to incorporate multiple disturbance types over a large geographical region in an evaluation of the effects of disturbance on ecosystem climate services. Future research utilizing both field and satellite observations in conjunction with ecosystem simulations are required to advance our understanding of ecosystem responses to interactions between climate and disturbance.

FIGURES AND TABLES

Figure Legends

Figure 2.1. (a) Map of ecoregions used in the study. Ecoregions were limited to eleven states (WA, OR, CA, ID, NV, AZ, MT, UT, WY, CO, and NM). (b) Location of disturbances across the western US. *Note that disturbances shown ARE NOT to size, actual pixel size is smaller than map representation.

Figure 2.2. Density distributions of JJA changes in (a) LST and (b) GPP following fire, bark beetle attack, defoliator attack, and UDs.

Figure 2.3. JJA change in response variables by ecoregion. Bar height is the mean response for the ecoregion; error bars represent standard deviation.

Figure 2.4. JJA change in LST (°C) following disturbance over the entire western US. See Figures S2-S4 for changes by ecoregion. In the case of bark beetles and defoliators, 'year of disturbance' is defined as the year in which damage reaches a level detectable in the EVI time series.

Figure 2.5. Percent JJA change in GPP following disturbance over the entire western US. See Figures S5-S7 for changes by ecoregion. In the case of bark beetles and defoliators, 'year of disturbance' is defined as the year in which damage reaches a level detectable in the EVI time series.

Figure 2.1.

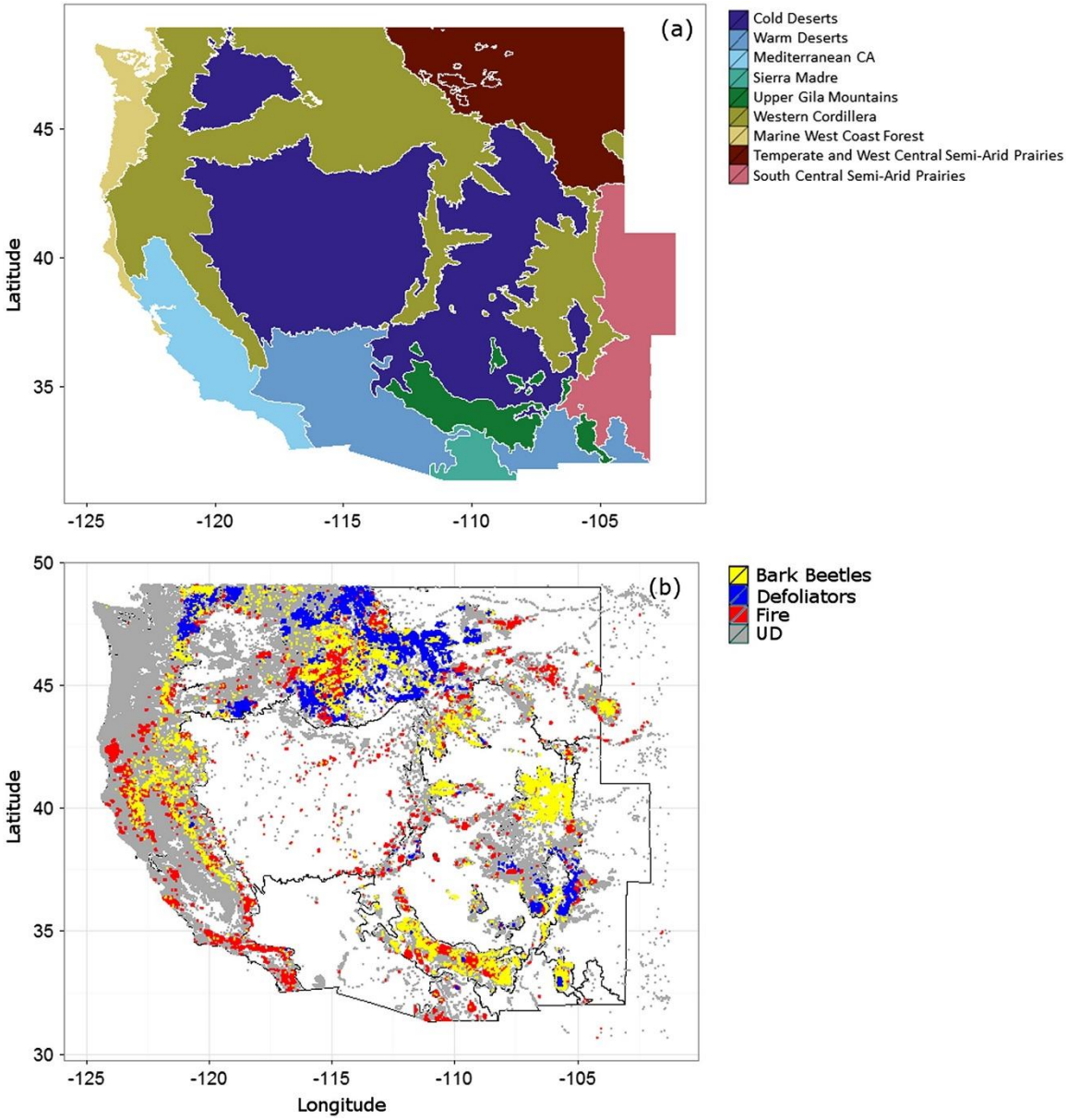
(a)
Cold Deserts
Warm Deserts
Mediterranean CA
Sierra Madre
Upper Gila Mountains
Western Cordillera
Marine West Coast Forest
Temperate and West Central Semi-Arid Prairies
South Central Semi-Arid Prairies
Latitude
45
40
35
-125
-120
-115
-110
-105
(b)
Bark Beetles
Defoliators
Fire
UD
Latitude
50
45
40
35
30
-125
-120
-115
-110
-105
Longitude

Figure 2.2.

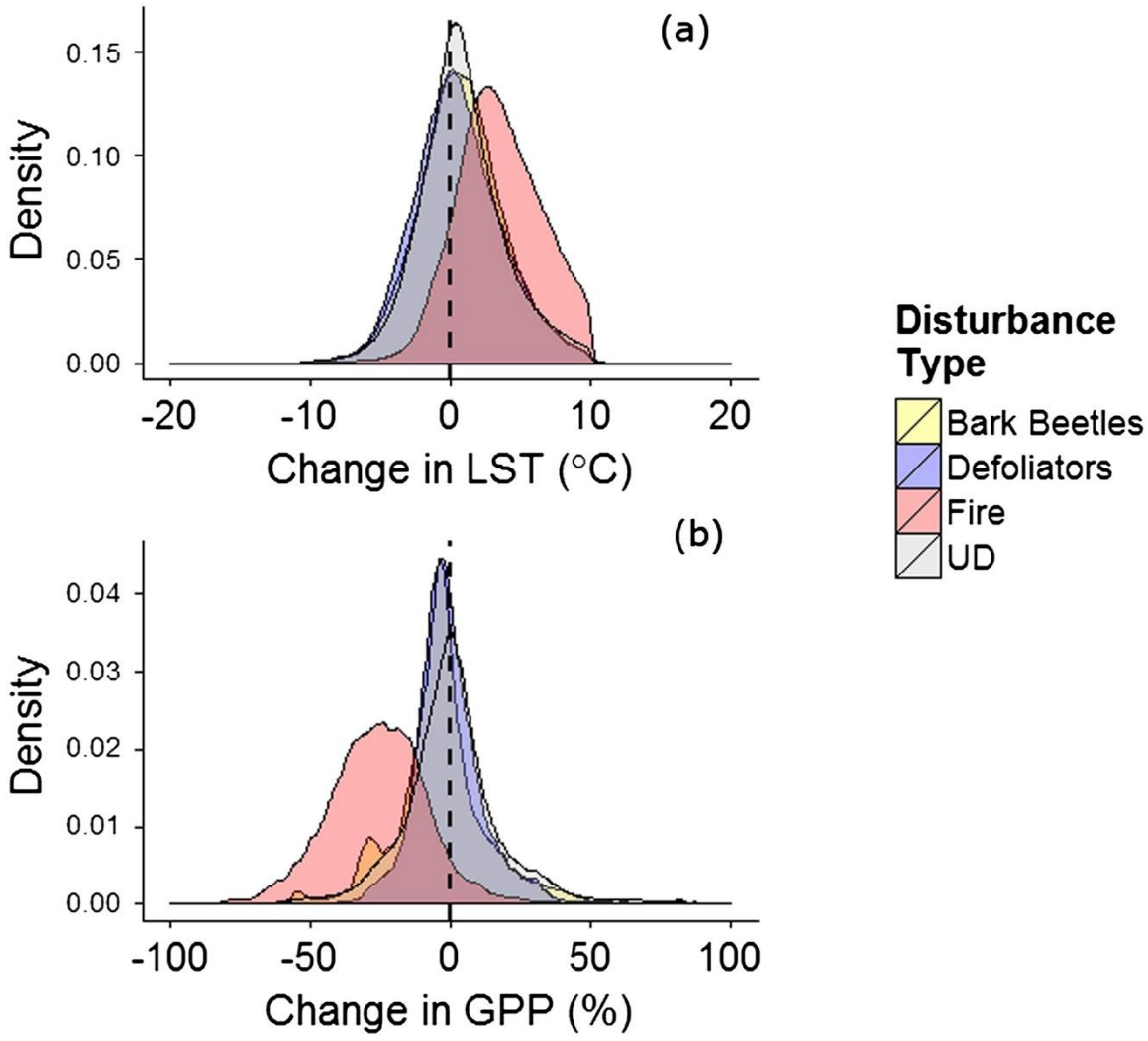
(a)
Density
0.15
0.10
0.05
0.00
-20
-10
0
10
20
Change in LST (°C)
(b)
Density
0.04
0.03
0.02
0.01
0.00
-100
-50
0
50
100
Change in GPP (%)
Disturbance Type
Bark Beetles
Defoliators
Fire
UD

Figure 2.3.

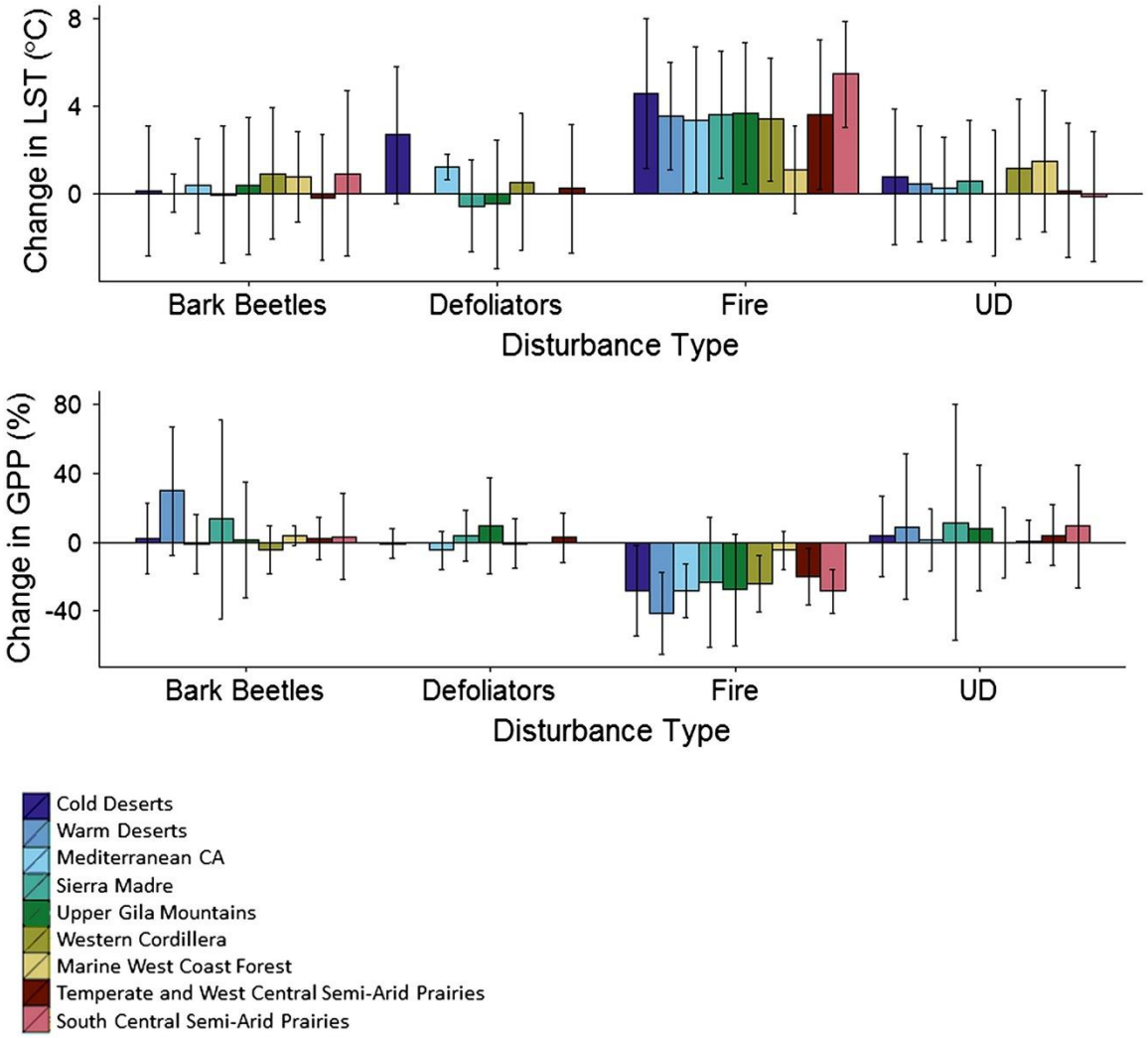
Change in LST (°C)
8
4
0
Bark Beetles
Defoliators
Fire
UD
Disturbance Type
Change in GPP (%)
80
40
0
-40
Bark Beetles
Defoliators
Fire
UD
Disturbance Type
Cold Deserts
Warm Deserts
Mediterranean CA
Sierra Madre
Upper Gila Mountains
Western Cordillera
Marine West Coast Forest
Temperate and West Central Semi-Arid Prairies
South Central Semi-Arid Prairies

Figure 2.4.

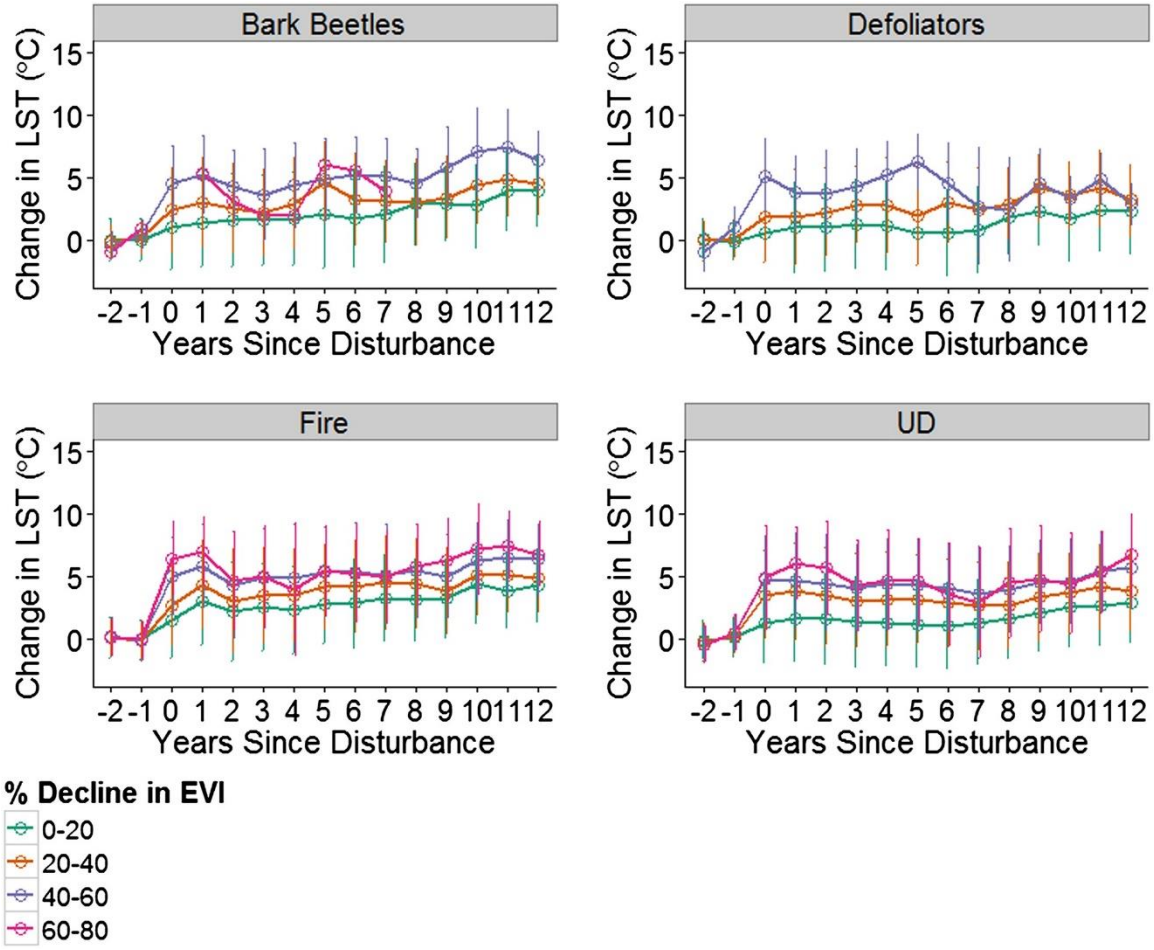
Bark Beetles
Defoliators
Fire
UD
Change in LST (°C)
Years Since Disturbance
% Decline in EVI
0-20
20-40
40-60
60-80

Figure 2.5.

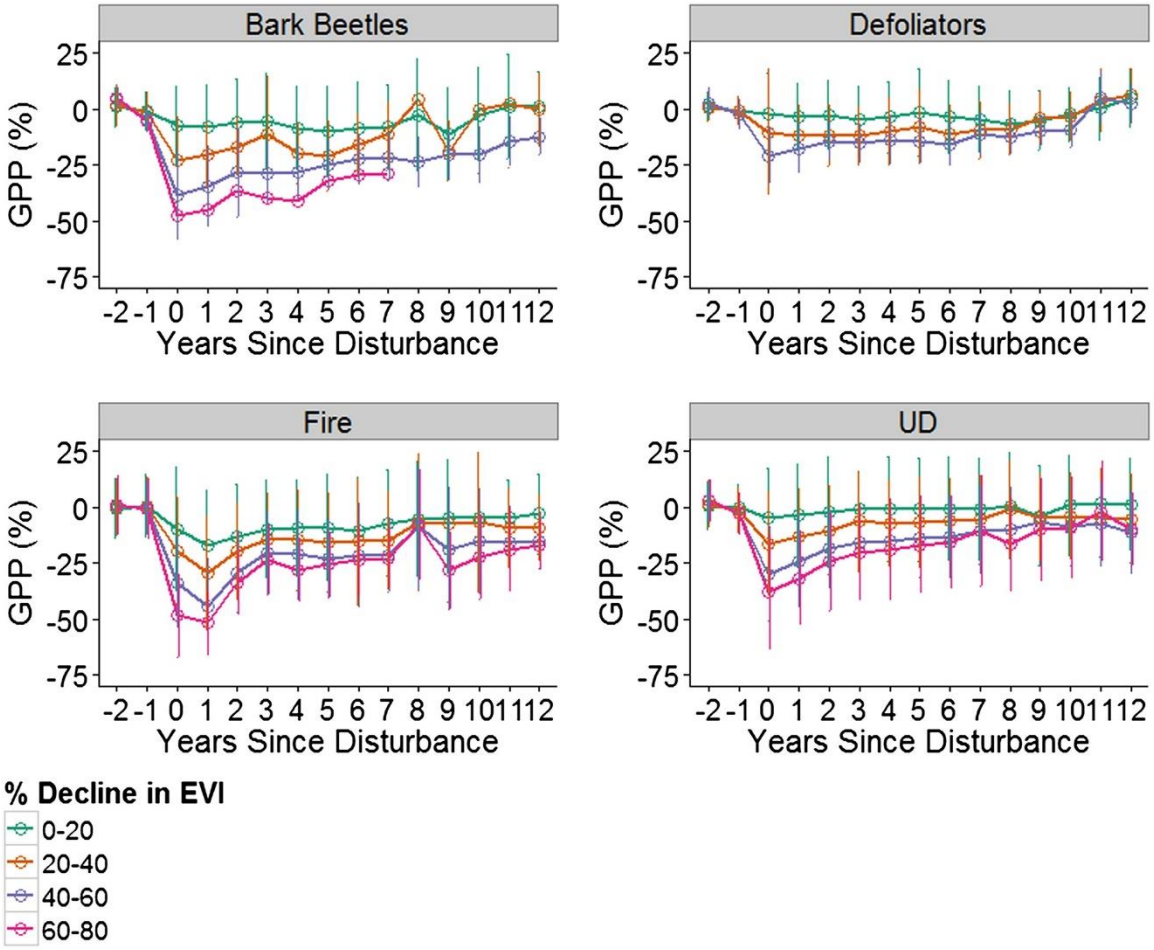
Bark Beetles
Defoliators
Fire
UD
GPP (%)
25
0
-25
-50
-75
-2 -1 0 1 2 3 4 5 6 7 8 9 10 11 12
Years Since Disturbance
% Decline in EVI
0-20
20-40
40-60
60-80

Tables

Table 2.1. Variables included in the Random forest models.*

Predictor Variable	Abbreviation	Reasoning
Severity (% Decline in EVI)	S	A higher degree of mortality (i.e., higher severity) in the pixel will separate it from the original state more than a lower degree of mortality.
Local Interannual Change in Air Temperature	T_{air}	A change in the average JJA air T will influence soil moisture and therefore latent heat exchange, surface temperatures, and photosynthesis (GPP).
Areal Extent	E_a	Disturbances that cover the entire pixel should have a larger impact on the response variables than small (< 1 pixel) disturbance patches. Responses to smaller disturbances may be diluted by undisturbed patches of forest.
Disturbance Type	D	Included for comparison with the above variables. Disturbance type should have a strong influence on the average LST, GPP, and C stock response because each disturbance type affects forest structure and composition differently.
Ecoregion	R	Also included for comparison with S, T_{air}, and E_a. Environmental characteristics, including soils, vegetation, climate, and hydrology, differ by ecoregion and may impact disturbance responses.

* S, T_{air}, and E_a are continuous variables. D and R are factors.

Table 2.2. Summary of Random Forest models used to predict LST and GPP.*

Response Variable	Predictor Variable	% Increase in MSE	Increase in RSS	RMSE	MBE	Model R^2	Testing n	Training n
LST	Severity	20.13	13.3×10^6	2.49	0	0.39	1465320	976855
	Change in Air T	16.25	10.6×10^6					
	Area	7.72	2.32×10^5					
	Disturbance Type	16.07	3.78×10^5					
	Ecoregion	15.45	2.03×10^5					
GPP	Severity	14.95	8.88×10^7	18.73	-0.03	0.45	1465320	976697
	Change in Air T	17.77	7.26×10^7					
	Area	10.42	2.36×10^7					
	Disturbance Type	11.12	3.30×10^7					
	Ecoregion	13.78	3.22×10^7					

* The model R^2 value is the correlation between values predicted by the model and the actual values in the 60% testing subset of the data. The '% Increase in MSE' is the increase in MSE that would occur if that predictor variable were removed from the model. The 'Increase in RSS' is the increase in RSS that would occur if the values of that variable were permuted across all nodes in all trees.

SUPPLEMENTARY INFORMATION

Supplemental Figure Legends

Figure S2.1. Recovery of JJA LST following fires. Legend values represent severity categories.

Figure S2.2. Recovery of JJA LST following bark beetle disturbance events. Legend values represent severity categories.

Figure S2.3. Recovery of JJA LST following defoliator disturbance events. Legend values represent severity categories.

Figure S2.4. Recovery of JJA LST following UD events. Legend values represent severity categories.

Figure S2.5. Recovery of JJA GPP following fires. Legend values represent severity categories.

Figure S2.6. Recovery of JJA GPP following bark beetle disturbance events. Legend values represent severity categories.

Figure S2.7. Recovery of JJA GPP following defoliator disturbance events. Legend values represent severity categories.

Figure S2.8. Recovery of JJA GPP following UD events. Legend values represent severity categories.

Figure S2.9. Nearest neighbor distance from detection points used in this paper to nearest Vegetation Change Tracker point in meters.

Figures S2.10. EVI-based severity and MTBS-defined severity for the 2011 Wallow Fire in Eastern Arizona.

Figure S2.1.

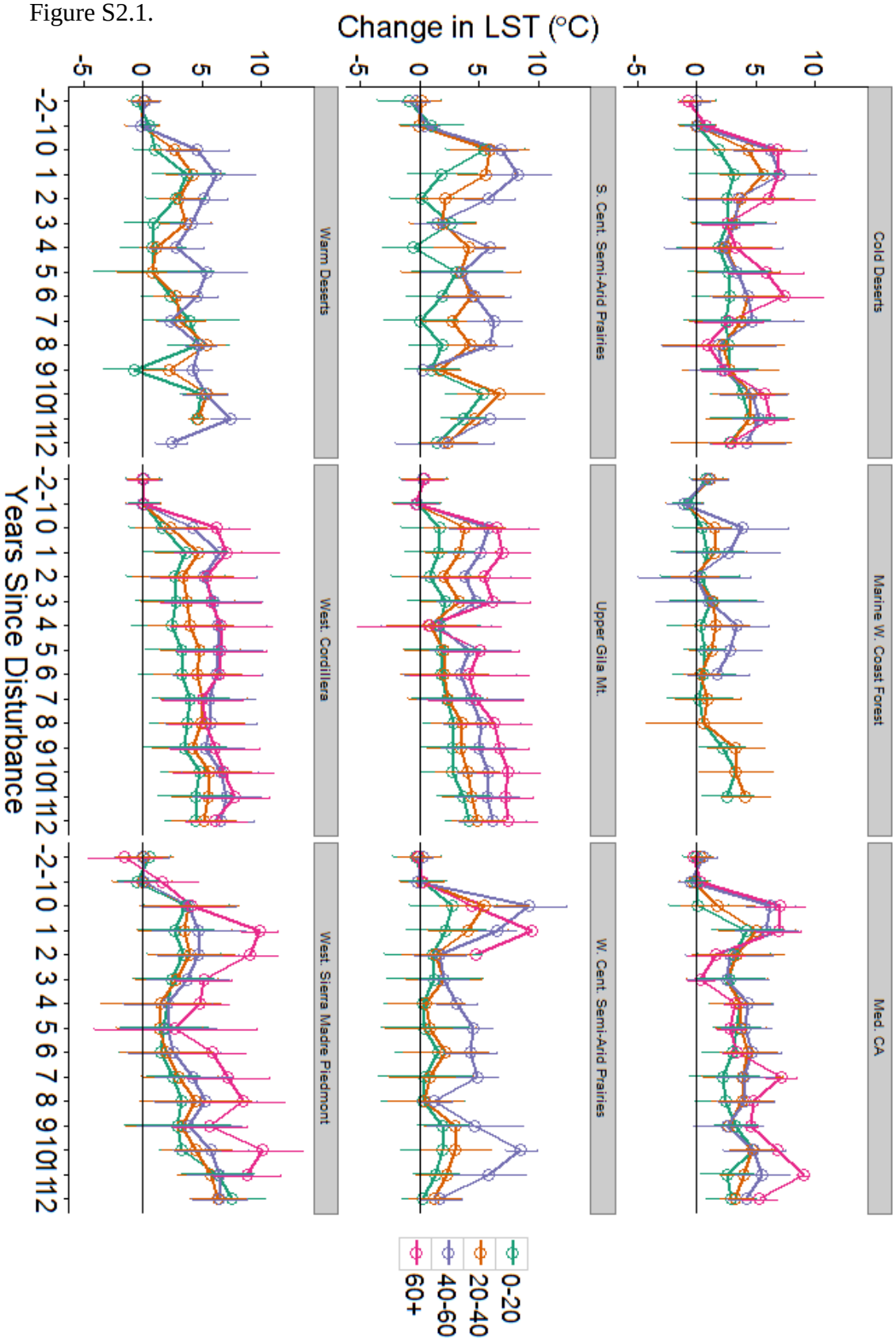
Change in LST (°C)
Cold Deserts
Marine W. Coast Forest
Med. CA
S. Cent. Semi-Arid Prairies
Upper Gila Mt.
W. Cent. Semi-Arid Prairies
Warm Deserts
West. Cordillera
West. Sierra Madre Piedmont
Years Since Disturbance
0-20
20-40
40-60
60+

Figures S2.2.

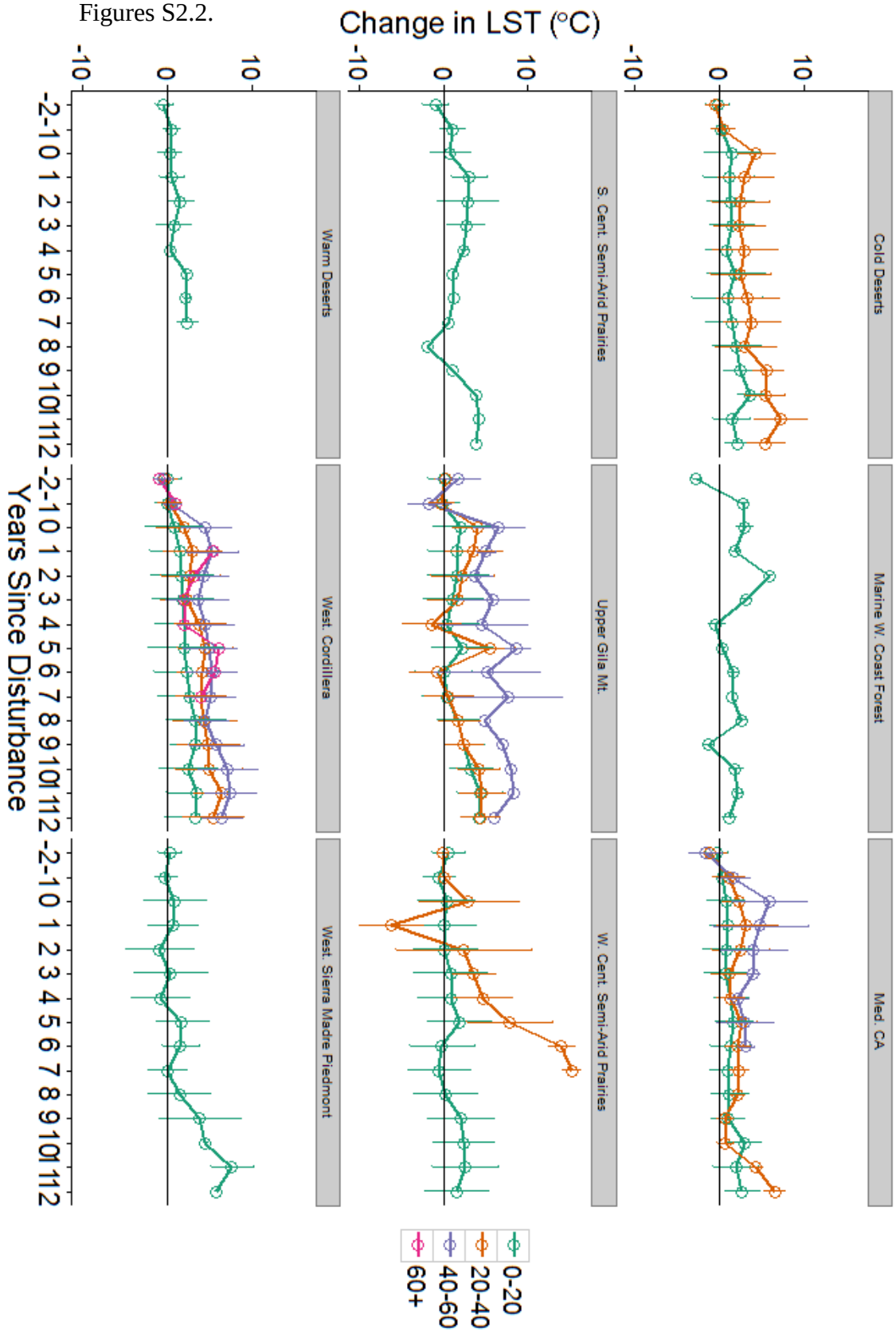
Change in LST (°C)
Cold Deserts
Marine W. Coast Forest
Med. CA
S. Cent. Semi-Arid Prairies
Upper Gila Mt.
W. Cent. Semi-Arid Prairies
Warm Deserts
West. Cordillera
West. Sierra Madre Piedmont
-10
0
10
-2 -1 0 1 2 3 4 5 6 7 8 9 10 11 12
Years Since Disturbance
0-20
20-40
40-60
60+

Figure S2.3.

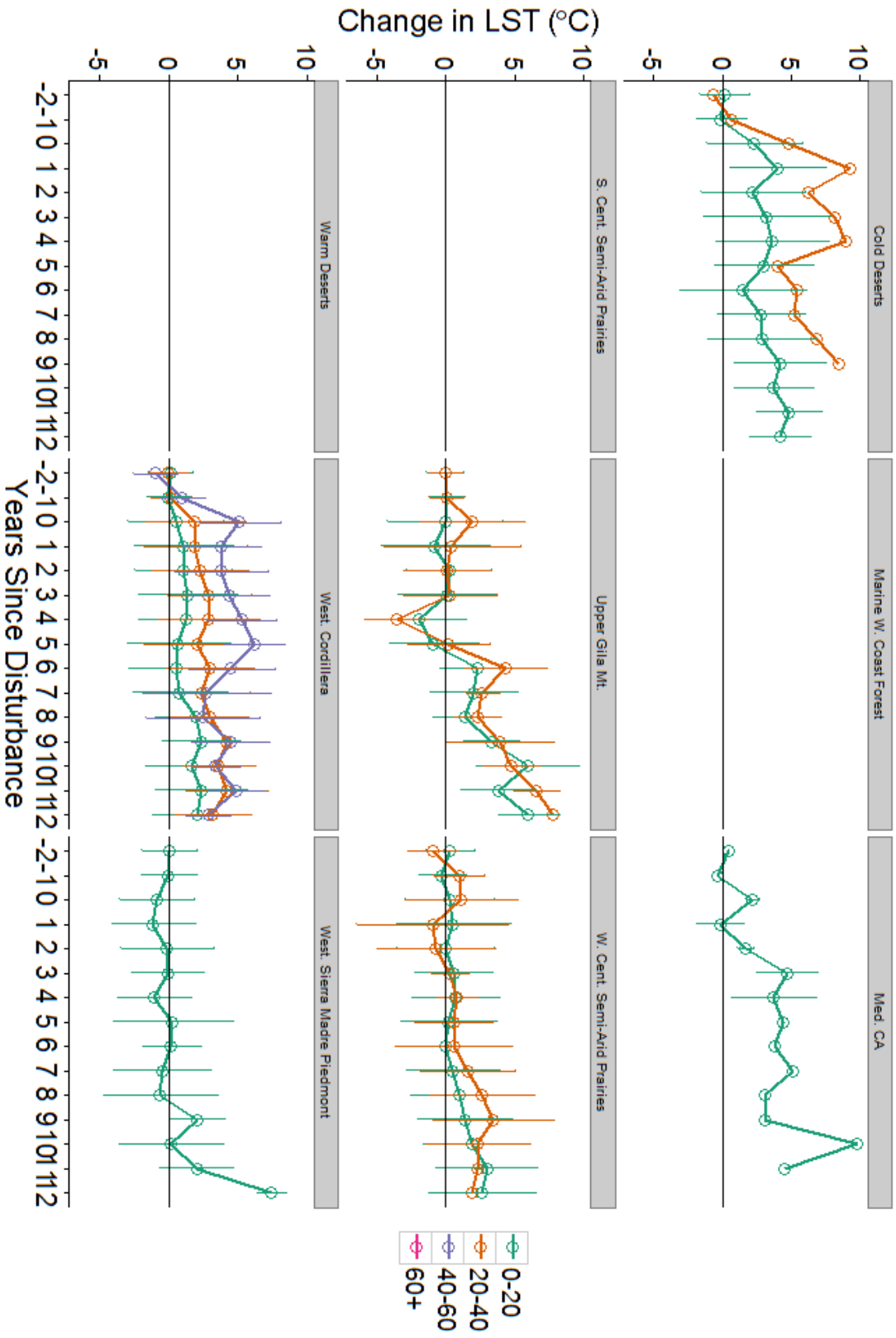
Change in LST (°C)
Cold Deserts
Marine W. Coast Forest
Med. CA
S. Cent. Semi-Arid Prairies
Upper Gila Mt.
W. Cent. Semi-Arid Prairies
Warm Deserts
West. Cordillera
West. Sierra Madre Piedmont
Years Since Disturbance
0-20
20-40
40-60
60+

Figures S2.4.

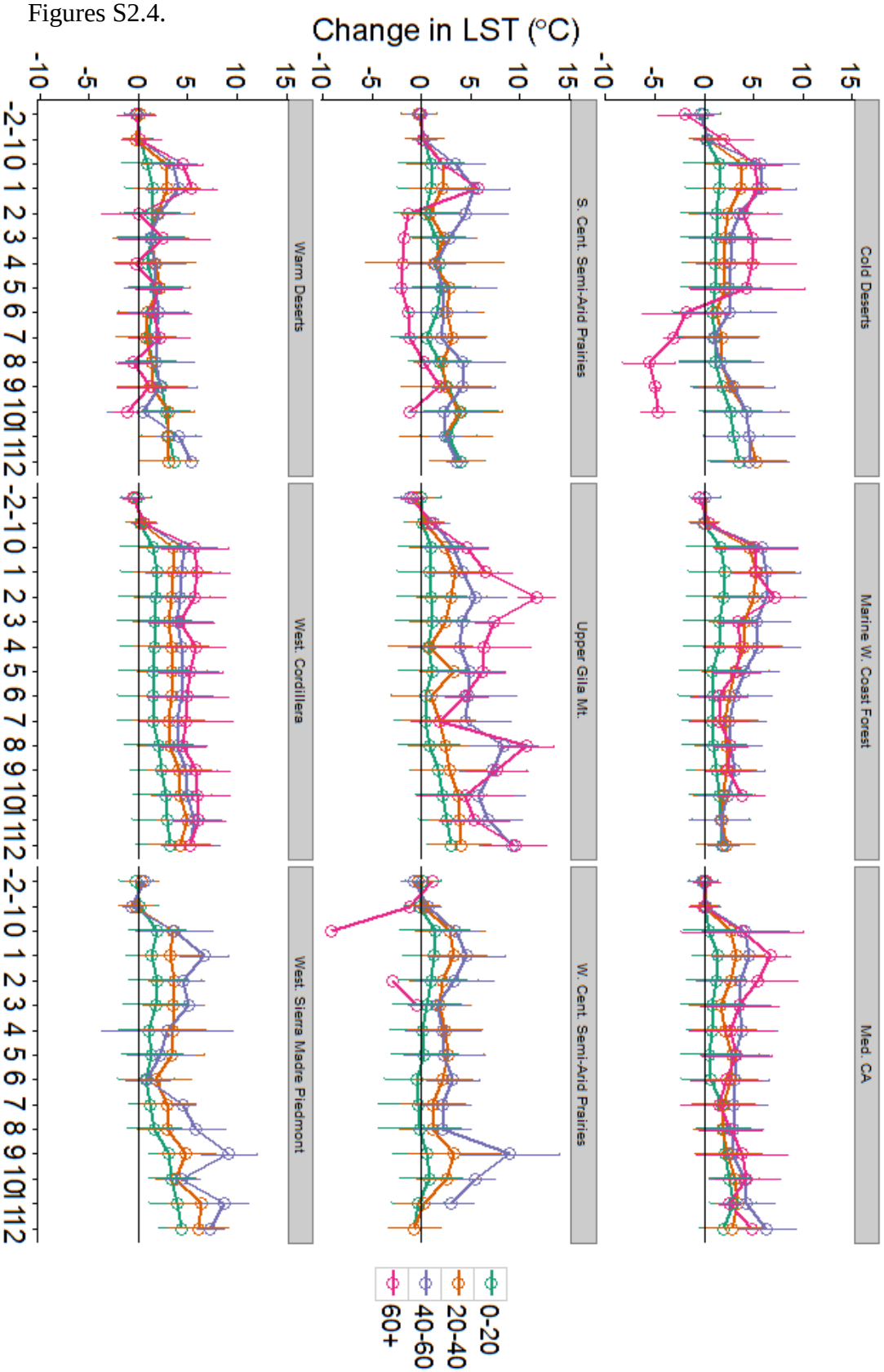
Change in LST (°C)
Cold Deserts
Marine W. Coast Forest
Med. CA
S. Cent. Semi-Arid Prairies
Upper Gila Mt.
W. Cent. Semi-Arid Prairies
Warm Deserts
West. Cordillera
West. Sierra Madre Piedmont
Years Since Disturbance
0-20
20-40
40-60
60+

Figures S2.5.

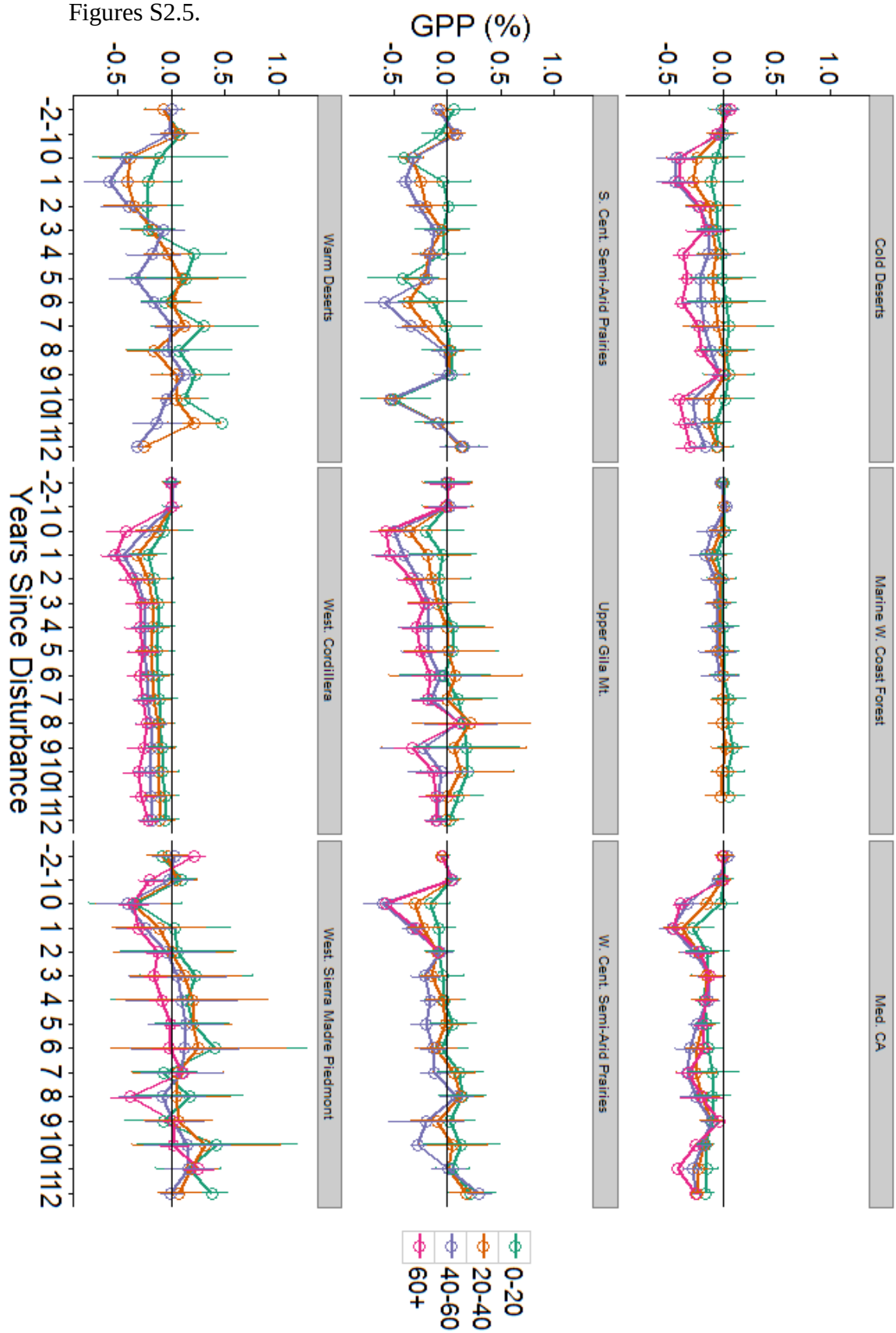
GPP (%)
-0.5
0.0
0.5
1.0
Cold Deserts
Marine W. Coast Forest
Med. CA
S. Cent. Semi-Arid Prairies
Upper Gila Mt.
W. Cent. Semi-Arid Prairies
Warm Deserts
West. Cordillera
West. Sierra Madre Piedmont
-2 -1 0 1 2 3 4 5 6 7 8 9 10 11 12
Years Since Disturbance
0-20
20-40
40-60
60+

Figure S2.6.

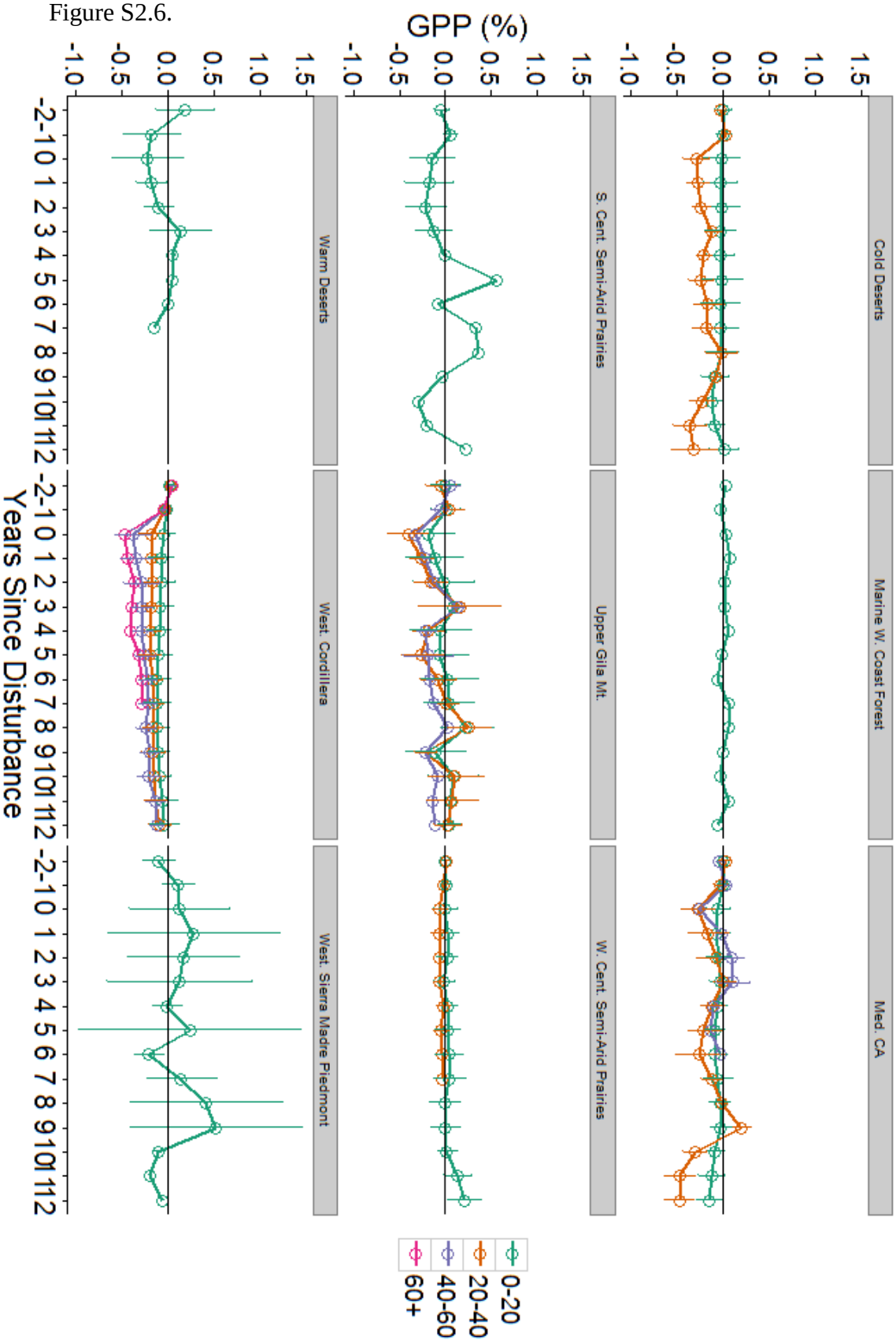
GPP (%)
Cold Deserts
Marine W. Coast Forest
Med. CA
S. Cent. Semi-Arid Prairies
Upper Gila Mt.
W. Cent. Semi-Arid Prairies
Warm Deserts
West. Cordillera
West. Sierra Madre Piedmont
Years Since Disturbance
0-20
20-40
40-60
60+

Figure S2.7.

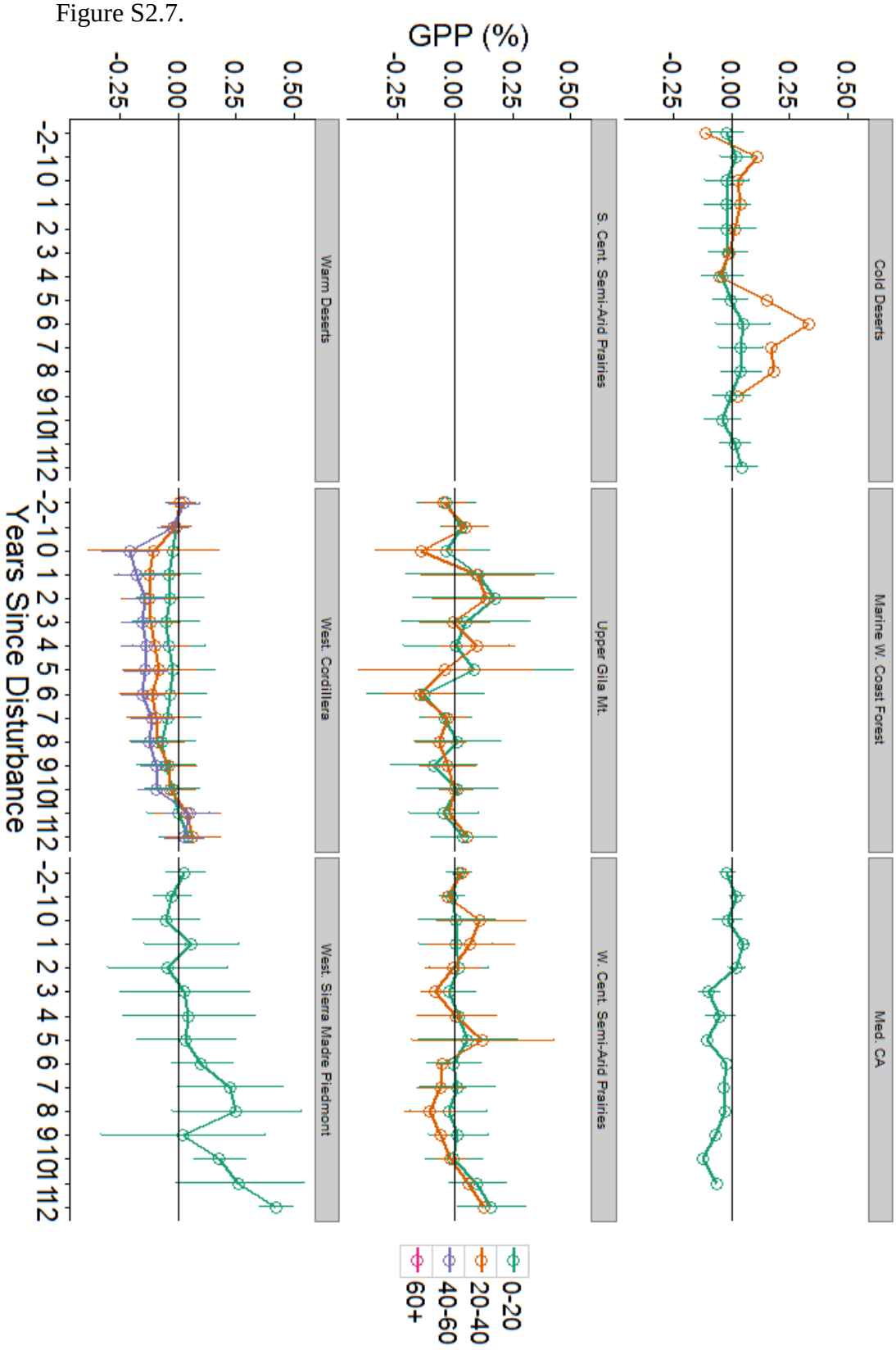
GPP (%)
0.50
0.25
0.00
-0.25
Cold Deserts
Marine W. Coast Forest
Med. CA
S. Cent. Semi-Arid Prairies
Upper Gila Mt.
W. Cent. Semi-Arid Prairies
Warm Deserts
West. Cordillera
West. Sierra Madre Piedmont
-2 -1 0 1 2 3 4 5 6 7 8 9 10 11 12
Years Since Disturbance
0-20
20-40
40-60
60+

Figure S2.8.

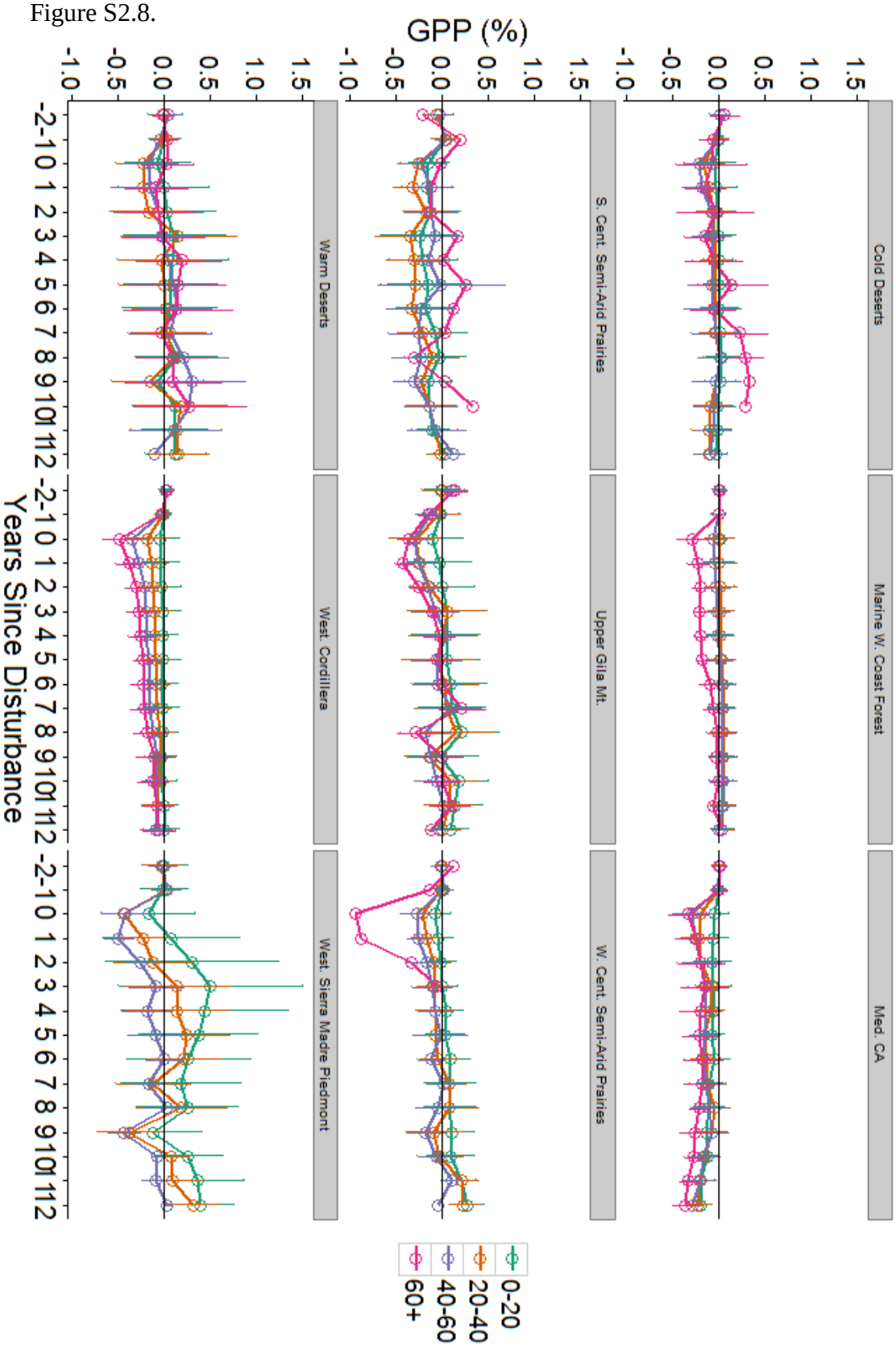
GPP (%)
Cold Deserts
Marine W. Coast Forest
Med. CA
S. Cent. Semi-Arid Prairies
Upper Gila Mt.
W. Cent. Semi-Arid Prairies
Warm Deserts
West. Cordillera
West. Sierra Madre Piedmont
Years Since Disturbance
0-20
20-40
40-60
60+

Figure S2.9.

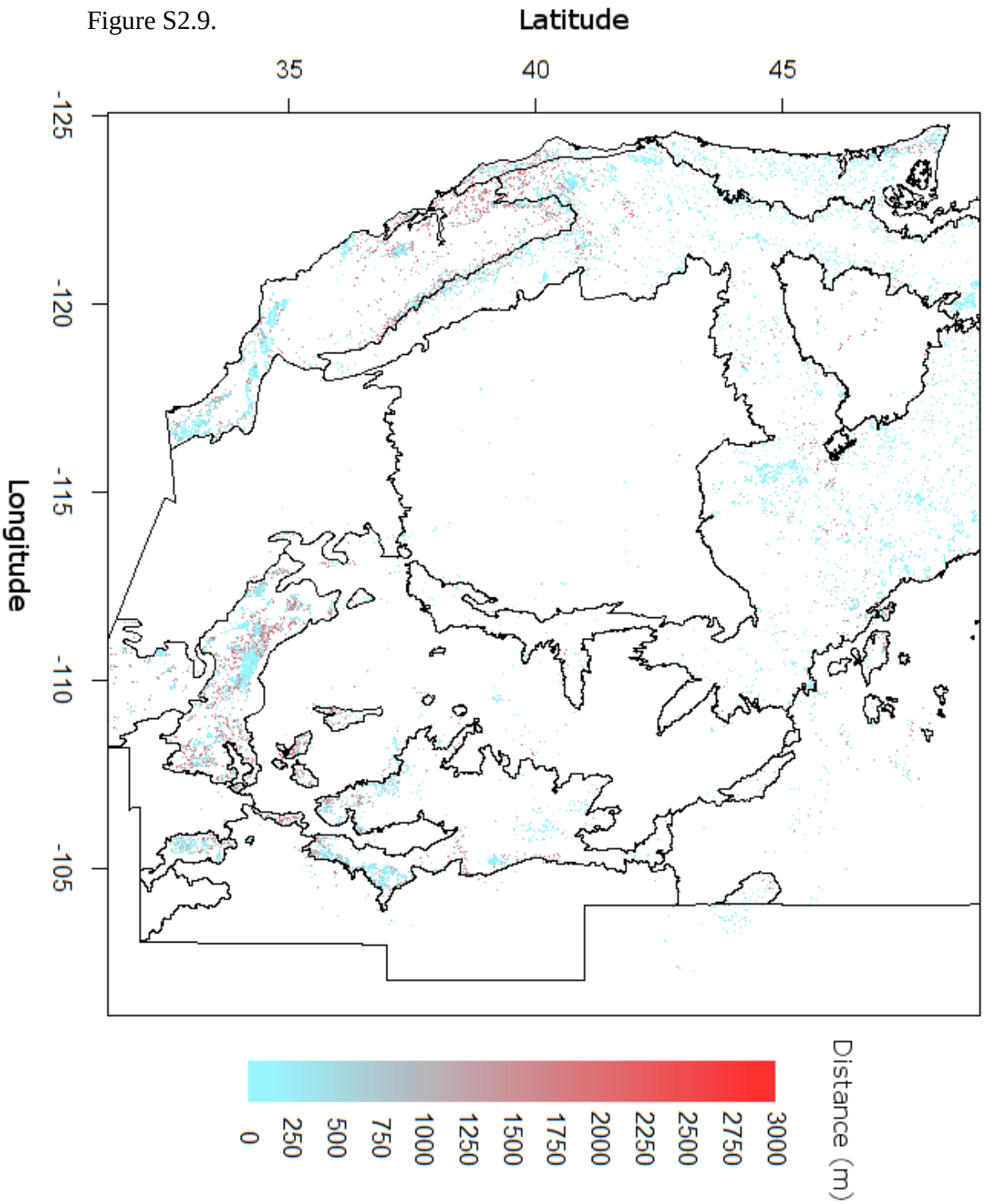
Latitude
35
40
45
Longitude
-125
-120
-115
-110
-105
Distance (m)
0
250
500
750
1000
1250
1500
1750
2000
2250
2500
2750
3000

Figure S2.10.

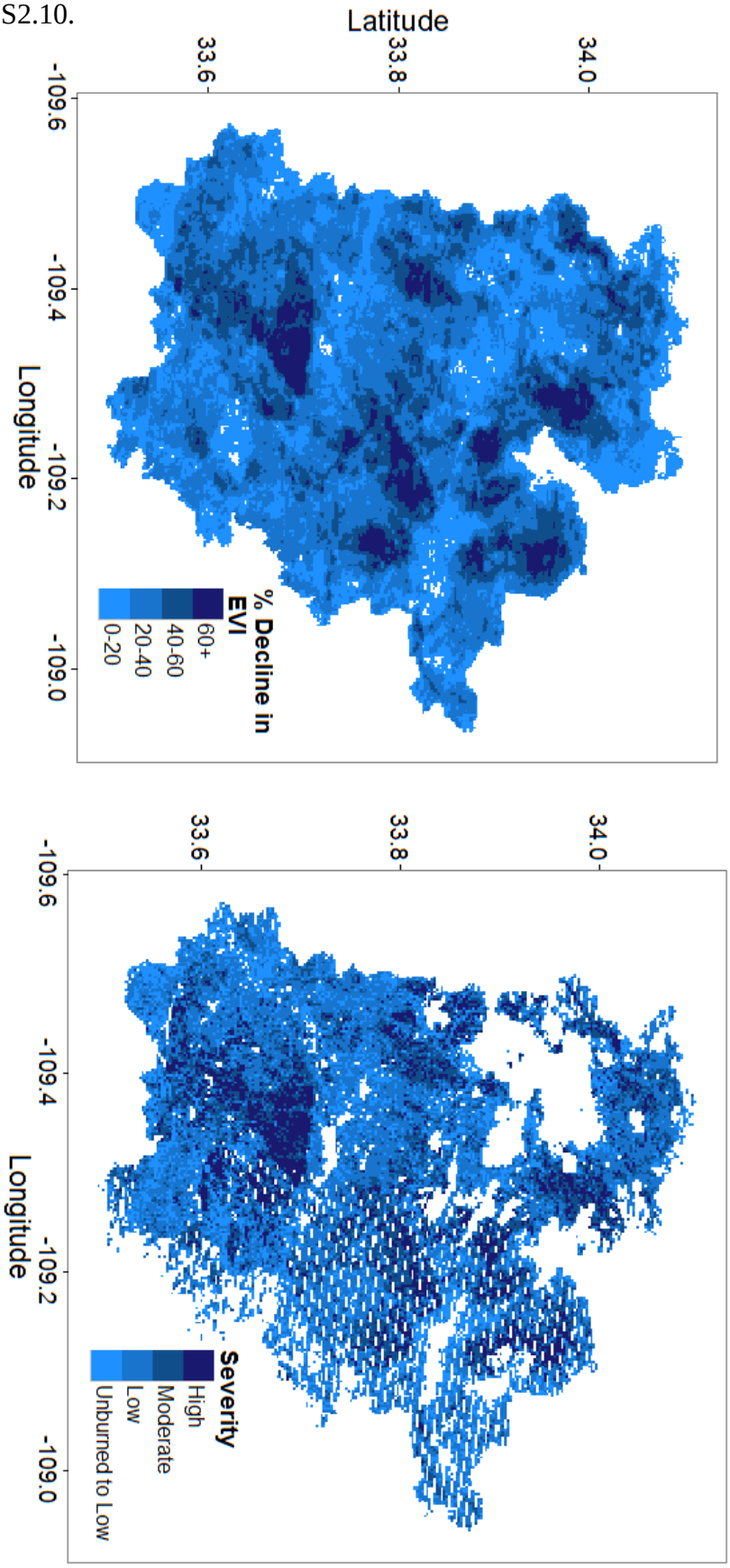
Latitude
33.6
33.8
34.0
-109.6
-109.4
-109.2
-109.0
Longitude
% Decline in EVI
60+
40-60
20-40
0-20
Severity
High
Moderate
Low
Unburned to Low

Supplementary Tables

Table S2.1. Area affected by detected disturbances in each ecoregion.*

Ecoregion	Bark Beetles (Mha)	Defoliators (Mha)	Fire (Mha)	Unknown (Mha)
Cold Deserts	0.003	0.001	0.033	0.307
Warm Deserts	0.000	0.000	0.002	0.029
Mediterranean CA	0.004	0.000	0.228	2.417
Sierra Madre	0.000	0.000	0.034	0.139
Upper Gila Mountains	0.174	0.008	0.348	2.134
Western Cordillera	0.499	0.249	0.943	5.868
Marine West Coast Forest	0.000	0.000	0.023	1.499
Temperate and West Central Semi-Arid Prairies	0.004	0.009	0.033	0.203
South Central Semi-Arid Prairies	0.000	0.000	0.002	0.068
Total Area (all ecoregions)	0.685	0.268	1.646	12.665
Total Area (all disturbance types and ecoregions)		15.264		

* Area is estimated by the area of a pixel by the number of pixels in each category. Pixels are 250 m x 250 m.

Table S2.2. Pre- to post-disturbance changes in JJA LST and GPP.**

Ecoregion	Change in LST (°C)	% Change in GPP
	Fires	
Cold Deserts	4.57 ± 3.45*	-28.19 ± 26.07*
Warm Deserts	3.55 ± 2.47*	-41.49 ± 23.81*
Mediterranean CA	3.36 ± 3.33*	-28.05 ± 15.62*
Sierra Madre	3.61 ± 2.91*	-23.17 ± 37.76*
Upper Gila Mountains	3.67 ± 3.23*	-27.64 ± 32.70*
Western Cordillera	3.39 ± 2.82*	-23.96 ± 16.09*
Marine West Coast Forest	1.10 ± 1.98*	-4.72 ± 11.38*
Temperate and West Central Semi-Arid Prairies	3.61 ± 3.43*	-19.96 ± 16.54*
South Central Semi-Arid Prairies	5.45 ± 2.42*	-28.47 ± 13.01*
$\bar{x}$	3.45 ± 3.02*	-25.05 ± 21.67*
	Bark Beetles	
Cold Deserts	0.12 ± 3.00	2.22 ± 20.75*
Warm Deserts	0.01 ± 0.87	29.86 ± 37.09*
Mediterranean CA	0.36 ± 2.16*	-1.02 ± 17.01
Sierra Madre	-0.05 ± 3.13	13.28 ± 58.20
Upper Gila Mountains	0.35 ± 3.12*	1.38 ± 33.87*
Western Cordillera	0.92 ± 3.00*	-4.43 ± 13.80*
Marine West Coast Forest	0.75 ± 2.07	3.56 ± 5.75
Temperate and West Central Semi-Arid Prairies	-0.18 ± 2.89	2.36 ± 12.43*
South Central Semi-Arid Prairies	0.91 ± 3.78	3.30 ± 25.19
$\bar{x}$	0.76 ± 3.04*	-2.84 ± 21.06*
	Defoliators	
Cold Deserts	2.68 ± 3.00*	-0.83 ± 8.68
Warm Deserts	NA	NA
Mediterranean CA	1.21 ± 0.58	-4.51 ± 10.97
Sierra Madre	-0.56 ± 2.12	3.87 ± 14.81
Upper Gila Mountains	-0.48 ± 2.94*	9.68 ± 27.91*
Western Cordillera	0.53 ± 3.13*	-0.66 ± 14.74*
Marine West Coast Forest	NA	NA
Temperate and West Central Semi-Arid Prairies	0.23 ± 2.94*	2.68 ± 14.40*
South Central Semi-Arid Prairies	NA	NA
$\bar{x}$	0.49 ± 3.12*	-0.23 ± 15.40*
	Unidentified Disturbances	
Cold Deserts	0.76 ± 3.08*	3.62 ± 23.36*
Warm Deserts	0.43 ± 2.64*	9.13 ± 42.16*
Mediterranean CA	0.22 ± 2.35*	1.31 ± 17.87*
Sierra Madre	0.54 ± 2.77*	11.48 ± 68.57*
Upper Gila Mountains	0.00 ± 2.88	8.03 ± 36.55*
Western Cordillera	1.12 ± 3.17*	-0.35 ± 20.28*
Marine West Coast Forest	1.48 ± 3.24*	0.85 ± 12.32*

Temperate and West Central Semi-Arid Prairies	0.15 ± 3.04*	4.11 ± 17.63*
South Central Semi-Arid Prairies	-0.15 ± 2.97*	9.26 ± 35.99*
$\bar{x}$	0.76 ± 3.03*	1.89 ± 24.20*

** Format is mean ± standard deviation. Highlighting indicates values that do not overlap zero. * indicates values that were significantly different from zero ($p < 0.01$) in a one sample t-test [R Core Team, 2013].

Table S2.3. Detection accuracy assessment using polygon data from USFS Aerial Detection Surveys (ADS) and Monitoring Trends in Burn Severity (MTBS). Table (a) contains overlap results for detections from this paper. Table (b) contains results for Vegetation Change Tracker (VCT) detection data. Polygon summaries are made for polygons that either contained detections or did not.

(a) BFAST

Disturbance	Validation Source	Severity Measure	Total Polygons	Polygons with Detections (%)	Total Polygon Area (Mha)	Polygons with Detections Area (Mha)(%)	Severity in Detected Polygons	Severity in Undetected Polygons	T-test p-value
Bark Beetles	Aerial Detection Surveys	Trees Per Acre	362636	24882 (7%)	8.01	3.20 (40%)	11.45	7.70	<0.01
Defoliators	Aerial Detection Surveys	Trees Per Acre	25218	8210 (33%)	3.08	2.19 (71%)	17.84	29.35	0.62
Fire	MTBS Data	Burn Severity	2564	2393 (93%)	28.83	27.54 (96%)	2.59	1.95	<0.01
UD	Aerial Detection Surveys		121847	8010 (7%)	1.88	0.73 (39%)	7.66	5.05	<0.01

(b) VCT

Disturbance	Validation Source	Severity Measure	Total Polygons	Polygons with Detections (%)	Total Polygon Area (Mha)	Polygons with Detections Area (Mha)(%)	Severity in Detected Polygons	Severity in Undetected Polygons	T-test p-value
Bark Beetles	Aerial Detection Surveys	Trees Per Acre	362636	16926 (5%)	8.01	4.09 (62%)	12.30	7.72	<0.01
Defoliators	Aerial Detection Surveys	Trees Per Acre	25218	6441 (26%)	3.08	2.11 (69%)	19.53	32.06	0.29
Fire	MTBS Data	Burn Severity	1988	1812 (91%)	14.16*	13.50 (95%)	2.59	1.85	<0.01
UD	Aerial Detection Surveys		121847	5409 (4%)	1.88	0.83 (44%)	8.26	5.06	<0.01

Table S2.4. Percent BFAST/Hansen dataset points within specified distances from VCT points.

Disturbance Type	Distance (m)	Percentage (%) BFAST/Hansen points
Fire	1000	96.77
	750	95.23
	500	92.44
	250	87.34
Bark Beetles	1000	75.88
	750	69.08
	500	60.58
	250	50.49
Defoliators	1000	68.23
	750	60.37
	500	51.50
	250	41.70
UDs	1000	59.98
	750	51.18
	500	41.76
	250	32.44
All disturbance types	1000	69.89
	750	62.61
	500	54.40
	250	45.60

CHAPTER 3

Application of random forest for the detection and attribution of forest disturbance

INTRODUCTION

Accurate assessments of current and future disturbance characteristics and trends are essential for understanding the ecological processes and interactions within and among landscapes [McDowell et al., 2015]. Current methods to detect forest disturbances use time series modeling or temporal decomposition on individual pixels (pixel of interest; POI) in order to detect when disturbances occur across landscapes [e.g., Kennedy et al., 2010; Verbesselt et al., 2010; Zhu et al., 2012]. These temporal approaches work well when applied to regions for which they have been tuned, but struggle when applied to new areas. Additionally, the temporal approaches require a separate method to be applied after the detection process in order to attribute the detected disturbances. Previous research has mentioned the potential for spatial spectral information to improve detection and attribution methods [Rich et al., 2010]. While several studies have used neighborhood pixel information (NPI) to attribute disturbances once detected using a temporal POI approach [Kennedy et al., 2015; Shimizu et al., 2017; Zhao et al., 2017], none have used spatial information simultaneously for the detection and attribution of disturbances. The incorporation of spatial data (e.g., NPI) may improve detection algorithms in addition to attribution algorithms by reducing the reliance of detection methods on perfect time series data and adherence of disturbance events to defined thresholds of change. However, despite the awareness of its potential uses, the reliance of most detection algorithms on computationally-intensive time series decomposition or modeling has limited the incorporation of spatial data thus far.

The advent of free, publicly-available, Landsat data in 2008 has made increasingly innovative methods for detecting and attributing forest disturbances possible

[McDowell et al., 2015]. For example, using dense time series of Landsat imagery, it is now possible to assess areas of forest loss and gain globally [Hansen et al., 2013]. However, it remains a challenge to efficiently and accurately detect and attribute forest disturbances across varying disturbance and forest types. It is especially difficult to detect low severity disturbances [Cohen et al., 2017]. Several model ensemble methods have been proposed to improve disturbance detection accuracy across varying forest types and for low intensity impacts. Ensemble approaches integrate results from multiple algorithms [Healey et al., 2018], or multiple spectral bands or indices [Cohen et al., 2018]. This approach substantially decreases both commission (i.e., false positive) and omission (i.e., false negative) errors, but are computationally intensive as many iterations of detection must be completed before the secondary classification process.

Researchers are beginning to incorporate API into attribution methods that make use of the temporal detection (POI) approaches [Kennedy et al., 2015; Shimizu et al., 2017; Zhao et al., 2017]; however, API may also be of use in the detection of forest disturbances. Disturbances do not occur in isolation, and therefore it is likely that if changes in the spectral band or index values are observed in a single pixel, neighboring pixels may also show similar changes. Thus, incorporating information on neighboring pixels into models of disturbance presence or absence may substantially improve our abilities to find disturbances of low severity or where time series data are incomplete or noisy due to the presence of clouds or snow. Additionally, the incorporation of API into the detection process enables a natural link of detection with attribution, making it possible to complete both processes using one analysis pipeline. For attribution, the characteristics of the neighboring pixels allow for differentiation between disturbance

types because disturbances often vary considerably in their spatial heterogeneity. For example, high severity fires may affect all pixels in an area similarly due to non-selective mortality or may impact all pixels within a short time frame. In contrast, a bark beetle outbreak might only affect some species in the area, leading to more patchy changes in spectral measures over the same area over a longer time period.

Adding NPI into the disturbance detection process requires the development of new detection methods. With temporal methods, each pixel is marked simply by the presence or absence of a clearly-defined change in the band or index. With the inclusion of NPI, this approach must be modified to look at the results of nearby pixels. Machine learning may help to solve this problem. Rather than look at the time series as something continuous, it is possible to break down the results of both temporal (POI) and spatial (NPI) components of the area (e.g., overall spectral change in the area, pre-break variance in spectral indices). The spatial and temporal components of each pixel represent potentially large numbers of variables, none of which are ideal for detecting disturbance on their own. It is more likely that a combination of the variables is best able to describe disturbed areas, but this presents a difficult problem for most user-defined models in that choosing the correct variables out of the many available requires a lot of time and effort. Machine learning methods are well-suited for this problem and are capable of efficiently using large quantities of variables to produce models to make decisions regarding the presence or absence of disturbance. This eliminates the need for the user to define complex rules governing when or where a disturbance can occur and allows for the incorporation of many variables that may be important for defining disturbance in a given area. Additionally, machine learning approaches such as Random Forest or Support

Vector Machines tend to be computationally efficient [Lippitt et al., 2008; Rodriguez-Galiano et al., 2012], reducing the resource requirements for the detection and attribution processes.

Machine learning has been applied to disturbance detection and attribution in several previous analyses, although primarily on either POI time series approaches [Huang et al., 2008; Lippitt et al, 2008; Rogan et al., 2008; Healey et al., 2018], or solely for attribution [Zhao et al., 2015; Shimizu et al., 2017]. Using only temporal spectral data, detection of partial forest harvest was up to 94% accurate in central Massachusetts [Lippitt et al., 2008], and detection of varying disturbances was ≥ 80% accurate in 19 Landsat scenes from around the world [Huang et al., 2008]. While both of these approaches are promising, they are limited by the training requirements and data preparation steps because high-quality, temporally-dense, Landsat data were not yet publicly available at the time of the studies. More recently, machine learning has been applied to the attribution of detected forest disturbances. Attribution accuracies of wildfires, harvests, and 'other disturbances' using Support Vector Machines in the Greater Yellowstone Ecosystem yielded 87% overall accuracy [Zhao et al., 2015], while attribution accuracies of harvests, 'water invasions', urbanization, 'other changes', and areas of recovery were ~85-96% accurate using a Random Forest approach in the Bago Mountains, Myanmar [Shimizu et al., 2017]. These applications show the promise of machine learning approaches for both detection and attribution. Using machine learning for both steps within a single analysis pipeline could result in similarly high accuracies as previous studies, while decreasing the amount of time and effort spent on the analysis. Additionally, while previous detection studies reported high accuracy results, they tended

to be focused on either single disturbance types or high severity disturbances. Combining detection and attribution steps while incorporating NPI could improve the reliability of results when searching for many disturbance types, including low severity disturbances.

Current methods for disturbance detection are less successful when applied to regions in which they were not developed [Cohen et al., 2017]. This represents a significant obstacle for the regular detection of disturbances globally. Detection algorithms do not work as well in areas for which they were not developed primarily because disturbances differ among ecosystems depending on myriad factors, including forest vegetation, climate, topography, and management. In short, parameters of forest disturbances are not stationary and models that assume stationarity are limited in their scope [e.g., Fotheringham et al., 1996]. By looking only at POI patterns of spectral change, it is extremely difficult to find reproducible patterns that will consistently find disturbances regardless of ecosystem properties. As mentioned previously, the use of a flexible machine learning framework that also incorporates NPI may reduce errors related to this issue. The ability of machine learning algorithms to relax assumptions of stationarity of model parameters may be beneficial in this circumstance, because different models may be fit to different regions without the user specified parameters that may be biased. Additionally, by incorporating NPI, the exact temporal patterns of specific regions matter less, as other variables are also considered. Finally, while this approach may help to improve the ability of disturbance detection and attribution methods to be applied more broadly, it may also help to elucidate how disturbance and forest characteristics change across space. Specifically, the output of methods such as Random Forest allow for the determination of variable importance, which may provide valuable

information about the typical temporal and spatial characteristics of disturbances among varying forest types. By understanding how disturbance characteristics vary across the landscape, we can work to further improve our detection and attribution methods, and also to enhance our understanding of disturbance impacts on ecosystem patterns and processes [Cooper et al., 2017].

Here, we test this concept by developing a new approach for both the detection and attribution of forest disturbances. In addition to using Random Forest models for both steps, we also incorporate spatial information on the area surrounding each POI. Our objectives with this new approach are to determine the usefulness of both temporal and spatial information for disturbance detection and attribution, and to determine whether a machine learning approach utilizing both types of information improves the accuracy of detection across multiple regions. We also seek to understand how disturbances differ across forest types, and how those differences might complicate traditional temporal approaches to disturbance detection. Specifically, with this approach, we ask, how do variables important for disturbance detection and attribution vary among regions?

METHODS

Site selection

Study sites (Fig. 3.1; Table 3.1) were selected to match those of previous studies presenting methods of disturbance detection using satellite imagery [Healey et al., 2018] so as to allow for direct comparison of our results with those from other analyses. These sites also represented a range of forest functional types and disturbance types. Sites selected included a warm summer Mediterranean mixed conifer forest in southwestern Oregon, a warm summer continental Mediterranean spruce-fir forest in northern

Colorado, a warm summer humid continental mixed pine forest in northeastern Minnesota, a warm summer humid continental spruce-fir forest in western Maine, humid subtropical mixed hardwood and pine forests in eastern Pennsylvania and New Jersey, and a humid subtropical mixed hardwood and pine forests in southern South Carolina. An additional Landsat scene covering the Olympic Peninsula in Washington state was included in the analysis to allow for a better understanding of the performance of the pipeline in an additional economically-important forest type (i.e., temperate rainforest/coastal mixed conifer), and to enhance our understanding of the ability of the pipeline in a natural forested system relative to a heavily human-impacted system. The added area, composed of mixed conifer forests shifting towards temperate rainforests in the western side of the peninsula, encompasses both Olympic National Park and national forest and private lands in which substantial clear-cutting has been practiced. This diversity of management provides a unique opportunity to analyze both human-caused and natural disturbances within a single region.

Random Forest models

Random Forest models were used for both the detection and attribution components of the pipeline developed for this study because they have proven to be effective in past approaches to the disturbance detection and attribution problems [Lippitt et al., 2008; Kennedy et al., 2015; Schroeder et al., 2017; Cohen et al., 2018; Healey et al., 2018]. Random Forest models use ensemble learning methods for classification or regression; here, we use them for classification. Random Forest models are randomized decision trees, which may be much less prone to model overfitting than ordinary decision tree methods. Random Forest models take multiple random subsets of the complete

training dataset and create decision trees with each subset. When data are then run through the model (i.e., set of decision trees), the result (disturbance class) with the most votes from all trees is the predicted class.

Data preparation

Forty-seven spatial and temporal variables were created in R as potential predictors for the disturbance detection Random Forest model (Fig. 3.2).Temporal variables were calculated using 2000-2016 NDVI time series for a single pixel, and spatial variables were calculated using 2000-2016 NDVI time series for all pixels within a 450m x 450m window around the pixel of interest. NDVI was selected for this analysis due to its widespread use in previous studies [e.g., Mildrexler et al., 2007; Verbesselt et al., 2012] and its relative simplicity to calculate. Temporal predictor variables were produced using several models fit to the time series, including a simple smoother (loess), a simple linear model [R Core Team, 2017], and a regression tree [Therneau et al., 2017]. These variables provided different information on breaks in the time series, overall trend, locations of maxima and minima, and trend in NDVI recovery if a negative break in the time series (decline in NDVI) occurred. Variables not derived via models provided further information on overall time series characteristics such as pre- and post-disturbance variation (Fig. 3.2). While many variables were included in the analysis, all were considered due to observed differences between disturbed pixel time series and undisturbed pixel time series.

NDVI data were prepared in Google Earth Engine using both Landsat 5 and Landsat 7 surface reflectance images. Areas with clouds, shadows, water, and snow were removed from all tiles from the study period (2000-2016) using the information included

in QA bands, which are derived using CFMask. The USGS surface reflectance data had been atmospherically-corrected using the LEDAPS pre-processing methods, and orthorectified prior to our use [https://landsat.usgs.gov/sites/default/files/documents/ledaps_product_guide.pdf]. Summertime mean (June-July-August; JJA) NDVI was calculated using all available annual imagery over the region and study period. If both Landsat 5 and Landsat 7 imagery were available, all surface reflectance images from both satellites were used in the calculation of the average. Data were aggregated from 30m to 90m resolution so as to reduce computational requirements, while maintaining the ability of the pipeline to assess stand-scale changes in NDVI.

Detection modeling

Data for Random Forest models were trained using a multi-step method. First, each Landsat scene was split into 9 blocks in order to reduce computational requirements. Either 0.01% of the data or 350 pixels were sampled from one block of the scene, depending on which sample was larger. For each pixel in the sample, human observers were shown a time series of NDVI images for the area surrounding the pixel, a recent true-color satellite image (via Google Earth), and a line plot of NDVI over the study period fitted with a loess curve. Observers marked each pixel with a binary value, either disturbed or undisturbed. These methods are very similar to those from TimeSync [Cohen et al., 2010], as they were derived from that training approach. We used similar methods developed in R for this analysis, rather than using TimeSync, because we wanted the resulting pipeline to be seamless. Using TimeSync would have meant that users would have to exit the pipeline, train data in a separate setting, and then export data and return

to the original pipeline. The streamlined method we have developed here will minimize the number of programs required by users of the pipeline.

Following training, a Random Forest model was fit with the ‘rf’ model option [Liaw & Wiener, 2002] in the ‘caret’ package in R [Kuhn, 2017]. All 47 variables were considered in the model. The resulting detection model was used to classify all pixels within each Landsat scene as either disturbed or undisturbed.

Attribution data preparation

Seventeen new spatial variables were created using the detection results to be used for attributing disturbances (Fig. 3.2). These variables relied on only those pixels which had been marked as disturbed by the initial model, and describe the similarity in disturbance characteristics within 450m x 450m windows surrounding each pixel (Fig. 3.2). For example, many of these variables describe how similar disturbed pixels were in terms of magnitude, duration, or other time series characteristics within neighboring areas.

Attribution modeling

Data for a second Random Forest model for attribution were trained with the initial variables in addition to the new spatial disturbance variables using the same method as for the detection data. However, in developing the training points for this model, points were labeled with the type of disturbance at each location rather than just the presence or absence of disturbance. When unsure of the disturbance type, we checked the point using historical imagery in Google Earth Pro. As the detection model had the potential to return false positives, we added a ‘0’ disturbance class indicating points where no disturbance had actually occurred. This allowed for the removal of detection

errors due to data abnormalities such as those resulting from the Landsat 7 failure of the scan line corrector. Other disturbances included biotic disturbances (e.g., bark beetles or defoliators), fire, harvest, wind, flooding or changes in river path, land use change (e.g., subdivision development), and landslides. These categories were user-defined and are therefore flexible for studies with varying objectives.

A model for the attribution of points was fit using the same method as the detection model. The resulting model was used to classify the pixels marked disturbance by the initial detection model into individual disturbance classes (Fig. 3.3). Output from this final step included a map of disturbance locations and types, as well as a map of disturbance year (Fig. 3.3). Disturbance year for each pixel was already determined for the creation of several spatial predictor variables (Fig. 3.2) using a simple time series break detection method [Zeileis et al., 2002; Zeileis et al., 2003].

Validation

The results of the attribution model were assessed using three measures. First, we assessed if a disturbance had actually occurred in the labeled points. Second, we assessed if no disturbance was present in the unlabeled points. Third, we assessed the accuracy of the disturbance date produced from the model. Out-of-bag accuracy assessments were completed using first historical satellite imagery in Google Earth Pro, and second, the training methods described previously. Validation was completed for two sections of each Landsat scene, both the block used for training as well as a separate block that was randomly selected from the remaining non-training blocks within the scene. Accuracy metrics were calculated using simple accuracy and Cohen's kappa statistic.

RESULTS

Detection and attribution accuracy

Detection errors varied considerably among the seven study regions. Simple commission rates were 12 ± 6% (accuracy of identified pixels, $\kappa = 0.77 \pm 0.12$), and omission rates were 17 ± 12% (accuracy of all disturbed pixels, $\kappa = 0.66 \pm 0.23$) (Fig. 3.4). Lower-severity areas of biotic disturbances in Northern Colorado led to the highest rate of false negative results (40%; $\kappa = 0.20$) (Fig. 3.5). The highest rates of false positives (23%; $\kappa = 0.54$) occurred in Eastern Pennsylvania. Incorrect attribution to disturbance type occurred at rates of 3 ± 3% ($\kappa = 0.95 \pm 0.06$) (Fig. 3.6), with the highest rates occurring in Oregon, and the lowest rates occurring in South Carolina (Fig. 3.6). It should be noted that South Carolina only had one major disturbance type, while Oregon had several. The most commonly misidentified disturbance type in Oregon was fire, which was most frequently misclassified as harvest.

The year of disturbance was identified correctly in 41-79% of the correctly-identified disturbances, with 73-95% of disturbances dated to within 3 years of the true disturbance date (Fig. 3.7). The lowest accuracy rate for disturbance year was in Minnesota, while the highest accuracy rate for disturbance year was in Oregon. All regions other than Minnesota were ≥59% accurate in correctly identifying the year of disturbance.

Accuracy rates were similar within the randomly-selected blocks outside the training area. Commission rates were 16 ± 7% (accuracy of identified pixels, $\kappa = 0.68 \pm 0.13$), and omission rates ranged were 11 ± 11% (accuracy of all disturbed pixels, $\kappa = 0.77 \pm 0.21$) (Fig. 3.4, Fig. 3.5). The highest and lowest rates of each error type occurred in the same regions as in the original validated training area. Incorrect attribution errors

occurred at similar rates as seen in the training area for most regions (Fig. 3.6). However, both Minnesota and Pennsylvania showed substantially higher mis-attribution rates (29% and 86%, respectively) due to the presence of novel, or differently represented, disturbance types in the randomly selected external blocks. The primary disturbance type in Pennsylvania shifted from harvest to land development, while in Minnesota there was significant mining activity in the external validation block that was mistaken for harvest. Accuracies for the disturbance date were similar to those from the primary training block (Fig. 3.7).

Geographic variation in disturbance characteristics

The variables selected to model disturbance presence/absence and type were inconsistent among regions (Table 3.2). However, each final detection and attribution model contained at least one spatial and one temporal variable. Temporal variables held more importance for determining the presence of disturbances, while spatial variables were more important for classifying the type of disturbance. There were no clear geographic patterns in variable importance.

The most important predictor variables for both detection and attribution models tended to relate to either the magnitude of the disturbance, the overall trend of the NDVI time series, or the minimum slope found between points in the time series (Table 3.2). Spatial equivalents of these variables were also deemed important in many of the models. Additionally, the loess slope variables tended to be much more important than the regression tree slope variables or raw time series slope variables, although some of those variables were among the top 5 most important variables in several models. Overall, disturbance dates (e.g., range in dates over the area) and durations were not especially

important in the models. Characteristics of NDVI in the area (e.g., average NDVI, variance in NDVI) were occasionally among the variables in the models.

Comparison of detection and attribution results from two forest regions

Products resulting from the introduced pipeline demonstrate how forest disturbance characteristics vary in different locations and how those differences might influence disturbance detection and attribution. We focused on results from two different forest types, coastal coniferous forests in Washington and humid subtropical mixed forests in South Carolina, to further demonstrate these patterns (Table 3.1). The primary disturbance types in Washington were timber harvest, wildfire, and changes in river paths, while the primary disturbance types in South Carolina were timber harvest and land development.

We were successful in locating a number of disturbance events in both locations (Fig. 3.8). The Washington state results were particularly striking in demonstrating differences in disturbance types and frequencies within and outside Olympic National Park. Disturbance locations were much more homogenous over the region in South Carolina. The difference in disturbance characteristics between the two regions was demonstrated well by observing the distributions of the variables used in the attribution models for each disturbance type (Fig. 3.9). Overall temporal patterns were similar between the two forested regions, both for disturbed and undisturbed pixels (Fig. 3.10). However, timber harvests in Washington tended to have greater magnitude drops in NDVI.

DISCUSSION

The results of this analysis were comparable to forest disturbance detection results from strictly temporal detection approaches. Similarly to other studies [e.g., Zhu et al., 2012; Cohen et al., 2018; Healey et al., 2018], our pipeline seemed to result in better accuracy for large, severe disturbances (e.g., clearcut harvests in western Washington), than for smaller and less severe disturbances (e.g., beetle-kill in some areas of northern Colorado). Additionally, while our detection year was close to the true disturbance year for large and severe disturbances, accuracy declined as disturbances became smaller, more spatially distributed, and less severe. Results may be improved by using finer resolution data and improving our methods for interpolating missing values of NDVI. Despite room for improvements, the similarity in detection accuracies between our approach that uses multiple time series-derived metrics, and other approaches that use time series decomposition and modeling, is promising. Specifically, while accuracy rates were not substantially improved, the method did improve the efficiency with which users might achieve those accuracy rates. Additionally, this method allows users to simultaneously detect and attribute disturbances rather than having to use two different approaches for each step.

The pipeline introduced here is one of the first, to our knowledge, to use spatial information (i.e., NPI) for both the detection and attribution of forest disturbances. Although not formally tested here, the incorporation of NPI has the potential to reduce the likelihood of false negatives and improve our ability to detect low severity disturbances or disturbances in areas with frequently cloudy or snowy conditions, as disturbances may be identified even if the pixel of interest does not show a clear drop in NDVI. This allows users to make use of more incomplete datasets and may therefore be

useful in areas of the world with less complete collections of satellite imagery. Additionally, the incorporation of NPI into disturbance detection allows for more clear-cut differentiation of data abnormalities from true disturbances, as forest disturbances tend to have fairly distinct spatial characteristics. Specifically, the incorporation of NPI is useful for removing false detections related to our use of Landsat 7 during the years in which the scan line corrector failed. While these areas were labeled using our detection model, composed of primarily POI variables, they were easy to remove (i.e., mark as false positives) in the secondary attribution step, which was completed using models composed primarily of NPI variables. Therefore, the incorporation of NPI into disturbance detection [Rich et al., 2010] has the potential to improve our ability to accurately and efficiently detect disturbances across a wide variety of forest types around the globe.

In addition to incorporating NPI to detection and attribution models, we also used machine learning (i.e., Random Forest) to classify pixels into disturbance and non-disturbance categories, and then into different types of disturbance. While several studies have made use of Random Forest models for the attribution component of this process, it is a novel application to also use those models for the detection component. We believe that this application simplifies and improves the detection component by limiting reliance on perfectly processed time series data. Rather than looking at the time series as a whole, the model uses general characteristics of the series, such as overall variance and slope, to create rules for what disturbed pixels look like relative to undisturbed pixels. Thus, while some undisturbed pixels may show declines in NDVI, they are not necessarily classified as disturbance because there are many variables involved in classification, not just the

presence or absence of a 'break.' The use of regionally-specific training data also improves the classification process, by allowing forests to have different 'typical' characteristics. For example, some forests show increasing trends in greenness over the study period, while others have slight depressions in some years due to a regional drought. The use of many variables in combination with localized training allows the algorithm to incorporate these characteristics, and is therefore more robust in the face of variable climate and differing forest ages. In short, most disturbances are more complicated than a simple temporal 'break' in spectral indices, and using a machine learning approach with many potential variables improves the region-to-region accuracy of detection and attribution algorithms substantially.

We considered a wide variety of potential variables in the detection and attribution classification models. Thus, the relative importance of those variables across regions is useful for determining patterns in disturbance characteristics across regions. None of the regional models used the exact same subset of variables for either detection or attribution. While all made use of at least one NPI and one POI variable in both detection and attribution components, the relative importance of those variables types differed considerably (Table 3.2; Figs. S3.1 & S3.2). We expected that there would be latitudinal or longitudinal patterns in variable importance, and therefore disturbance characteristics; however, consistent patterns were not apparent in our results despite clear variation in importance among regions. We believe that this is due primarily to differences in the background (i.e., undisturbed) forest conditions, although it is also possible that we simply did not use a large enough sample of regions to determine patterns of variable importance. It was necessary to spend considerable time familiarizing

ourselves with the characteristics of the forest both in terms of appearance and general time series characteristics, before completing the training for each region because the typical characteristics differed considerably. As such, while disturbances may be similar in many respects between regions, the environment in which they occur may not be and may in fact be more important than the disturbance characteristics themselves when searching for disturbances.

Cohen et al. [2017] found that detection algorithms are substantially less successful when applied to regions in which they were not developed. Our results suggest that this may be due to the differences in how disturbed areas relate to undisturbed areas within regions. As mentioned previously, while disturbance characteristics may be similar across some regions, the background forest conditions in which those disturbances occur may differ considerably. However, in addition to background conditions, the actual disturbance characteristics themselves also differ considerably, especially when shifting across management zones [Niemelä, 1999] and from evergreen to deciduous forests. A semi-arid, evergreen forest managed for recreation and fire risk mitigation will differ completely in terms of both background and 'typical' disturbance relative to a humid subtropical, deciduous forest managed for timber harvest. These readily apparent differences between forest types and disturbance regimes likely account for the poor transferability of POI-based disturbance detection approaches to different regions without substantial re-tuning. A similar approach to that introduced here, whereby training data for each region are used to create completely different models for separate regions, may prove useful in the future. This method could be scaled rapidly by compiling a database of training points. However, a necessary intermediate step is to

determine the density of training data required to produce sufficiently accurate results while minimizing effort. It would also be helpful to determine the region size within which predictions are most accurate (i.e., Landsat scene, ecoregion, etc.).

This approach remains a challenge over large regions due to the uncertainty surrounding required training point density. Currently, the pipeline developed for the analysis is most useful at the local to landscape scale. At these scales, users may quickly train points for their study region and produce accurate detection and attribution results in a matter of hours, depending on computational resources. The analysis presented here was completed on a single desktop computer with four cores and <8 gigabytes of memory, with a single Landsat scene taking 2 days of computing time from the beginning of the analysis to the end. This makes the approach very accessible for most ecologists and may therefore prove useful for studies in which high-resolution disturbance data are required over a landscape. Additionally, as the approach does not depend on any one type of data, multiple data types and resolutions can easily be used depending on the desired results. While we use upscaled Landsat data here, future analyses could use 30m resolution Landsat data or 250m MODIS vegetation index data. Additionally, we used NDVI for the spectral index. However, other studies have demonstrated that shortwave infrared (SWIR)-based indices are much more effective for disturbance detection [Schultz et al., 2016; Cohen et al., 2018]. These indices could be applied to this approach easily, potentially improving detection accuracy. Additional increases in accuracy might be achieved by also integrating factors such as topographic wetness index, or land surface temperature.

While the pipeline created for this analysis demonstrates the potential for improvement in current disturbance detection and attribution approaches, there are several limitations to the current analysis. First, our results were limited by the use of only summertime NDVI values for the analysis. We masked out clouds, cloud shadows, and other areas marked as being of low quality, but this resulted in a significant number of pixels with large chunks of missing data. For this study, we filled in these pixels with NDVI averages. This approach led to flattened time series in which trends in NDVI over time were less visible and therefore less able to be classified. The use of spatial information mitigated this problem somewhat, but a better method for the interpolation of missing data points, or the use of better-prepared data [e.g., Robinson et al., 2017], would further improve the algorithm. A separate problem with this approach is the need for good training data for both the detection and attribution models. Most disturbance models require some tuning for each region in which they are applied, so this is not a unique problem to this approach. However, this approach relies solely on those training data for determining the accuracy of the models and is therefore capable of producing both extremely good or extremely poor results depending on the abilities of the trainer. When using this pipeline, it is very necessary to become familiar with the typical characteristics of the region and to train a sufficient number of points so that a few mistaken training points do not have too strong an influence on the results. More work should be done to determine both the best density of training points and the sensitivity of the models to the presence of 'bad' training points [e.g., Rogan et al., 2008].

CONCLUSIONS

Disturbance detection and attribution methods may be improved through the incorporation of spatial information in addition to temporal information. Detection and attribution may also be made more efficient and regionally-robust by using machine learning (e.g., Random Forest) approaches with many potential predictor variables rather than strictly temporal pixel-level data. We found that while accuracy varied across regions and among disturbance types, the false positive and negative rates using these new methods were similar to those from strictly temporal approaches. In addition, we found that the variables important for disturbance detection and attribution varied considerably across regions, with at least one spatial and one temporal variable included in each model. This suggests that both disturbance characteristics and the environment in which they occur vary considerably by forest type and local environmental conditions. These differences may explain why other algorithms are very successful in one region, while losing much of their accuracy in others. The pipeline introduced here was aimed at demonstrating how spatial information and a machine learning approach could be used to improve the efficiency of current detection and attribution methods. However, the resulting methods may be useful when applied to landscape-level studies and are freely available online as a set of scripts and functions. With continued improvements of both this and previously-developed detection and attribution algorithms, we will soon be able to accurately and efficiently detect forest disturbances at the global scale.

FIGURES AND TABLES

Figure Legends

Figure 3.1. Location of Landsat scenes around the United States. Black boxes show the bounding boxes around the scenes.

Figure 3.2. Full set of variables considered for the Random Forest detection and attribution models. Gridded boxes show the spatial domain of each variables (in grey). For disturbance spatial variables, the grey-shaded boxes represent pixels in which example disturbances were detected during the detection phase of the pipeline. These variables were not considered for the detection model as they are derived from that model. The red asterisk in the spatial variable gridded box shows the pixel of interest, used to calculate the ratio of that pixel's value relative to all values in the box. Variable markers are as follows: (1) associated with disturbance characteristics, (2) associated with general time series characteristics, (3) disturbance timing, (4) associated with overall forest NDVI characteristics, (*) characterization of average trend over the area, (**) measure of the variable texture over the area, (***) measure of the POI relative to the neighboring pixels.

Figure 3.3. Pipeline for detecting and attributing forest disturbances using Landsat data. Grey boxes represent the final output images.

Figure 3.4. Omission (false negative) and commission (false positive) error rates for each region, based on the validation samples.

Figure 3.5. Classified omission errors. Error type represents the type of disturbance that was missed. (a) bars show validation results from the original training block (not including the training points), while (b) bars show validation results from the randomly-selected alternative block.

Figure 3.6. Classified incorrect attribution errors. Error type represents the actual type of disturbance vs. the labeled type of disturbance (labeled / actual). Maine had no misattributed disturbances because all disturbances were of a single type. (a) bars show validation results from the original training block (not including the training points), while (b) bars show validation results from the randomly-selected alternative block.

Figure 3.7. Distance in years between detected disturbance date and actual disturbance date within validation samples for each region.

Figure 3.8. Example output for the (a) Washington, and (b) Colorado regions. Colors show disturbance type, while the saturation of the color indicates the disturbance date.

Figure 3.9. Density plots of the variables in the Random Forest attribution model for the (a) Washington state and (b) Colorado Landsat scenes, separated by disturbance type.

Figure 3.10. Time series of summertime (JJA) NDVI for (a, b) Washington, and (c, d) Colorado. Example undisturbed pixels are shown in the top panels (a, c), and example

disturbed pixels are shown in the bottom panels (b, d). The grey line is the fitted loess curve for the time series.

Figure 3.1.

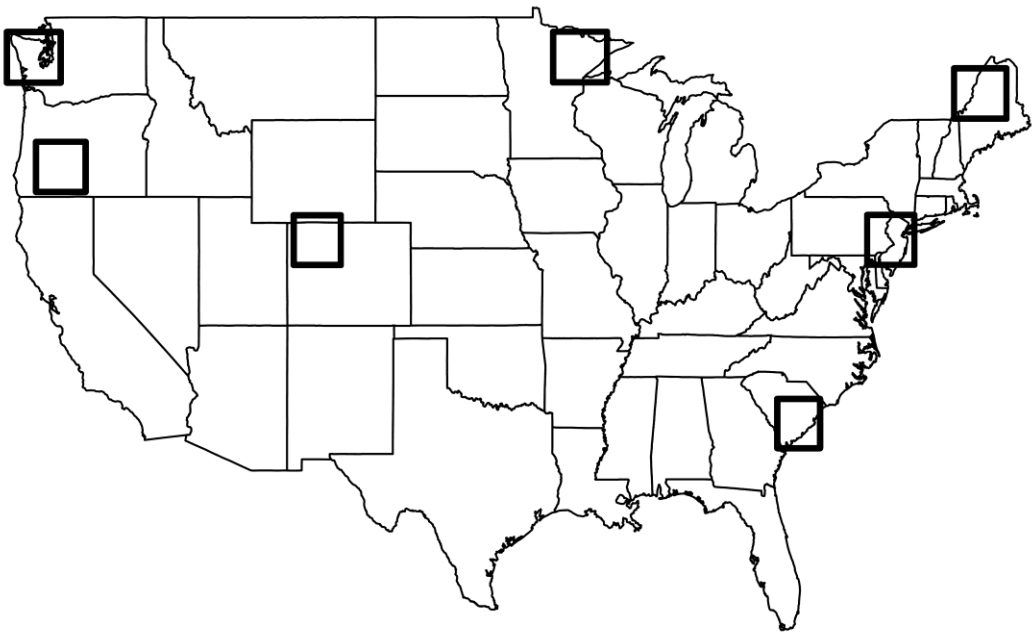

Figure 3.2.

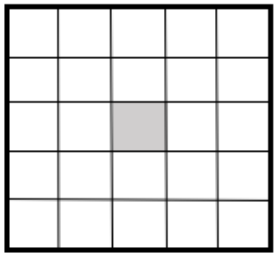

Temporal Variables

- Magnitude[1]
- Duration[1]
- Overall TS slope[2]
- Minimum TS slope[1]
- Variance in TS slope[2]
- Overall loess slope[2]
- Minimum loess slope[1]
- Maximum loess slope[2]
- Median loess slope[2]
- Variance in loess slope[2]
- Date of loess minimum[3]
- Range of loess fitted NDVI[4]
- NDVI Range[4]
- NDVI mean average deviance (MAD)[4]
- NDVI Variance[4]
- Median NDVI[4]
- Maximum NDVI[4]
- Minimum NDVI[4]
- Ratio of NDVI MAD to mean[4]
- Pre- dist. NDVI variance[4]
- Post-dist. NDVI variance[4]
- Ratio of pre- to post-dist. variance[4]
- Detected TS break date[3]
- Min. slope of RPART model[1]
- Max. Slope of RPART model[2]
- Date of RPART minimum[3]

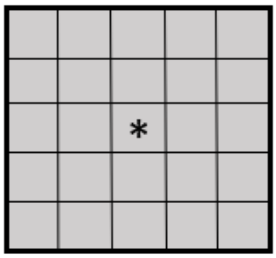

Spatial Variables

- Median magnitude[1*]
- Range in magnitude[1**]
- Ratio of magnitude[1***]
- Median duration[1*]
- Range in duration[1**]
- Ratio of duration[1***]
- Median minimum loess slope[1*]
- Range in minimum loess slope[1**]
- Ratio of minimum loess slope[1***]
- Median maximum loess slope[2*]
- Range in maximum loess slope[2**]
- Ratio of maximum loess slope[2***]
- Median median loess slope[2*]
- Range in median loess slope[2**]
- Ratio of median loess slope[2***]
- Range of date of loess minimum[3**]
- Range of detected TS break date[3**]
- Median ratio of pre- to post-dist. variance[4*]
- Range in ratio of pre- to post-dist. variance[4**]

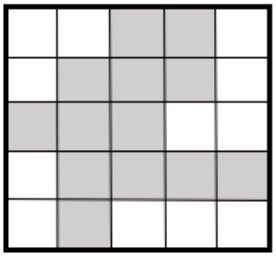

Disturbance Spatial Variables

- Median magnitude[1*]
- Range in magnitude[1**]
- Median duration[1*]
- Range in duration[1**]
- Median minimum loess slope[1*]
- Range in minimum loess slope[1**]
- Median maximum loess slope[2*]
- Range in maximum loess slope[2**]
- Median median loess slope[2*]
- Range of median loess slope[2**]
- Median date of loess minimum[3*]
- Range in date of loess minimum[3**]
- Median detected TS break date[3*]
- Range in detected TS break date[3**]
- Median overall TS slope[2*]
- Range in overall TS slope[2**]
- Number of pixels[**]

Figure 3.3.

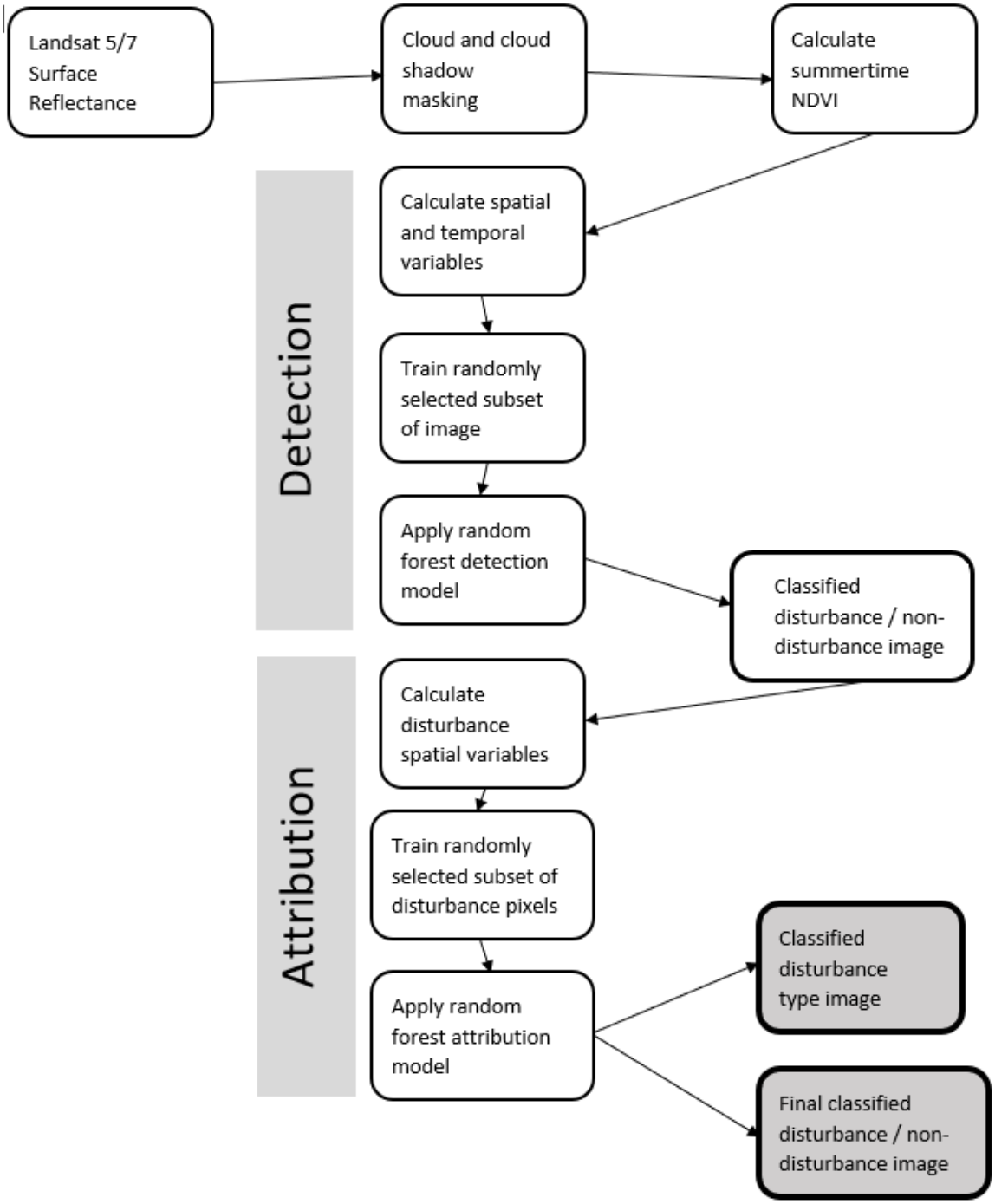
Landsat 5/7 Surface Reflectance
Cloud and cloud shadow masking
Calculate summertime NDVI
Detection
Calculate spatial and temporal variables
Train randomly selected subset of image
Apply random forest detection model
Classified disturbance / non-disturbance image
Attribution
Calculate disturbance spatial variables
Train randomly selected subset of disturbance pixels
Apply random forest attribution model
Classified disturbance type image
Final classified disturbance / non-disturbance image

Figure 3.4.

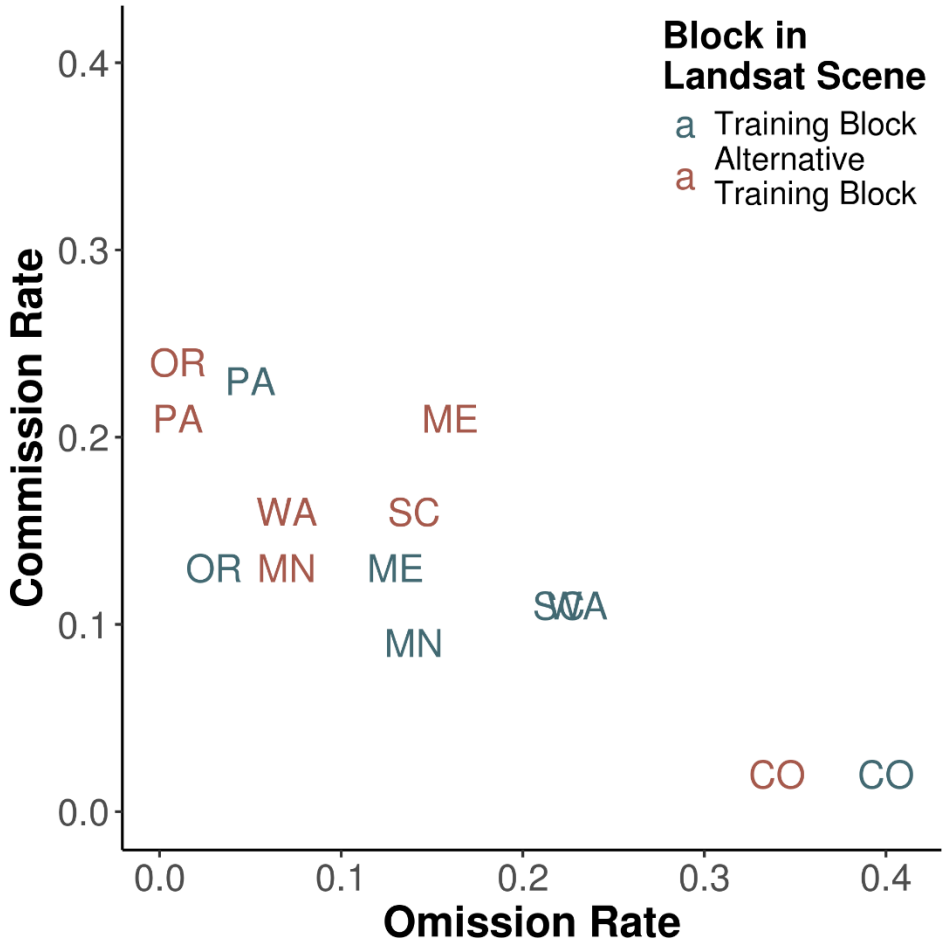
Block in
Landsat Scene
a Training Block
a Alternative
Training Block
Commission Rate
0.4
0.3
0.2
0.1
0.0
OR
PA
PA
ME
WA
SC
OR
MN
ME
MN
CO
CO
0.0
0.1
0.2
0.3
0.4
Omission Rate

Figure 3.5.

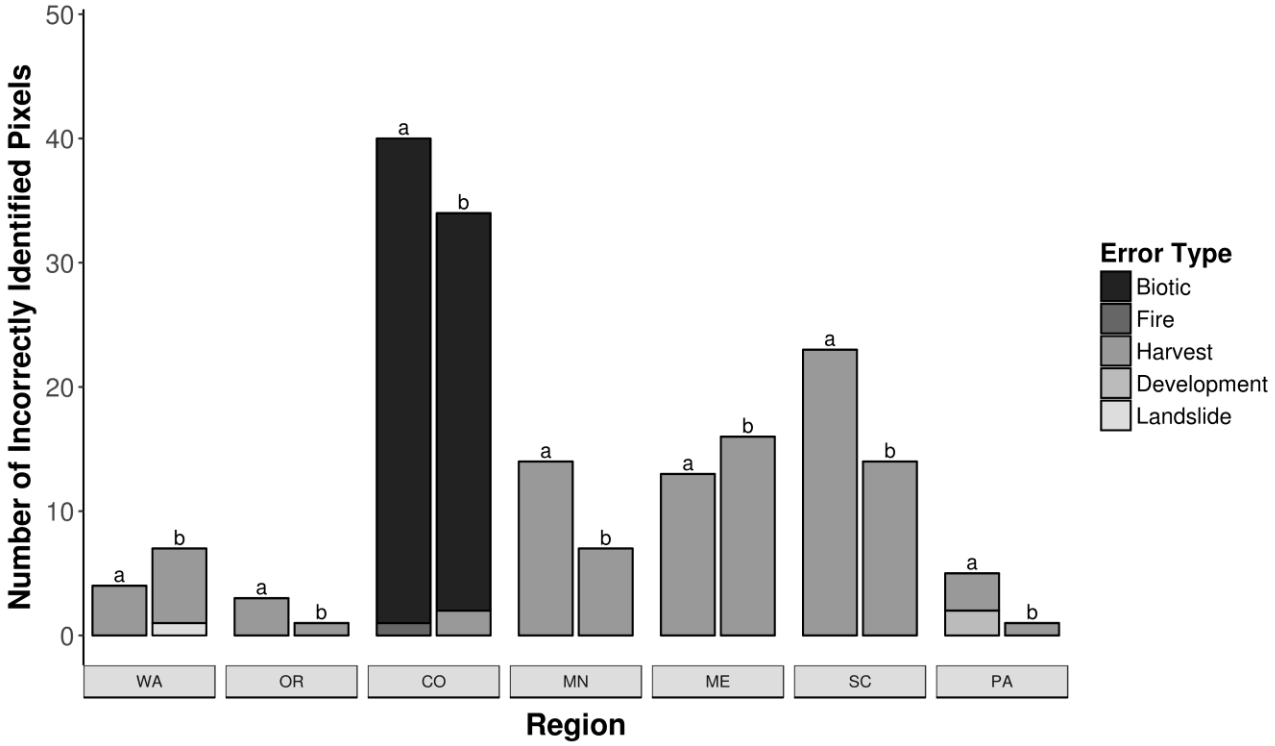
Number of Incorrectly Identified Pixels
50
40
30
20
10
0
a
b
a
b
a
b
a
b
a
b
a
b
a
b
WA
OR
CO
MN
ME
SC
PA
Region
Error Type
Biotic
Fire
Harvest
Development
Landslide

Figure 3.6.

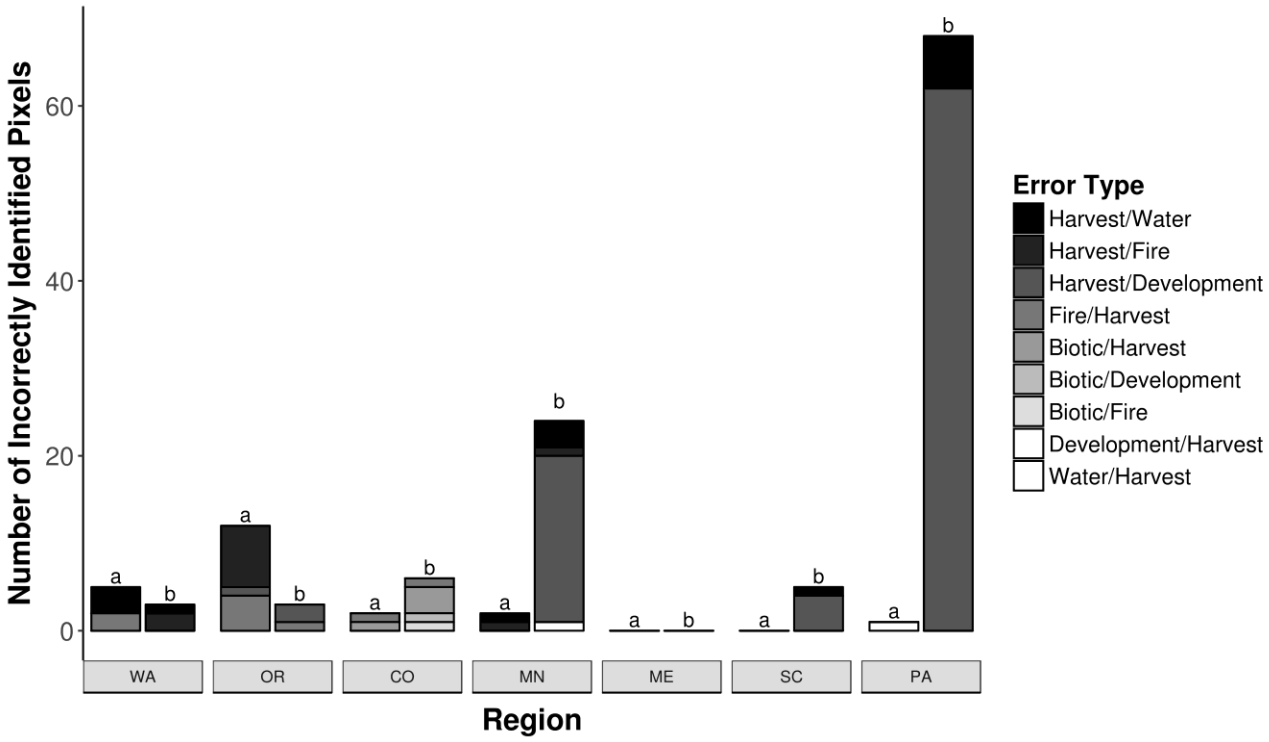
Number of Incorrectly Identified Pixels
0
20
40
60
a
b
a
b
a
b
a
b
a
b
a
b
a
b
WA
OR
CO
MN
ME
SC
PA
Region
Error Type
Harvest/Water
Harvest/Fire
Harvest/Development
Fire/Harvest
Biotic/Harvest
Biotic/Development
Biotic/Fire
Development/Harvest
Water/Harvest

Figure 3.7.

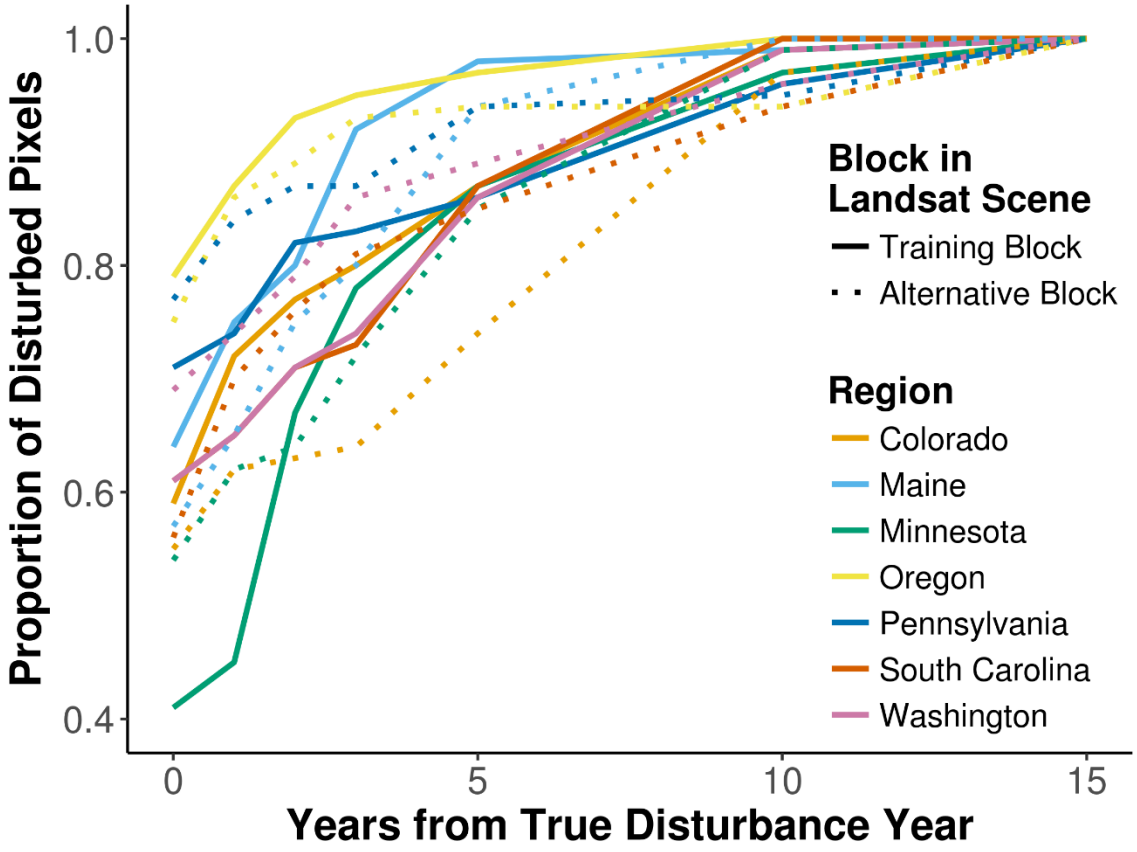
Proportion of Disturbed Pixels
1.0
0.8
0.6
0.4
0
5
10
15
Years from True Disturbance Year
Block in Landsat Scene
Training Block
Alternative Block
Region
Colorado
Maine
Minnesota
Oregon
Pennsylvania
South Carolina
Washington

Figure 3.8.

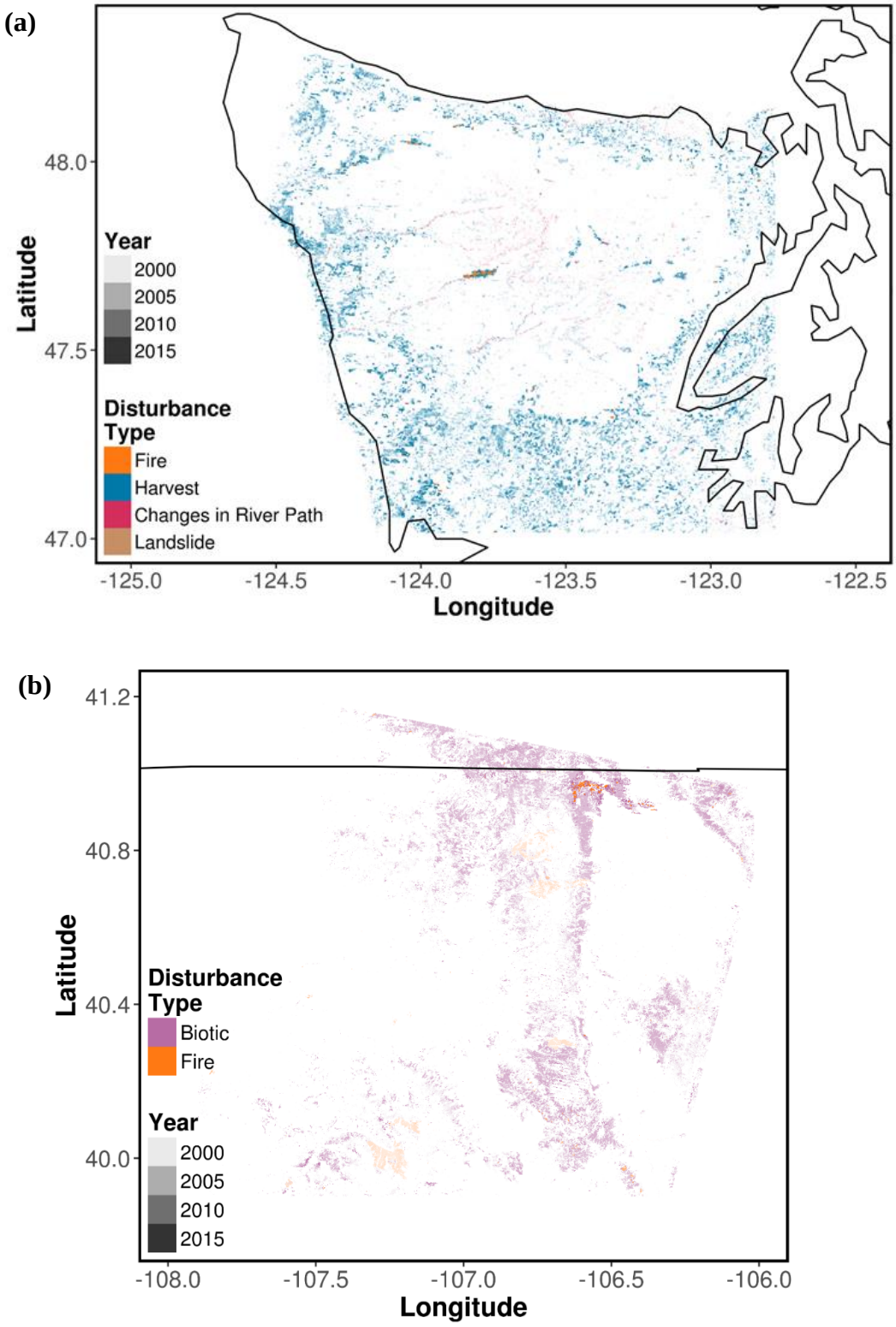
(a)
48.0
47.5
47.0
Latitude
Year
2000
2005
2010
2015
Disturbance Type
Fire
Harvest
Changes in River Path
Landslide
-125.0
-124.5
-124.0
-123.5
-123.0
-122.5
Longitude
(b)
41.2
40.8
40.4
40.0
Latitude
Disturbance Type
Biotic
Fire
Year
2000
2005
2010
2015
-108.0
-107.5
-107.0
-106.5
-106.0
Longitude

Figure 3.9.

(a)

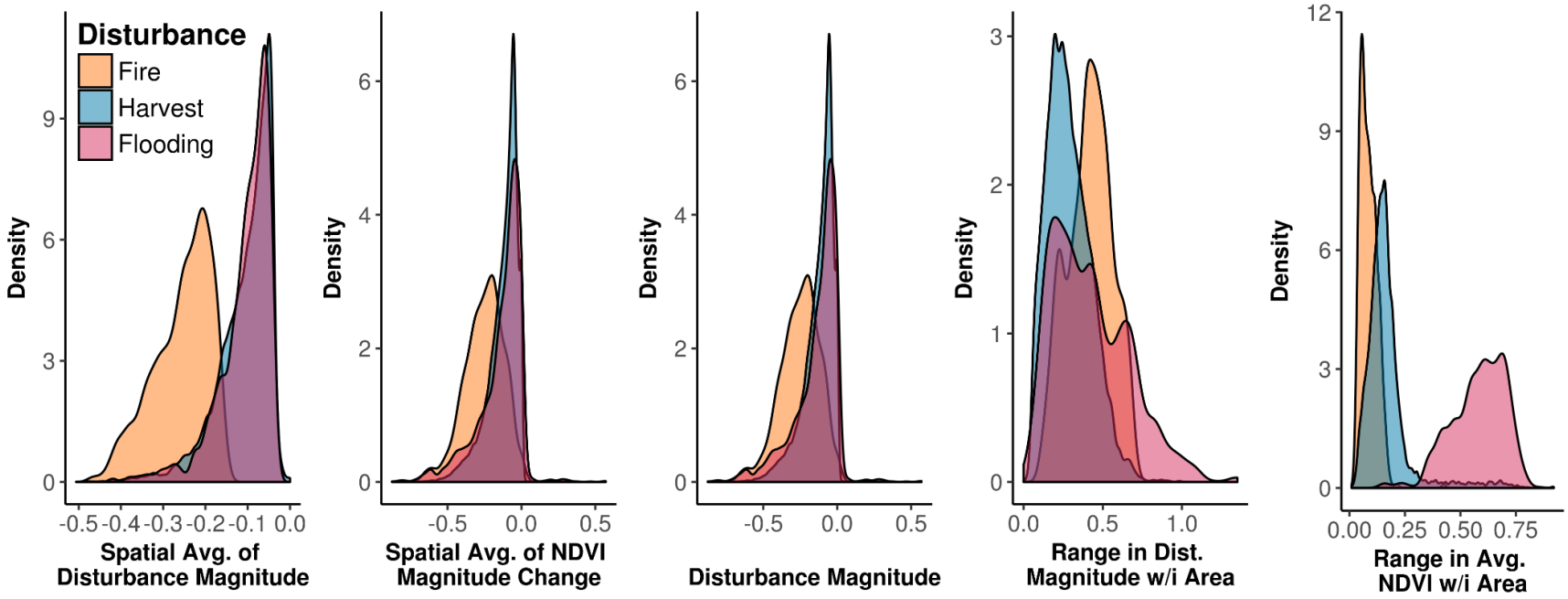
Disturbance
Fire
Harvest
Flooding
Density
Spatial Avg. of Disturbance Magnitude
Spatial Avg. of NDVI Magnitude Change
Disturbance Magnitude
Range in Dist. Magnitude w/i Area
Range in Avg. NDVI w/i Area

(b)

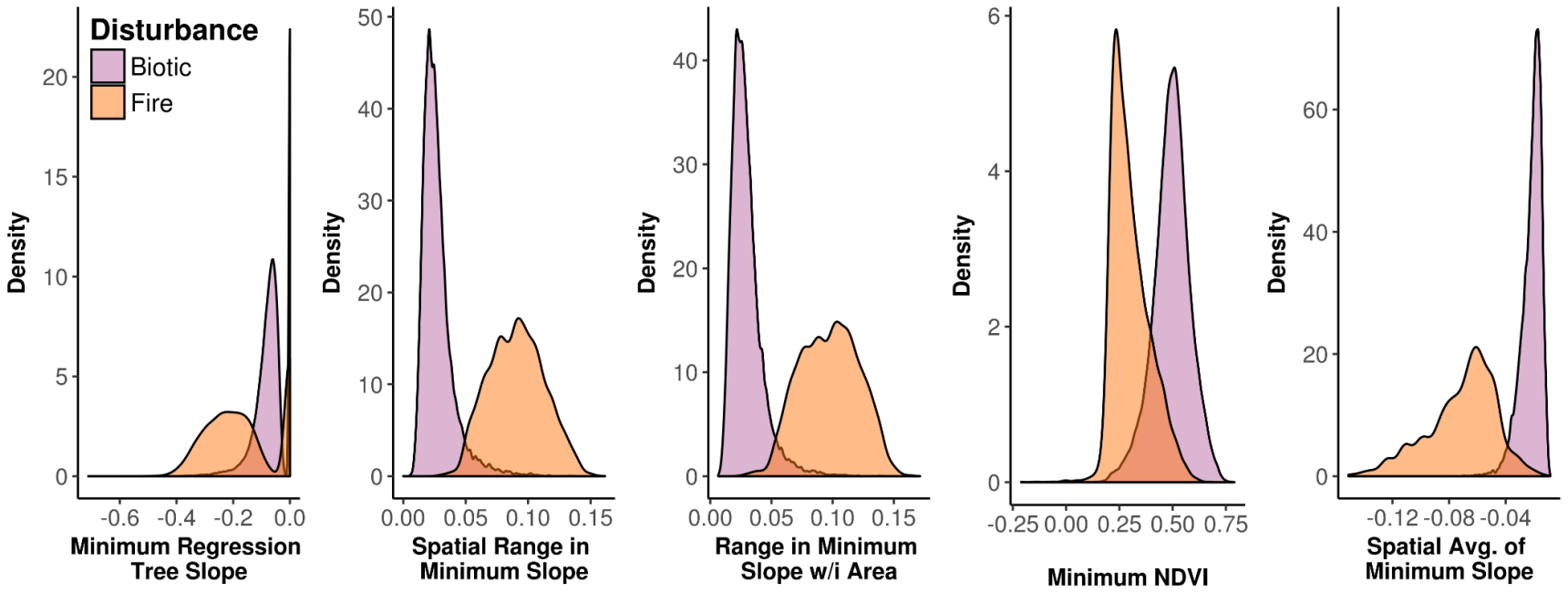
Disturbance
Biotic
Fire
Density
Minimum Regression Tree Slope
Spatial Range in Minimum Slope
Range in Minimum Slope w/i Area
Minimum NDVI
Spatial Avg. of Minimum Slope

Figure 3.10.

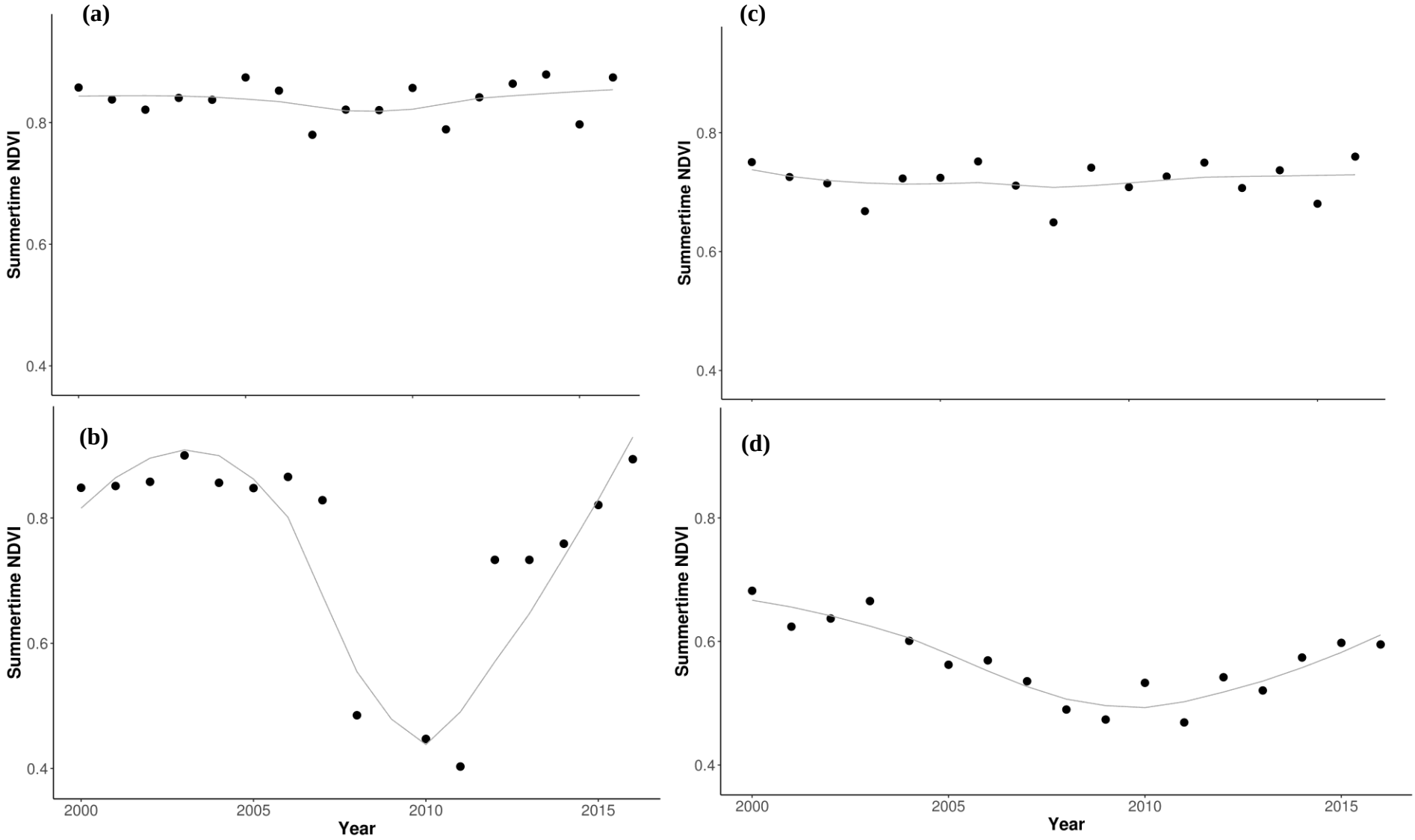

Tables

Table 3.1. Landsat scene paths and rows, along with the primary disturbance types within each scene.

Region Name	*Landsat Path*	*Landsat Row*	*Primary Disturbance Types*
Washington (WA)	47	27	Harvest, Fire, River Changes
Oregon (OR)	45	30	Fire, Harvest
Colorado (CO)	35	32	Fire, Bark Beetle Outbreaks
Minnesota (MN)	27	27	Harvest, Flooding
Maine (ME)	12	28	Harvest
South Carolina (SC)	16	37	Harvest
Pennsylvania (PA)	14	32	Land Development

Table 3.2. Variables included in the final Random Forest detection and attribution models for each Landsat scene, indicated by the abbreviation for the primary state that they overlap.

	Region						
	WA	**OR**	**CO**	**MN**	**ME**	**SC**	**PA**
Detection Model	1. Median NDVI change in area	1. Median minimum loess slope in area	1. Overall loess slope	1. Median loess slope ratio of pixel to area	1. Minimum loess slope	1. Variance in loess slope	1. Median loess slope
	2. Disturbance magnitude	2. Variance in loess slope	2. Minimum loess slope	2. Minimum loess slope ratio of pixel to area	2. Median loess slope	2. Minimum loess slope	2. Area range of pre- to post-disturbance variance
	3. Median minimum loess slope in area	3. Minimum loess slope	3. Median minimum loess slope in area	3. Median loess slope range in area	3. Minimum TS slope	3. Median NDVI change in area	3. Variance TS slope
	4. Overall loess slope	4. Minimum RPART slope	4. Median NDVI change in area	4. Variance in loess slope	4. Variance TS slope	4. Post-disturbance TS variance	4. Minimum loess slope ratio of pixel to area
	5. Median loess slope	5. Mean NDVI change in area	5. Disturbance magnitude	5. Median loess slope	5. Minimum loess slope ratio of pixel to area	5. Median minimum loess slope in area	5. Median of mean loess slope in area
Attribution Model	1. Median magnitude of nearby disturbed pixels	1. Median median NDVI of nearby disturbed pixels	1. Minimum RPART slope	1. Post-disturbance TS variance	1. Range in NDVI	1. Median NDVI	1. Median NDVI change in area
	2. Median NDVI change in area	2. Median minimum loess slope in nearby disturbed pixels	2. Range in minimum loess slope in nearby disturbed pixels	2. Pre- to post-disturbance variance ratio	2. Median maximum loess slope in nearby disturbed pixels	2. Median disturbance duration in nearby disturbed pixels	2. Disturbance magnitude
	3. Disturbance magnitude	3. Median maximum loess slope in area	3. Range in minimum loess slope in area	3. Pixel to area ratio of pre- to post-disturbance variance ratio	3. Maximum loess slope	3. Median median NDVI in nearby disturbed pixels	3. Median magnitude of nearby disturbed pixels
	4. Range in disturbance magnitude in area	4. Average NDVI	4. Minimum NDVI	4. Median maximum loess slope in nearby disturbed pixels	4. Variance in NDVI	4. Maximum NDVI	4. Overall TS slope
	5. Range in median NDVI in nearby disturbed pixels	5. Range in maximum loess slope in nearby disturbed pixels	5. Median minimum loess slope in nearby disturbed pixels	5. Median NDVI change in area	5. Range in disturbance magnitude in area	5. Median minimum loess slope in nearby disturbed pixels	5. Median disturbance duration in nearby disturbed pixels

SUPPLEMENTARY INFORMATION

Supplemental Figure Legends

Figure S3.1. Relative importance for the top 5 most important variables in the Random Forest detection model.

Figure S3.2. Relative importance for the top 5 most important variables in the Random Forest attribution model.

Figure S3.1.

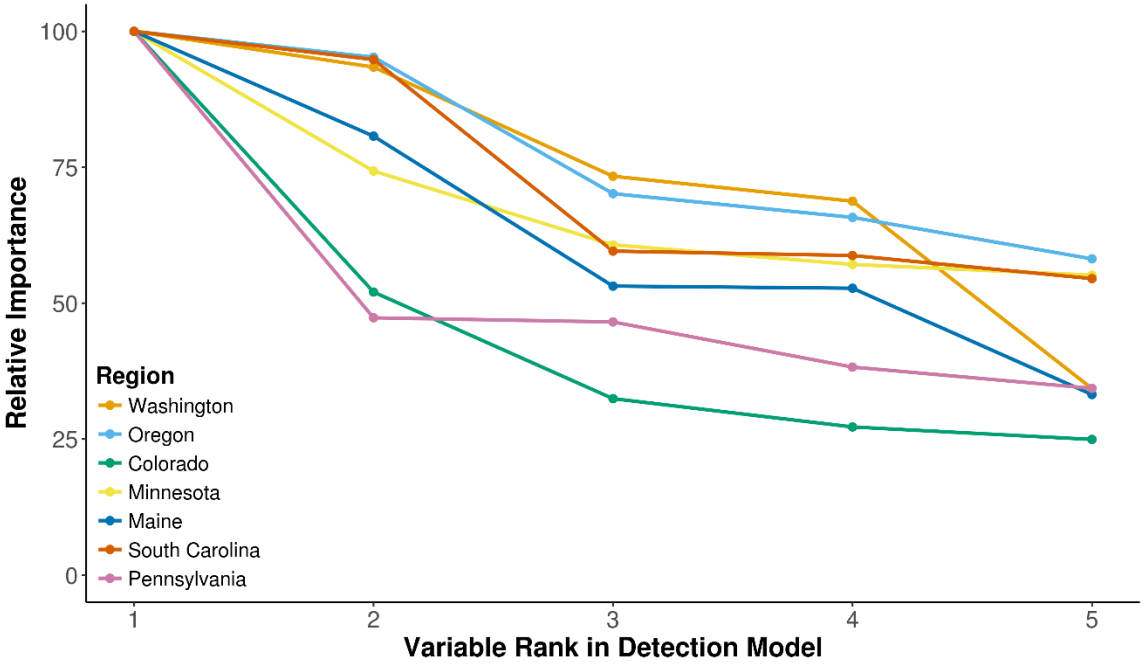
Relative Importance
100
75
50
25
0
1
2
3
4
5
Variable Rank in Detection Model
Region
Washington
Oregon
Colorado
Minnesota
Maine
South Carolina
Pennsylvania

Figure S3.2.

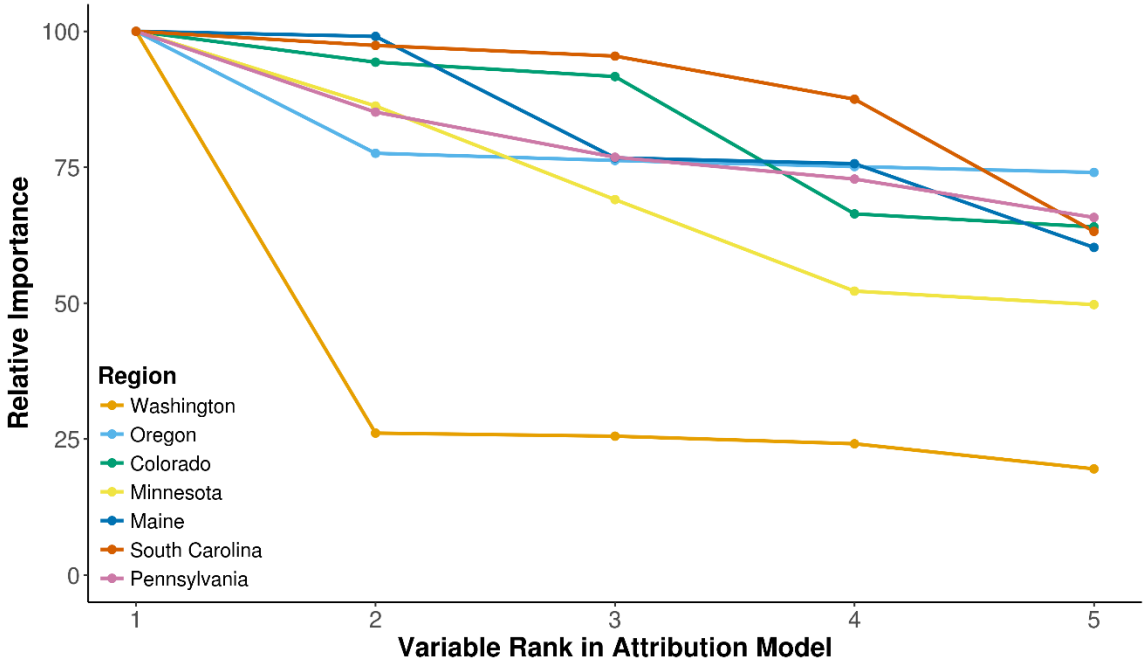
Relative Importance
100
75
50
25
0
Region
Washington
Oregon
Colorado
Minnesota
Maine
South Carolina
Pennsylvania
1
2
3
4
5
Variable Rank in Attribution Model

CONCLUDING REMARKS

Contributions

The work completed for this dissertation has resulted in several important contributions. I have discovered that forest disturbances have the potential to influence forest productivity well into the future, and that disturbance impacts vary considerably even across relatively small climatic gradients. Previous research had also suggested the potential for bark beetle outbreaks to result in phenotypic or genetic changes in pine populations, but this study demonstrates that those shifts may be limited to low elevation, or water-limited, sites. This new finding is important to managers deciding where best to focus treatments aimed at limiting bark beetle outbreaks. Additionally, I was surprised to learn that beetles tend to attack faster-growing lodgepole pine. This finding adds to the argument that timber plantations may want to focus on increasing phenotypic and genetic variability in order to enhance plantation resilience to future disturbances. Secondly, I have demonstrated that the variability in disturbance impacts among forest types and locations. In addition to variation in the long-term biochemical impacts of beetle outbreaks across climatic gradients, there is also substantial variability in the short-term biophysical impacts of several disturbance types. Previous research has discussed the potential for fires and bark beetle outbreaks to impact climate at large scales over long periods of time. The results from chapters 1 and 2 indicate that while this may be true when considering very large and severe disturbances, the specific impacts of each disturbance event are much more nuanced and depend on individual forest characteristics and the climate during which the disturbance occurs.

Both chapters 1 and 2 indicated the need for better methods with which to detect and attribute forest disturbances. As such, a third contribution that I have made to advancing our understanding of disturbance ecology is the detection and attribution pipeline introduced in chapter 3. This new method will better enable researchers and managers to locate and assess forest disturbances over many different forested areas. This contribution is particularly important because no combined detection and attribution methods existed previously, and most separate detection and attribution methods are computationally intensive and time consuming. The approach introduced here is more efficient and easy to use than previous methods, while limiting concurrent reductions in accuracy.

Next Steps

Looking forward, there are several directions for this research to continue to progress. First, the methods and results from this research could be used to further investigate the biochemical and biophysical impacts of disturbance by informing mechanistic model-based studies. Modeling would enable a better understanding of the carbon, nutrient, and energy dynamics of forested ecosystems over a range of time scales and future climatic scenarios. Using the methods from chapter 3, model simulations of disturbances could be improved through a better understanding of the spatial and temporal characteristics of disturbances. Furthermore, the results of chapter 1 demonstrate that models may need to account for changes in forest growth and productivity following disturbances; the results of that study also give a preliminary measure of those changes. The results of chapter 2, that disturbance impacts on LST and

GPP differ by ecoregion, would help to define the typical impacts of forest disturbances by ecoregion.

In addition to further understanding disturbance impacts through modeling, another future direction for the work completed for chapter 3 is to improve on the methods in order to make them more accessible. Specifically, the pipeline could be developed into an R package or a command line program. This change would enable more researchers to use fine-resolution disturbance information in their analyses, and potentially greatly enhance our understanding of disturbance dynamics.

REFERENCES

Adams, H.D., Guardiola-Claramonte, M., Barron-Gafford, G.A., Villegas, J.C., Breshears, D.D., Zou, C.B., *et al.* (2009), Temperature sensitivity of drought-induced tree mortality portends increased regional die-off under global-change-type drought, *PNAS, 106* (17), 7063–7066.

Alberto, F.J., Aitken, S.N., Alía, R., González-Martínez, S.C., Hänninen, H., Kremer, A., *et al.* (2013), Potential for evolutionary responses to climate change–evidence from tree populations, *Global Change Biology, 19* (6), 1645-1661.

Allen, C.D., Macalady, A.K., Chenchouni, H., Bachelet, D., McDowell, N., Vennetier, M., *et al.* (2010), A global overview of drought and heat-induced tree mortality reveals emerging climate change risks for forests, *Forest Ecology and Management, 259* (4), 660–684.

Amiro, B.D., Barr, A.G., Barr, J.G., Black, T.A., Bacho, R., Brown, M., *et al.* (2010), Ecosystem carbon dioxide fluxes after disturbance in forests of North America, *Journal of Geophysical Research – Biogeosciences, 115* (G00K02).

Amman, G.D. & Baker, B.H. (1972), Mountain pine beetle influence on lodgepole pine stand structure, *Journal of Forestry*, *70* (4), 204-209.

Anderegg, W.R.L., Kane, J.M. & Anderegg, L.D.L. (2013), Consequences of widespread tree mortality triggered by drought and temperature stress, *Nature Climate Change*, *3* (1), 30–36.

Assal, T.J., Sibold, J. & Reich, R. (2014), Modeling a historical mountain pine beetle outbreak using Landsat MSS and multiple lines of evidence, *Remote Sensing of Environment*, *155*, 275-288.

Bechtold, W.A. & Patterson, P.L. (2005), *The enhanced forest inventory and analysis program - national sampling design and estimation procedures* (Vol. 80), Asheville, North Carolina: US Department of Agriculture Forest Service, Southern Research Station.

Bentz, B.J., Régnière, J., Fettig, C.J., Hansen, E.M., Hayes, J.L., Hicke, J.A., *et al.* (2010), Climate change and bark beetles of the western United States and Canada: direct and indirect effects, *BioScience*, *60* (8), 602–613.

Bentz, B.J., Boone, C. & Raffa, K.F. (2015), Tree response and mountain pine beetle attack preference, reproduction and emergence timing in mixed whitebark and lodgepole pine stands, *Agricultural and Forest Entomology*, *17* (4), 421-432.

Berg, E.E., Henry, J.D., Fastie, C.L., De Volder, A.D. & Matsouka, S.M. (2006), Spruce beetle outbreaks on the Kenai Peninsula, Alaska, and Kluane National Park and Reserve, Yukon Territory: relationship to summer temperatures and regional

differences in disturbance regimes, *Forest Ecology and Management*, *227* (3), 219-232.

Bigler, C. & Veblen, T.T. (2009), Increased early growth rates decrease longevities of conifers in subalpine forests, *Oikos*, *118* (8), 1130-1138.

Biondi, F. & Qeadan, F. (2008), A theory-driven approach to tree-ring standardization: defining the biological trend from expected basal area increment, *Tree-Ring Research*, *64* (2), 81-96.

Björklund, N. & Lindgren, B.S. (2009), Diameter of lodgepole pine and mortality caused by the mountain pine beetle: factors that influence their relationship and applicability for susceptibility rating, *Canadian Journal of Forest Research*, *39* (5), 908-916.

Bonan, G.B. (2008), Forests and climate change: forcings, feedbacks, and the climate benefits of forests, *Science*, *320* (5882), 1444–1449.

Bond-Lamberty, B., Peckham, S.D., Ahl, D.E. & Gower, S.T. (2007), Fire as the dominant driver of central Canadian boreal forest carbon balance, *Nature*, *450* (7166), 89–92.

Boone, C.K., Aukema, B.H., Bohlmann, J., Carroll, A.L. & Raffa, K.F. (2011), Efficacy of tree defense physiology varies with bark beetle population density: a basis for positive feedback in eruptive species, *Canadian Journal of Forest Research*, *41* (6), 1174-1188.

Borkhuu, B., Peckham, S.D., Ewers, B.E., Nortan, U. & Pendall, E. (2015) Does soil respiration decline following bark beetle induced forest mortality? Evidence from a lodgepole pine forest, *Agricultural and Forest Meteorology*, *214*, 201-207.

Breshears, D.D., Myers, O.B., Meyer, C.W., Barnes, F.J., Zou, C.B., Allen, C.D., *et al.* (2009) Tree die-off in response to global change-type drought: mortality insights from a decade of plant water potential measurements, *Frontiers in Ecology and the Environment, 7* (4), 185-189.

Bright, B.C., Hicke, J.A. & Meddens, A.J.H. (2013), Effects of bark beetle-caused tree mortality on biogeochemical and biogeophysical MODIS products, *Journal of Geophysical Research - Biogeosciences, 118* (3), 974–982.

Brown, M.G., Black, T.A., Nesic, Z., Fredeen, A.L., Foord, V.N., Spittlehouse, D.L., *et al.* (2012) The carbon balance of two lodgepole pine stands recovering from mountain pine beetle attack in British Columbia, *Agricultural and Forest Meteorology, 153,* 82- 93.

Buck, A.L. (1981), New equations for computing vapor pressure and enhancement factor, *Journal of Applied Meteorology*, *20* (12), 1527-1532.

Bunn, A.G., Korpela, M., Biondi, F., Campelo, F., Mérian, P., Qeadan, F. & Zang, C. (2015), dplR: Dendrochronology Program Library in R. R package version 1.6.2.

Carroll, A.L., Taylor, S.W., Régnière, J. & Safranyik, L. (2003), Effect of climate change on range expansion by the mountain pine beetle in British Columbia, *Mountain Pine Beetle Symposium: Challenges and Solutions, Oct. 30-31, 2003. Kelowna BC. Natural Resources Canada, Information Report BC-X-399, Victoria*. 223-232.

Chapman, T.B., Veblen, T.T. & Schoennagel, T. (2012), Spatiotemporal patterns of mountain pine beetle activity in the southern Rocky Mountains, *Ecology*, *93* (10), 2175-2185.

Chhin, S., Hogg, E.T., Lieffers, V.J. & Huang, S. (2008), Potential effects of climate change on the growth of lodgepole pine across diameter size classes and ecological regions, *Forest Ecology and Management*, *256* (10), 1692-1703.

Christiansen, E., Waring, R.H. & Berryman, A.A. (1987), Resistance of conifers to bark beetle attack: searching for general relationships, *Forest Ecology and Management*, *22* (1-2), 89-106.

Cohen, W.B., Yang, Z. & Kennedy, R. (2010), Detecting trends in forest disturbance and recovery using yearly Landsat time series: 2. TimeSync—Tools for calibration and validation, *Remote Sensing of Environment*, *114* (12), 2911-2924.

Cohen, W.B., Healey, S.P., Yang, Z., Stehman, S.V., Brewer, C.K., Brooks, E.B., *et al.* (2017), How similar are forest disturbance maps derived from different Landsat time series algorithms?, *Forests*, *8* (4), 98.

Cohen, W.B., Yang, Z., Healey, S.P., Kennedy, R.E. & Gorelick, N. (2018) A LandTrendr multispectral ensemble for forest disturbance detection, *Remote Sensing of Environment*, *205*, 131-140.

Cooper, L.A., Ballantyne, A.P., Holden, Z.A. & Landguth, E.L. (2017) Disturbance impacts on land surface temperature and gross primary productivity in the western United States, *Journal of Geophysical Research: Biogeosciences*, *122* (4), 930-946.

Coops, N.C. & Wulder, M.A. (2010), Estimating the reduction in gross primary production due to mountain pine beetle infestation using satellite observations, *International Journal of Remote Sensing*, *31* (8), 2129-2138.

Cybis Elektronik, (2014), "CDendro and CooRecorder."

Dale, V.H., Joyce, L.A., McNulty, S., Neilson, R.P., Ayres, M.P., Flannigan, M.D., *et al.* (2001), Climate change and forest disturbances, *BioScience*, *51* (9), 723-734.

de la Mata, R., Hood, S. & Sala, A. (2017), Insect outbreak shifts the direction of selection from fast to slow growth rates in the long-lived conifer Pinus ponderosa, *PNAS*, *114* (28), 7391-7396.

DiMiceli C.M., Carroll, M.L., Sohlberg, R.A., Huang, C., Hansen, M.C. & Townshend, J.R.G. (2011), Annual global automated MODIS Vegetation Continuous Fields (MOD44B) at 250 m spatial resolution for data years beginning day 65, 2000-2010, collection 5 percent tree cover, *University of Maryland, College Park, MD, USA*.

DeVries, B., Verbesselt, J., Kooistra, L. & Herold, M. (2015), Robust monitoring of small-scale forest disturbances in a tropical montane forest using Landsat time series, *Remote Sensing of Environment*, *161*, 107–121.

Dillon, G.K., Holden, Z.A., Morgan, P., Crimmins, M.A., Heyerdahl, E.K. & Luce, C.H. (2011), Both topography and climate affected forest and woodland burn severity in two regions of the western US, 1984 to 2006, *Ecosphere*, *2* (12), 1-33.

Dobrowski, S.Z., Abatzoglou, J., Swanson, A.K., Greenberg, J.A., Mynsberge, A.R., Holden, Z.A. & Schwartz, M.K. (2013), The climate velocity of the contiguous United States during the 20th century, *Global Change Biology*, *19* (1), 241–251.

Dutrieux, L.P., Verbesselt, J., Kooistra, L. & Herold, M. (2015), Monitoring forest cover loss using multiple data streams, a case study of a tropical dry forest in Bolivia, *ISPRS Journal of Photogrammetry and Remote Sensing*, *107*, 112–125.

Edburg, E.L., Hicke, J.A., Lawrence, D.M. & Thornton, P.E. (2011) Simulating coupled carbon and nitrogen dynamics following mountain pine beetle outbreaks in the western United States, *Journal of Geophysical Research - Biogeosciences*, *116*, G04033.

Eidenshink, J., Schwind, B., Brewer, K., Zhu, Z.L., Quayle, B. & Howard, S. (2007), A Project for Monitoring Trends in Burn Severity, *Fire Ecology*, *3* (1), 3–21.

Esri (2010), ArcGIS Desktop: Release 10, *Redlands, CA: Environmental Systems Research Institute*.

Fernández-de-Uña, L., McDowell, N.G., Cañellas, I. & Gea-Izquierdo, G. (2016), Disentangling the effect of competition, CO2 and climate on intrinsic water-use efficiency and tree growth, *Journal of Ecology*, *104* (3), 678-690.

Ferrenberg, S., Kane, J.M. & Mitton, J.B. (2014), Resin duct characteristics associated with tree resistance to bark beetles across lodgepole and limber pines, *Oecologia*, *174* (4), 1283-1292.

Foster, J.R., Burton, J.I., Forrester, J.A., Liu, F., Muss, J.D., Sabatini, F.M., *et al.* (2010), Evidence for a recent increase in forest growth is questionable, *PNAS, 107* (21), E86-E87.

Fotheringham, A.S., Charlton, M. & Brunsdon, C. (1996), The geography of parameter space: an investigation of spatial non-stationarity, *Int. J. Geographical Information Systems, 10* (5), 605-627.

Franklin, J.F., Spies, T.A., Van Pelt, R., Carey, A.B., Thornburgh, D.A., Lindenmayer, D.B., *et al.* (2002), Disturbances and structural development of natural forest ecosystems with silvicultural implications, using Douglas-fir forests as an example, *Forest Ecology and Management, 155* (13), 399–423.

Fulé, P.Z., Covington, W.W. & Moore, M.M. (1997), Determining reference conditions for ecosystem management of southwestern ponderosa pine forests, *Ecological Applications, 7* (3), 895–908.

Ghimire, B., Williams, C.A., Collatz, G.J., Vanderhoof, M., Rogan, J., Kulakowski, D. & Masek, J.D. (2015) Large carbon release legacy from bark beetle outbreaks across Western United States, *Global Change Biology, 21* (8), 3087-3101.

Hall, R.J., Skakun, R.S. & Arsenault, E.J. (2006), Remotely sensed data in the mapping of insect defoliation, *Understanding forest disturbance and spatial pattern: Remote sensing and GIS approaches*, 85-111.

Hanks, L.M., Paine, T.D., Millar, J.G., Campbell, C.D. & Schuch, U.K. (1999), Water relations of host trees and resistance to the phloem-boring beetle Phoracantha semipunctata F. (Coleoptera: Cerambycidae), *Oecologia*, *119*(3), 400-407.

Hansen, M.C., Potapov, P.V., Moore, R., Hancher, M., Turubanova, S., Tyukavina, A., *et al.* (2013), High-resolution global maps of 21st-century forest cover change, *Science*, *342* (6160), 850-853.

Hanson, P.J. & J.F. Weltzin (2000), Drought disturbance from climate change: response of United States forests, *Science of the Total Environment*, *262* (3), 205–220.

Hart, S.J., Veblen, T.T., Eisenhart, K.S., Jarvis, D. & Kulakowski, D. (2014), Drought induces spruce beetle (Dendroctonus rufipennis) outbreaks across northwestern Colorado, *Ecology*, *95* (4), 930-939.

Healey, S.P., Cohen, W.B., Yang, Z., Brewer, C.K., Brooks, E.B., Gorelick, N., *et al.* (2018), Mapping forest change using stacked generalization: An ensemble approach, *Remote Sensing of Environment*, *204*, 717-728.

Herms, D.A. & Mattson, W.J. (1992), The dilemma of plants: to grow or defend, *The Quarterly Review of Biology, 67* (3), 283-335.

Heyder, U., Schaphoff, S., Gerten, D. & Lucht, W. (2011), Risk of severe climate change impact on the terrestrial biosphere, *Environmental Research Letters*, *6*(3), 34-36.

Hicke, J.A., Logan, J.A., Powell, J. & Ojima, D.S. (2006), Changing temperatures influence suitability for modeled mountain pine beetle (Dendroctonus ponderosae) outbreaks in the western United States, *Journal of Geophysical Research - Biogeosciences*, *111* (G2).

Hicke, J.A., Allen, C.D., Desai, A.R., Dietze, M.C., Hall, R.J., Hogg, E.H.T., *et al.* (2012), Effects of biotic disturbances on forest carbon cycling in the United States and Canada, *Global Change Biology*, *18*(1), 7–34.

Hicke, J.A., Meddens, A.J.H., Allen, C.D. & Kolden, C.A. (2013), Carbon stocks of trees killed by bark beetles and wildfire in the western United States, *Environmental Research Letters*, *8*, 035032.

Hicke, J.A., Meddens, A.J.H. & Kolden, C.A. (2016), Recent tree mortality in the western United States from bark beetles and forest fires, *Forest Science*, *62* (2), 141-153.

Holden, Z.A., Morgan, P. & Evans, J.S. (2009), A predictive model of burn severity based on 20 year satellite-inferred burn severity data in a large southwestern US wilderness area, *Forest Ecology and Management*, *258* (11), 2399–2406.

Holmes, R. (1983), Computer Assisted Quality Control in Tree-Ring Dating and Measurement, *Tree-Ring Bulletin, 44*, 69-75.

Hood, S. & Sala, A. (2015), Ponderosa pine resin defenses and growth: metrics matter, *Tree Physiology*, *35* (11), 1223-1235.

Huang, C., Song, K., Kim, S., Townshend, J.R., Davis, P., Masek, J.G. & Goward, S.N. (2008), Use of a dark object concept and support vector machines to automate forest cover change analysis, *Remote Sensing of Environment*, *112* (3), 970-985.

Huang, C., Goward, S.N., Masek, J.G., Thomas, N., Zhu, Z. & Vogelmann, J.E. (2010), An automated approach for reconstructing recent forest disturbance history using dense Landsat time series stacks, *Remote Sensing of Environment*, *114* (1), 183-198.

Huete A., Didan, K., Miura, T., Rodriguez, E.P., Gao, X. & Ferreira, L.G. (2002), Overview of the radiometric and biophysical performance of the MODIS vegetation indices, *Remote Sensing of Environment*, *83* (1-2), 195-213.

Irvine, J., Law, B.E. & Hibbard, K.A. (2007) Postfire carbon pools and fluxes in semiarid ponderosa pine in Central Oregon, *Global Change Biology*, *13* (8), 1748-1760.

Jassby A.D. & Cloern, J.E. (2015), wq: some tools for exploring water quality monitoring data, R package version 0.4.3.

Johnson, E.A., Miyanishi, K. & Weir, J.M.H. (1998), Wildfires in the western Canadian boreal forest: Landscape patterns and ecosystem management, *Journal of Vegetation Science*, *9* (4), 603–610.

Johnson, E.W. & Ross, J. (2008), Quantifying error in aerial survey data, *Australian Forestry*, *71* (3), 216-222.

Johnson, E.W. & Wittwer, D. (2008), Aerial detection surveys in the United States, *Australian Forestry*, *71* (3), 212-215.

Kane, J.M. & Kolb, T.E. (2010), Importance of resin ducts in reducing ponderosa pine mortality from bark beetle attack, *Oecologia*, *164* (3), 601-609.

Kellndorfer J., Walker, W., LaPoint, E., Bishop, J., Cormier, T., Fiske, G., *et al.* (2012), NACP aboveground biomass and carbon baseline data, v. 2 (NBCD 2000), U.S.A. 2000, data set, *Available online (http://daac.ornl.gov) from ORNL DAAC, Oak Ridge, TN*.

Kennedy, R.E., Yang, Z. & Cohen, W.B. (2010), Detecting trends in forest disturbance and recovery using yearly Landsat time series: 1. LandTrendr—Temporal segmentation algorithms, *Remote Sensing of Environment*, *114* (12), 2897-2910.

Klutsch, J.G., Negron, J.F., Costello, S.L., Rhoades, C.C., West, D.R., Popp, J. & Caissie, R. (2009), Stand characteristics and downed woody debris accumulations associated with a mountain pine beetle (Dendroctonus ponderosae Hopkins) outbreak in Colorado, *Forest Ecology and Management*, *258* (5), 641-649.

Knapp, P.A., Soulé, P.T. & Maxwell, J.T. (2013), Mountain pine beetle selectivity in old-growth ponderosa pine forests, Montana, USA, *Ecology and Evolution*, *3* (5), 1141-1148.

Kuhn, M., with contributions from Wing, J., Weston, S., Williams, A., Keefer, C., Engelhardt, A., *et al.* (2017), caret: Classification and Regression Training, R package version 6.0-78.

Kurz, W.A., Dymond, C.C., Stinson, G., Rampley, G.J., Neilson, E.T., Carroll, A.L., *et al.* (2008), Mountain pine beetle and forest carbon feedback to climate change, *Nature*, *452* (7190), 987–990.

Lahr, E.C. & Krokene, P. (2013), Conifer stored resources and resistance to a fungus associated with the spruce bark beetle Ips typographus, *PloS One*, *8* (8), 72405.

Larsson, L. (2014), CooRecorder and Cdendro programs of the CooRecorder/Cdendro package version 7.7.

Law, B.E., Sun, O.J., Campbell, J., Van Tuyl, S. & Thornton, P.E. (2003), Changes in carbon storage and fluxes in a chronosequence of ponderosa pine, *Global Change Biology, 9* (4), 510–524.

Liaw, A. & Wiener, M. (2002), Classification and Regression by randomForest, *R News 2* (3), 18--22.

Lippitt, C.D., Rogan, J., Li, Z., Eastman, J.R. & Jones, T.G. (2008), Mapping selective logging in mixed deciduous forest, *Photogrammetric Engineering & Remote Sensing*, *74* (10), 1201-1211.

Littell, J.S., McKenzie, D., Peterson, D.L. & Westerling, A.L. (2009), Climate and wildfire area burned in western U.S. ecoprovinces, 1916–2003, *Ecological Applications, 19* (4), 1003–1021.

Littell, J.S., Oneil, E.E., McKenzie, D., Hicke, J.A., Lutz, J.A., Norheim, R.A. & Elsner, f M.M. (2010), Forest ecosystems, disturbance, and climatic change in Washington State, USA, *Climatic Change*, *102* (1), 129-158.

Liu H.Q. & Huete, A.R. (1995), A feedback based modification of the NDVI to minimize canopy background and atmospheric noise, *IEEE Transactions on Geoscience and Remote Sensing, 33* (2), 457-465.

Lo, Y.H., Blanco, J.A., Seely, B., Welham, C. & Kimmins, J.H. (2010), Relationships between climate and tree radial growth in interior British Columbia, Canada, *Forest Ecology and Management*, *259* (5), 932-942.

Logan, J.A. & Powell, J.A. (2001), Ghost forests, global warming, and the mountain pine beetle (Coleoptera: Scolytidae), *American Entomologist*, *47* (3), 160.

Niemelä, J. (1999), Management in relation to disturbance in the boreal forest, *Forest Ecology and Management*, *115* (2-3), 127-134.

Maness, H., Kushner, P.J. & Fung, I. (2013), Summertime climate response to mountain pine beetle disturbance in British Columbia, *Nature Geoscience*, *6* (1), 65–70.

McDowell, N.G., Coops, N.C., Beck, P.S., Chambers, J.Q., Gangodagamage, C., Hicke, J.A., *et al.* (2015), Global satellite monitoring of climate-induced vegetation disturbances, *Trends in Plant Science*, *20* (2), 114-123.

McMahon S.M., Parker, G.G. & Miller, D.F. (2010), Evidence for a recent increase in forest growth, *PNAS, 107* (8), 3611-3615.

Meddens, A.J.H., Hicke, J.A. & Ferguson, C.A. (2012), Spatiotemporal patterns of observed bark beetle-caused tree mortality in British Columbia and the western United States, *Ecological Applications*, *22* (7), 1876–1891.

Meigs, G.W., Donato, D.C., Campbell, J.L., Martin, J.G. & Law, B.E. (2009) Forest fire impacts on carbon uptake, storage, and emission: the role of burn severity in the Eastern Cascades, Oregon, *Ecosystems, 12* (8), 1246-1267.

Mildrexler, D.J., Zhao, M., Heinsch, F.A. & Running, S.W. (2007) A new satellite-based methodology for continental-scale disturbance detection, *Ecological Applications*, *17* (1), 235-250.

Millar, C.I., Westfall, R.D., Delany, D.L., Bokach, M.J., Flint, A.L. & Flint, L.E. (2012), Forest mortality in high-elevation whitebark pine (Pinus albicaulis) forests of eastern California, USA; influence of environmental context, bark beetles, climatic water deficit, and warming, *Canadian Journal of Forest Research*, *42* (4), 749-765.

Millar, C.I. & Stephenson, N.L. (2015), Temperate forest health in an era of emerging megadisturbance, *Science*, *349* (6250), 823–826.

Mitchell, R.G., Waring, R.H. & Pitman, G.B. (1983), Thinning lodgepole pine increases tree vigor and resistance to mountain pine beetle, *Forest Science*, *29* (1), 204-211.

Mitton, J.B. & Ferrenberg, S.M. (2012), Mountain pine beetle develops an unprecedented summer generation in response to climate warming, *The American Naturalist*, *179* (5), E163-E171.

Montana Natural Heritage Program (1993-2017).

Moore, D.J.P., Trahan, N.A., Wilkes, P., Quaife, T., Stephens, B.B., Elder, K., *et al.* (2013), Persistent reduced ecosystem respiration after insect disturbance in high elevation forests, *Ecology Letters*, *16* (6), 731–737.

Morehouse, K., Johns, T., Kaye, J. & Kaye, A. (2008) Carbon and nitrogen cycling immediately following bark beetle outbreaks in southwestern ponderosa pine forests, *Forest Ecology and Management, 255* (7), 2698-2708.

Moreira, X., Mooney, K.A., Rasmann, S., Petry, W.K., Carrillo-Gavilán, A., Zas, R. & Sampedro, L. (2014), Trade-offs between constitutive and induced defences drive geographical and climatic clines in pine chemical defences, *Ecology Letters*, *17* (5), 537-546.

O'Halloran, T.L., Law, B.E., Goulden, M.L., Wang, Z., Barr, J.G., Schaaf, C., *et al.* (2012), Radiative forcing of natural forest disturbances, *Global Change Biology*, *18* (2), 555–565.

Omernik J.M. (1987), Ecoregions of the coterminous United States, *Annals of the Association of American Geographers*, 77 (1), 118-125.

Omernik J.M. & Griffith, G.E. (2014), Ecoregions of the conterminous United States: evolution of a hierarchical spatial framework, *Environmental Management*, *54* (6)**,** 1249-1266.

Pachauri, R.K., Allen, M.R., Barros, V.R., Broome, J., Cramer, W., Christ, R., *et al.* (2014), *Climate change 2014: synthesis report. Contribution of Working Groups I, II and III to the fifth assessment report of the Intergovernmental Panel on Climate Change* (p. 151), IPCC.

Pec, G.J., Karst, J., Sywenky, A.N., Cigan, P.W., Erbilgin, N., Simard, S.W. & Cahill, J.F. (2015), Rapid Increases in forest understory diversity and productivity following a mountain pine beetle (Dendroctonus ponderosae) outbreak in pine forests, *PLoS One*, *10* (4), e0124691.

Penn, C.A., Bearup, L.A., Maxwell, R.M. & Clow, D.W. (2016), Numerical experiments to explain multiscale hydrological responses to mountain pine beetle tree mortality in a headwater watershed, *Water Resources Research, 52* (4), 3143-3161.

Pinnell, S. (2016), Resin duct defenses in Ponderosa pine during a mountain pine beetle outbreak: Genetic effects, mortality, and relationships with growth.

Pregitzer, K.S. & Euskirchen, E.S. (2004), Carbon cycling and storage in world forests: biome patterns related to forest age, *Global Change Biology*, *10* (12), 2052–2077.

PRISM Climate Group (2011), PRISM climate data, *Oregon State University, Corvallis, OR.*

R Core Team (2013), R: A language and environment for statistical computing, *R Foundation for Statistical Computing, Vienna, Austria.*

R Core Team (2017), R: A language and environment for statistical computing, *R Foundation for Statistical Computing, Vienna, Austria.*

Raffa, K.F. & Berryman, A.A. (1983), The role of host plant resistance in the colonization behavior and ecology of bark beetles (Coleoptera: Scolytidae), *Ecological Monographs*, *53* (1), 27-49.

Raffa, K.F. (1988), The mountain pine beetle in western North America, *Dynamics of Forest Insect Populations*, 505-530.

Raffa, K.F., Aukema, B.H., Bentz, B.J., Carroll, A.L., Hicke, J.A., Turner, M.G. & Romme, W.H. (2008), Cross-scale Drivers of Natural Disturbances Prone to Anthropogenic Amplification: The Dynamics of Bark Beetle Eruptions, *Bioscience*, *58* (6), 501.

Randerson, J.T., Liu, H., Flanner, M.G., Chambers, S.D., Jin, Y., Hess, P.G., *et al.* (2006), The impact of boreal forest fire on climate warming, *Science*, *314* (5802), 1130–1132.

Reed, D.E., Ewers, B.E. & Pendall, E. (2014), Impact of mountain pine beetle induced mortality on forest carbon and water fluxes, *Environmental Research Letters*, *9* (10), 105004.

Reed, C.C., Ballantyne, A.P., Cooper, L.A. & Sala, A. (2018) Limited evidence for CO2-related growth enhancement in northern Rocky Mountain lodgepole pine populations across climate gradients, *Global Change Biology*.

Rich, R.L., Frelich, L., Reich, P.B. & Bauer, M.E. (2010), Detecting wind disturbance severity and canopy heterogeneity in boreal forest by coupling high-spatial resolution satellite imagery and field data, *Remote Sensing of Environment*, *114* (2), 299-308.

Robinson, N.P., Allred, B.W., Jones, M.O., Moreno, A., Kimball, J.S., Naugle, D.E., *et al.* (2017), A Dynamic Landsat Derived Normalized Difference Vegetation Index (NDVI) Product for the Conterminous United States, *Remote Sensing*, *9* (8), 863.

Rodriguez-Galiano, V.F., Ghimire, B., Rogan, J., Chica-Olmo, M. & Rigol-Sanchez, J.P. (2012), An assessment of the effectiveness of a random forest classifier for land-cover classification, *ISPRS Journal of Photogrammetry and Remote Sensing*, *67*, 93-104.

Rogan, J., Franklin, J., Stow, D., Miller, J., Woodcock, C. & Roberts, D. (2008), Mapping land-cover modifications over large areas: A comparison of machine learning algorithms, *Remote Sensing of Environment*, *112* (5), 2272-2283.

Ruel, J. & Whitham, T.G. (2002), Fast-growing juvenile pinyons suffer greater herbivory when mature, *Ecology*, *83* (10), 2691-2699.

Safranyik, L. & Carroll, A.L. (2006), *The biology and epidemiology of the mountain pine beetle in lodgepole pine forests.*

Sangüesa-Barreda, G., Linares, J.C. & Camarero, J.J. (2015), Reduced growth sensitivity to climate in bark-beetle infested Aleppo pines: Connecting climatic and biotic drivers of forest dieback, *Forest Ecology and Management*, *357*, 126-137.

Schultz, M., Clevers, J.G., Carter, S., Verbesselt, J., Avitabile, V., Quang, H.V. & Herold, M. (2016), Performance of vegetation indices from Landsat time series in deforestation monitoring, *International Journal of Applied Earth Observation and Geoinformation*, *52*, 318-327.

Seager, R., Ting, M., Held, I., Kushnir, Y., Lu, J., Vecchi, G., *et al.* (2007), Model projections of an imminent transition to a more arid climate in southwestern North America, *Science, 316* (5828), 1181-1184.

Seidl, R., Schelhaas, M.J., Rammer, W. & Verkerk, P.J. (2014), Increasing forest disturbances in Europe and their impact on carbon storage, *Nature Climate Change, 4*, 806-810.

Shimizu, K., Ahmed, O.S., Ponce-Hernandez, R., Ota, T., Win, Z.C., Mizoue, N. & Yoshida, S. (2017), Attribution of Disturbance Agents to Forest Change Using a Landsat Time Series in Tropical Seasonal Forests in the Bago Mountains, Myanmar, *Forests*, *8* (6), 218.

Shrimpton, D.M. & Thomson, A.J. (1985), Relationship between phloem thickness and lodgepole pine growth characteristics, *Canadian Journal of Forest Research*, *15* (5), 1004-1008.

Simard, M., Powell, E.N., Raffa, K.F. & Turner, M.G. (2012), What explains landscape patterns of tree mortality caused by bark beetle outbreaks in Greater Yellowstone?, *Global Ecology and Biogeography, 21* (5), 556-567.

Sobrino, J.A., Jimenez-Munoz, J.C. & Paolini, L. (2004), Land surface temperature retrieval from LANDSAT TM 5, *Remote Sensing of Environment, 90* (4), 434-440.

Sousa, W.P. (1984), The role of disturbance in natural communities, *Annual Review of Ecology and Systematics, 15*, 353-391.

Speckman, H.N., Frank, J.M., Bradford, J.B., Miles, B.L., Massman, W.J., Parton, W.J. & Ryan, M.G. (2015) Forest ecosystem respiration estimated from eddy covariance and chamber measurements under high turbulence and substantial tree mortality from bark beetles, *Global Change Biology, 21* (2), 708-721.

Stephens, S.L., Boerner, R.E., Moghaddas, J.J., Moghaddas, E.E., Collins, B.M., Dow, C.B., *et al.* (2012), Fuel treatment impacts on estimated wildfire carbon loss from forests in Montana, Oregon, California, and Arizona, *Ecosphere*, *3* (5), 1-17.

Stokes, M.A. & Smiley, T.L. (1968), *An introduction to tree-ring dating*, Chicago: University of Chicago Press.

Therneau, T., Atkinson, B. & Ripley, B. (2017), rpart: Recursive partitioning and regression trees. R package version 4.1-11.

Townshend, J., Hansen, M., Carroll, M., DiMiceli, C., Sohlberg, R. & Huang, C. (2011), User Guide for the MODIS Vegetation Continuous Fields Product Collection 5 Version 1, *University of Maryland.*

Trumbore, S., Brando, P. & Hartmann, H. (2015), Forest health and global change, *Science, 349* (6250), 814-818.

USDA Forest Service, Forest Health Protection and its partners (2000-2014), Aerial detection survey data.

Vanderhoof, M., Williams, C.A., Ghimire, B. & Rogan, J. (2013), Impact of mountain pine beetle outbreaks on forest albedo and radiative forcing, as derived from Moderate Resolution ImagingSpectroradiometer, Rocky Mountains, USA, *Journal of Geophysical Research - Biogeosciences*, *118* (4), 1461-1471.

Veblen, T.T., Hadley, K.S., Reid, M.S. & Rebertus, A.J. (1991), The response of subalpine forests to spruce beetle outbreak in Colorado, *Ecology, 72* (1)**,** 213-231.

Venables, W.N. & Ripley, B.D. (2002), Modern applied statistics with S, fourth edition, *Springer, New York, New York.*

Verbesselt, J., Hyndman, R., Newnham, G. & Culvenor, D. (2010a), Detecting trend and seasonal changes in satellite image time series, *Remote Sensing of Environment*, *114* (1), 106–115.

Verbesselt, J., Hyndman, R., Zeileis, A. & Culvenor, D. (2010b), Phenological change detection while accounting for abrupt and gradual trends in satellite image time series, *Remote Sensing of Environment*, *114* (12), 2970–2980.

Verbesselt, J., Zeileis, A. & Herold, M. (2012) Near real-time disturbance detection using satellite image time series, *Remote Sensing of Environment*, *123*, 98-108.

Waring, R.H. & Pitman, G.B. (1983), Physiological stress in lodgepole pine as a precursor for mountain pine beetle attack, *Journal of Applied Entomology*, *96* (1-5), 265-270.

Watson, R.T., Zinyowera, M.C. & Moss, R.H. (1998), The regional impacts of climate change: an assessment of vulnerability, *Cambridge University Press, Cambridge.*

Watts, L.M. & Laffan, S.W. (2014), Effectiveness of the BFAST algorithm for detecting vegetation response patterns in a semi-arid region, *Remote Sensing of Environment*, *154*, 234–245.

Weng, Q., Lu, D. & Schubring, J. (2004), Estimation of land surface temperature-vegetation abundance relationship for urban heat island studies, *Remote Sensing of Environment, 89* (4), 467-483.

Westerling, A.L., Turner, M.G., Smithwick, E.A.H., Romme, W.H. & Ryan, M.G. (2011), Continued warming could transform Greater Yellowstone fire regimes by mid-21st century, *PNAS, 108* (32), 13165–13170.

Wiedinmyer, C., Quayle, B., Geron, C., Belote, A., McKenzie, D., Zhang, X., *et al.* (2006), Estimating emissions from fires in North America for air quality modeling, *Atmospheric Environment, 40* (19), 3419-3432.

Williams, C.A., Collatz, G.J., Masek, J. & Goward, S.N. (2012), Carbon consequences of forest disturbance and recovery across the conterminous United States, *Global Biogeochemical Cycles*, *26* (1), GB1005.

Yanchuk, A.D., Murphy, J.C. & Wallin, K.F. (2008), Evaluation of genetic variation of attack and resistance in lodgepole pine in the early stages of a mountain pine beetle outbreak, *Tree Genetics & Genomes*, *4* (2), 171-180.

Zeileis, A., Leisch, F., Hornik, K. & Kleiber, C. (2002), strucchange: An R Package for Testing for Structural Change in Linear Regression Models, *Journal of Statistical Software, 7* (2), 1-38.

Zeileis, A., Kleiber, C., Kraemer, W. & Hornik, K. (2003), Testing and Dating of Structural Changes in Practice, *Computational Statistics & Data Analysis, 44,* 109-123.

Zhao, F., Huang, C. & Zhu, Z. (2015), Use of vegetation change tracker and support vector machine to map disturbance types in greater yellowstone ecosystems in a 1984–2010 Landsat time series, *IEEE Geoscience and Remote Sensing Letters*, *12* (8), 1650-1654.

Zhu, Z., Woodcock, C.E. & Olofsson, P. (2012), Continuous monitoring of forest disturbance using all available Landsat imagery, *Remote Sensing of Environment*, *122*, 75-91.

Zuur, A.F., Ieno, E.N., Walker, N., Savaliev, A.A. & Smith, G.M. (2009), *Mixed effects models and extensions in ecology with R,* New York, NY: Springer Science and Business Media.